11-13-2013

Minimization of Cost and CO2 Emissions for Rectangular Spread Footings Subjected to Biaxial Loading

Andrew Kary Mehdi Assadollahi

MINIMIZATION OF COST AND CO_2 EMISSIONS FOR RECTANGULAR SPREAD FOOTINGS SUBJECTED TO BIAXIAL LOADING

by

Andrew Kary Mehdi Assadollahi

A Dissertation

Submitted in Partial Fulfillment of the

Requirements for the Degree of

Doctor of Philosophy

Major: Engineering

The University of Memphis

December 2013

ACKNOWLEDGEMENTS

There are several people who have provided a great amount of time and effort to aid me in the completion of this dissertation. I am thankful for all of the encouragement and guidance that Dr. Camp has provided me as my faculty advisor and mentor over the years. His continuing friendship and patience have made it possible for me to achieve all of my goals during my graduate school career. I would like to thank Dr. Pezeshk for giving me the opportunity to attend The University of Memphis and be a part of the Civil Engineering Department. I would also like to thank the Pezeshk family for their unending support, encouragement, and friendship since my childhood. I am thankful for all of Dr. Meier's wisdom and patience that he has provided me throughout my graduate career. I am thankful for all of the professional advice which Dr. Arellano and Dr. Elsayed have provided me over the years.

There are also several teachers and professors who have had a significant impact on my academic and personal growth over the years. Most notably, I would like to thank: Ms. Paris, Mrs. Duncan, Mrs. Antignane, Mr. Berretta, Mrs. Comas, Mr. Box, Mr. Kolodziej, Mr. Wong, Mr. Rocha, Mr. McGinnis, Dr. Lin, Dr. Malasri, Dr. Madhavan, Dr. Becker, Dr. Bedrossian, Dr. Ivey, Dr. Palazolo, Dr. Segui, Dr. Abdelnaby, and Dr. Latifi. I would like to thank Master Brumley and the Taekwondo University family for teaching me the importance of courtesy, integrity, perseverance, self-control, and having an indomitable spirit. All of these qualities have not only proven to be essential in graduate school but also in life. I would also like to thank Mr. Farrar and Dr. Ramirez for saving my computer on numerous occasions from various illnesses, as well as Mrs. Meier for her everlasting positive attitude.

Without my close friends keeping me sane, my graduate career would have ended a long time ago. I would like to thank Anthony, Daniel, Mark, Thomas, Teddy, Alan, Parsa, Taylor, Duncan, Nikko, Annie, Lauren, Masood, Hanan, Moji, Alireza, and Ali. I would like to thank my best friend Andy, and his family, for being like a second family to me since I was five years old. I would especially like to thank Sanaz, my office mate for the past three years, for her support and friendship and for putting up with all of my annoyances. I would also like to thank my kitty for keeping me company every night as I lie awake pondering my future.

Lastly, I would like to thank my family for their unending love and support, throughout my entire life. My parents Ali and Janet Assadollahi have been a constant source of love and encouragement. My father's perseverance towards excellence coupled with my mother's compassion and patience have given me the tools to accomplish things I never imagined. With every timeout, spanking, and grounding came an important life lesson. I also want to thank my sisters Andrea and Ariann Assadollahi, who have always supported me in all of my endeavors, except during arguments. I could not have made it this far without my family.

ABSTRACT

Assadollahi, Andrew Kary Mehdi. Ph.D. The University of Memphis. December 2013. Minimization of Cost and CO_2 Emissions for Rectangular Spread Footings Subjected to Biaxial Loading. Major Professor: Charles Camp, Ph.D.

A Big Bang-Big Crunch (BB-BC) optimization algorithm was applied to the analysis and design of reinforced concrete spread footings subjected to concentric, uniaxial, and biaxial loading. For spread footings subjected to eccentric loading conditions, it is convenient to assume that the entire base of the footing remains in contact with the soil, resulting in a compressive bearing pressure distribution. However, this assumption does not accurately describe the nature of the bearing pressure distribution. Analysis procedures for spread footings subjected to eccentric loading conditions that allow uniaxial and biaxial uplift were developed. From these formulations, an analysis chart of the bearing pressure surface equations for one, two, and three footing corners detached was developed to determine percentages of detachment along the edges of a spread footing that is subjected to biaxial uplift.

In addition to assuming that the entire footing base remains in compression, it is common to make several other simplifying assumptions when designing spread footings subjected to uniaxial and biaxial loading. A BB-BC optimization algorithm is applied in order to compare spread footing designs based upon theoretical analysis procedures and designs based upon simplifying assumptions.

Since cost has always been an integral part of engineering design and CO_2 emissions are becoming of greater concern, a multi-objective optimization was utilized to develop relationships between cost and CO_2 emissions associated with the design of reinforced spread footings subjected to concentric, uniaxial, and biaxial loading.

TABLE OF CONTENTS

LIST OF TABLES

LIST OF FIGURES

xiii

CHAPTER 1

INTRODUCTION

Reinforced concrete spread footings are one of the most common geo-structures in engineering practice. In the analysis and design of spread footings, the interaction between the soil and the reinforced concrete poses many challenges to the designer: the footing must safely and reliably support the superstructure, provide stability against soil bearing capacity failure and excessive settlement, and limit the stresses in the concrete. In addition to these design objectives, there are many requirements that a reinforced spread footing must satisfy: it must have sufficient shear and moment capacities in both of the plan dimensions, the bearing capacity of the concrete cannot be exceeded, and the configuration of the steel reinforcement must meet all building code requirements.

Uniaxial loading occurs on a spread footing when the applied force acts through a point displaced from the center along one of the principal axes, or if there is a moment load applied to the footing. The eccentricity is the perpendicular distance from the center of the footing to the applied load. For a moment loading, the equivalent eccentricity is calculated as the applied moment divided by the applied vertical column load. Biaxial loading occurs when the applied force acts through a point displaced from the center along both of the principal directions. In this case, there are two eccentricity values, which are the perpendicular distances from the center of the footing to the applied load. For moment loading; there are two applied moments, each about one of the principal axes. When designing a spread footing with eccentric loading, it is convenient and typical for the entire base of the footing to be in compression.

Economical design is essential in the practice of engineering. However, a detailed method for developing low-cost designs of reinforced concrete spread footings is relatively new (Wang and Kulhawy 2008, Wang 2009, and Khajehzadeh et al. 2011). In addition, there has been no investigation into the development of low-cost and low-CO_2 emission designs that consider both the geotechnical and structural limit states.

According to the United Nations Intergovernmental Panel on Climate Change (UNIPCC 2007), there has been a significant increase in the build-up of global greenhouse gases (GHG) in the atmosphere due to human activities since the pre-industrial times. The production of Portland cement, the principal binder used in concrete, is responsible for large emissions of carbon dioxide (CO_2) (Mehta 2002). Due to increased demand for concrete products and structures, the carbon footprint of the cement industry almost doubled between 1990 and 2005 (Mehta 2009). As a result of the concerns of the increased levels of GHG, design and construction methods have moved towards more sustainable materials, designs, and construction practices. With the variety and number of concrete structures in the world, consideration of the impacts of CO_2 emissions on their design is both a suitable and prudent area of research.

In practice, simplifying and conservative assumptions for the analysis of spread footings are made which yield over-designed results. If cost or the emission of CO_2 is not a concern; that is, if they are negligible compared to the cost or CO_2 emissions of the entire project, then using simplifying design assumptions is acceptable. However, if the material and construction costs or CO_2 emissions of the spread footing are not considered negligible, then using simplifying design assumptions which not only yields over-

designed footings, but also leads to inflated costs or CO_2 emissions, may not be acceptable.

To analyze and design a reinforced concrete spread footing while minimizing cost or CO_2 emissions, optimization algorithms may be employed. Big Bang-Big Crunch (BB-BC) has been shown to be a computationally efficient heuristic method to solve a variety of optimization problems. The most powerful concept proposed by Erol and Eksin (2006) in their original BB-BC algorithm involved exploiting the power of the mean. Historically, Galton (1907) proposed that the average or weighted-average of a group of estimates can be remarkably accurate. Erol and Eksin (2006) coupled the Galtonian principle of the accuracy of the mean with an abstract model of the lifecycle of the universe to develop the BB-BC algorithm.

The BB-BC algorithm has been shown to outperform many other evolutionary methods in a variety of optimization problems. Erol and Eksin (2006) established that a simple BB-BC algorithm can outperform enhanced and classic genetic algorithms (GA) for many benchmark optimization functions. Camp (2007) and Kaveh and Talatahari (2009 and 2010) proposed hybrid forms of the BB-BC algorithm to solve structural engineering optimization problems. Results indicated that these hybrid BB-BC algorithms improved both the quality of the optimization and its computational efficiency when compared to published solutions generated by GA and ant colony optimization (ACO).

While there is little research on optimization of spread footings, the literature has numerous studies on optimizing the design of reinforced concrete structures. For example, Sarma and Adeli (1998) present a comprehensive review of papers on cost

optimization of concrete structures. Coello et al. (1997), Rafiqa and Southcombea (1998), Rajeev and Krishnamoorthy (1998), Camp et al. (2003), Lee and Ahn (2003), Lepš and Šejnoha (2003), Sahaba et al. (2004), Govindaraj and Ramasamy (2005), Kwak and Kim (2008, 2009), and Camp and Huq (2013) all applied various types of GAs to the cost optimization of reinforced concrete structures. Paya et al. (2008), Perea et al. (2008), and Paya-Zaforteza et al. (2009) optimized reinforced concrete structures using simple and hybrid simulated annealing (SA) algorithms. Camp and Akin (2012) used a hybrid BB-BC algorithm to develop low-cost retaining wall designs and Villalba et al. (2010) optimized reinforced concrete retaining walls for CO_2 emissions using SA. Yepes et al. (2012) developed an innovative hybrid multistart optimization strategic method based on a variable neighborhood search threshold acceptance strategy to optimize reinforced concrete retaining walls for cost and CO_2 emissions.

CHAPTER 2

OBJECTIVES

Since the design of spread footings is a common practice among geotechnical and structural engineers; the optimization of spread footings subjected to concentric and eccentric loads is a prudent area of research. When designing a spread footing due to eccentric loading, it is typical and convenient that the entire base of the footing be in compression. By designing a spread footing such that the footing base is in full compression, the footing will typically be much larger than what is required to satisfy all of the geotechnical and structural service and ultimate limit states. In an effort to design smaller, yet adequate spread footings, there has been some limited research on uniaxial and biaxial uplift (Highter and Anders 1985, Irles and Irles 1994, Wilson 1997, Rodriguez-Gutierrez and Aristizabal-Ochoa 2012). In addition, knowledge of the soil pressure distribution for spread footings subjected to uplift may be necessary to evaluate an existing footing in which the original loading pattern has been modified. Therefore, the first objective of this research is to develop analysis procedures for reinforced concrete spread footings which are subjected to uniaxial and biaxial uplift.

In all fields of engineering, the comparison of theoretical analysis procedures with simplified analysis procedures is an important discussion among engineers. In practice, many simplifying design assumptions are made that can yield over-designed, conservative results. However, many of these simplifying assumptions may not be necessary and often lead to inflated costs and increased CO_2 emissions. A second objective of this research is to compare spread footing designs, subjected to eccentric

loading, using the developed theoretical analysis procedures with designs based on simplifying assumptions, commonly used in practice, using optimization techniques.

Economical designs have always been important to engineers, with concerns about the impacts of GHGs, reducing CO_2 emissions is becoming a valid objective in engineering design. The third objective of this research is to study of the relationship between cost and CO_2 emissions by applying the optimization procedure to a multi-objective fitness function.

CHAPTER 3

GEOMECHANICS

Biaxial eccentric loading is encountered when an applied force acts through a point displaced from the center of the footing along both of the principal directions or there are two applied moments, each about one of the principal axes. Uniaxial eccentric loading occurs if a force acts through a point displaced from the center of the footing along only one of the principal directions or there is one applied moment. In this research the spread footings is assumed to be perfectly rigid and the soil is assumed to be homogeneous, uniform, isotropic, cohesionless, and behave linear-elastically. Since the spread footing is assumed to be rigid, the distribution of the subgrade reaction is independent of the degree of compressibility of the subgrade. During eccentric loading, a non-uniform bearing pressure distribution is produced. If there are no eccentricities or applied moments, the loading condition is concentric and a uniform bearing pressure distribution occurs. All procedures developed in this research are based on the assumption that the ground water table is located well below the foundation.

Two eccentric loading conditions are considered: eccentricities within and outside of the kern of the footing. The kern area of a rectangular cross section is defined as the area in which a load is applied such that no tensile stresses develop. If a load is applied outside of the kern; one, two, or three corners of the cross section will develop tensile stresses. For the application of spread footings, it is assumed that tensile stresses are not transmitted to the soil from the footing. Because of this, when there is loading on a spread footing outside of the kern area, detachment of the footing from the soil will occur.

7

Meyerhof (1953) developed the effective area method for the analysis of spread footings due to biaxial bending. Teng (1962) developed an analysis chart with accompanying equations to evaluate the four corner bearing pressures for footings subjected to biaxial uplift. Higher and Anders (1985) developed another effective area method along with a set of design charts for the analysis of footings subjected to biaxial uplift. Irles and Irles (1994) developed analytical solutions for finding the percentage of the dimensions of footings that become detached during biaxial uplift by geometrically modeling the bearing pressure distribution. Wilson (1997) modeled the bearing pressure distribution beneath a footing experiencing biaxial uplift using planar geometric solids. The focus of this chapter is the development of equations to model the bearing pressure distribution beneath a rectangular footing subjected to eccentric loading in which one, two, or three corners become detached from the soil. In addition to governing equations, an analysis chart is developed for the determination of the corner bearing pressures when uplift occurs.

3.1 Biaxial Loading

Figure 1 shows a schematic of a spread footing subjected to biaxial loading where the origin is taken to be the center of the footing and the applied force is P, the length of the footing is L, the width is B, the eccentricity along the x-axis is e_x, and the eccentricity along the y-axis is e_y. Due to symmetry, only positive eccentricities are considered.
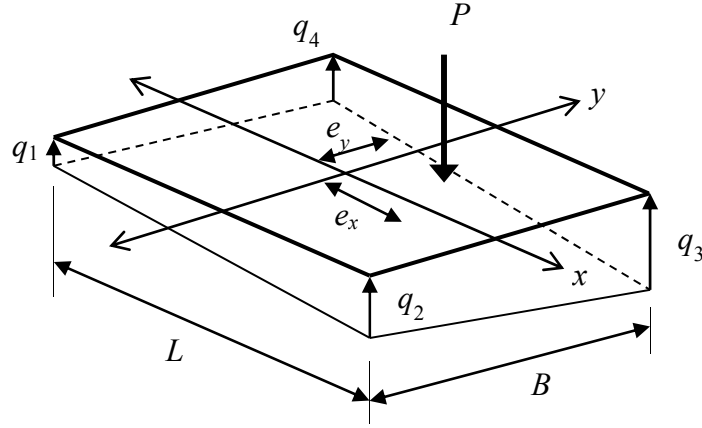
Figure 1. Spread Footing Subjected to Biaxial Loading.

When a footing is subjected to biaxial loading and there is no detachment of the soil (the entire bearing surface is in compression), the well-known bending formula is applied to determine the bearing stresses at the four corners of the footing as

$$q_{[1-4]} = \frac{P}{BL} \pm \frac{M_x c_y}{I_x} \pm \frac{M_y c_x}{I_y} \qquad (1)$$

where M_x is the moment about the x-axis, I_x is the moment of inertia about the x-axis, c_y is half of the footing width, M_y is the moment about the y-axis, I_y is the moment of inertia about the y-axis, and c_x is half of the footing length. Substituting values for the moment of inertia terms, defining the moment about the x-axis as Pe_y, and defining the moment about the y-axis as Pe_x yields:

$$q_{[1-4]} = \frac{P}{BL}\left(1 \pm \frac{6e_y}{B} \pm \frac{6e_x}{L}\right) \qquad (2)$$

The locations of P that cause the minimum corner pressure, q_1, to become zero define the portion of the kern boundary for positive eccentricities. The minimum bearing pressure, q_1, is given by:

$$q_1 = \frac{P}{BL}\left(1 - \frac{6e_y}{B} - \frac{6e_x}{L}\right)$$ (3)

When Equation (3) equals zero, the kern boundary is:

$$\frac{6e_y}{B} + \frac{6e_x}{L} = 1$$ (4)

Therefore, when the left side of Equation (4) is larger than 1, a portion of the footing will become detached from the soil, assuming that the soil cannot support tension, and Equation (1) is no longer applicable for determining the bearing pressures at the four corners of the footing.

Analytical solutions for the case of biaxial uplift will be based upon the formulation for a rectangular element with associated interpolation functions. The choice of a rectangular element formulation is made because the analysis of only rectangular spread footings is considered in this research. Figure 2 shows a general rectangular element.
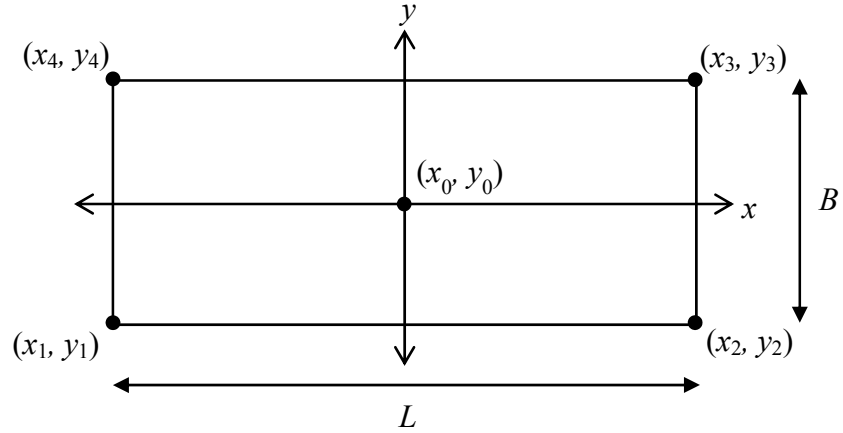
Figure 2. Rectangular Element.

For the purposes of this research, the initial point shown in Figure 2 will be taken as the origin, located at the center of the element. For the application of spread footings, there are four degrees of freedom, one for each node, which are designated by the four corner bearing stresses, q_1, q_2, q_3, and q_4. The general rectangular interpolation functions N_i are:

$$N_i(x,y) = \begin{pmatrix} \dfrac{(x_2-x)(y_3-y)}{(x_2-x_1)(y_3-y_1)} \\[2ex] \dfrac{(x_1-x)(y_3-y)}{(x_1-x_2)(y_3-y_2)} \\[2ex] \dfrac{(x_1-x)(y_1-y)}{(x_1-x_3)(y_1-y_3)} \\[2ex] \dfrac{(x-x_2)(y_1-y)}{(x_4-x_2)(y_1-y_4)} \end{pmatrix} \tag{5}$$

Figure 3 shows plots of each rectangular interpolation function.

11
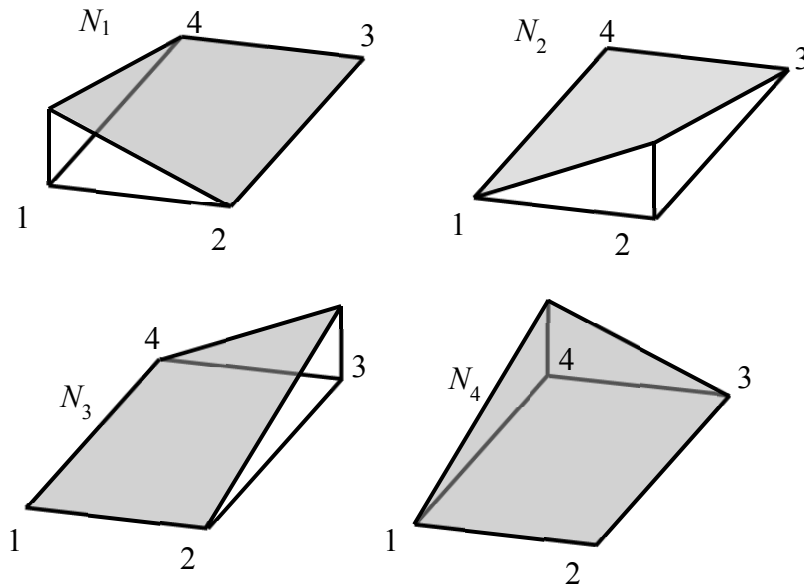
Figure 3. Plots of Interpolation Functions.

The shapes of the interpolation functions are such that there is no curvature in the directions parallel to the sides of the element; however, there is a twist in each of the plots for $N_i(x, y)$ that is caused by the bilinear xy term. This model fits the description of the assumed bearing pressure distribution beneath a rectangular spread footing subjected to biaxial loading.

In order to develop a relationship for the bearing pressure surface beneath a rectangular spread footing, first the four corner stresses q_j are defined as a column vector as:

$$q_j = \begin{pmatrix} q_1 \\ q_2 \\ q_3 \\ q_4 \end{pmatrix} \tag{6}$$

The geometric boundary conditions of a rectangular spread footing are defined by the coordinates (x_1,y_1), (x_2,y_2), (x_3,y_3), (x_4,y_4) as:

$$
\begin{aligned}
(x_1,y_1) &= \left(-\frac{L}{2},-\frac{B}{2}\right) \\
(x_2,y_2) &= \left(\frac{L}{2},-\frac{B}{2}\right) \\
(x_3,y_3) &= \left(\frac{L}{2},\frac{B}{2}\right) \\
(x_4,y_4) &= \left(-\frac{L}{2},\frac{B}{2}\right)
\end{aligned} \tag{7}
$$

Substituting the boundary conditions given by Equation (7) into the shape function formulations given in Equation (5) defines the spread footing geometry in terms of the rectangular element shape functions. This is given as:

$$
N_i(x,y) = \frac{1}{BL}\begin{bmatrix} \left(x-\frac{L}{2}\right)\left(y-\frac{B}{2}\right) \\ \left(x+\frac{L}{2}\right)\left(\frac{B}{2}-y\right) \\ \left(x+\frac{L}{2}\right)\left(y+\frac{B}{2}\right) \\ \left(\frac{L}{2}-x\right)\left(y+\frac{B}{2}\right) \end{bmatrix} \tag{8}
$$

13

The superposition of the four corner stresses with the shape functions defines the bearing pressure surface beneath a rectangular spread footing and is achieved by performing the following operation:

$$q(x,y) = q_j^T N_i(x,y) \tag{9}$$

Evaluating the vector multiplication in Equation (9) gives the general relationship for the bearing pressure surface beneath a rectangular spread footing as:

$$q(x,y) = \frac{q_1}{BL}\left(y - \frac{B}{2}\right)\left(x - \frac{L}{2}\right) - \frac{q_2}{BL}\left(y - \frac{B}{2}\right)\left(x + \frac{L}{2}\right) \\ + \frac{q_3}{BL}\left(y + \frac{B}{2}\right)\left(x + \frac{L}{2}\right) - \frac{q_4}{BL}\left(y + \frac{B}{2}\right)\left(x - \frac{L}{2}\right) \tag{10}$$

During uniaxial loading, the bilinear xy terms cancel and Equation (10) simplifies to a planar surface. For uniaxial loading along the positive x-axis, $q_2 = q_3$ and $q_1 = q_4$. If uniaxial loading is along the positive y-axis, $q_3 = q_4$ and $q_1 = q_2$. For the case of concentric loading, the four corner pressures are equal and all of the variable terms cancel, resulting in Equation (10) being constant.

Since a rectangular spread footing is symmetric, the load P may fall in any of the four quadrants of the footing. Figure 4 shows a rectangular spread footing with the load P having positive eccentricities. For loading within the other three quadrants, the kern boundary is developed in a similar manner. The kern is the diamond-shaped area bounded by four linear relationships.
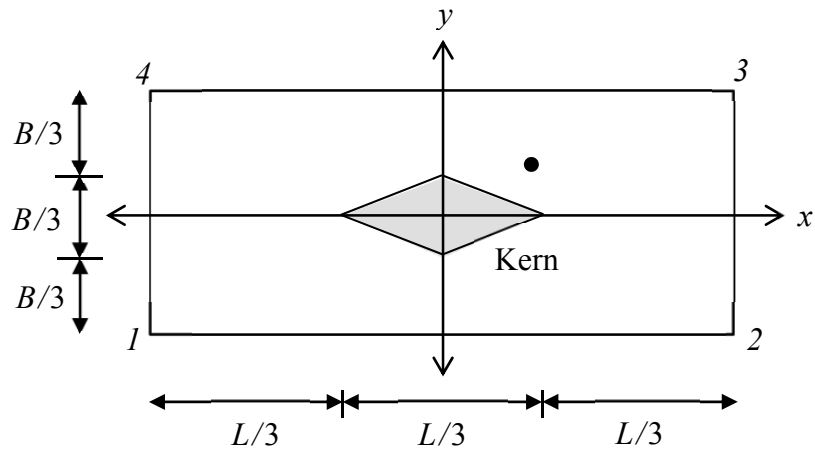
Figure 4. Spread Footing with Load in Quadrant I.

Depending on where the load is located with respect to the kern boundary, only Corner 1 may become detached (Case 1), Corners 1 and 4 may become detached (Case 2), Corners 1 and 2 may become detached (Case 3), or Corners 1, 2, and 4 may become detached (Case 4). Different sets of boundary conditions are applied to Equation (10) for each of the four cases of biaxial uplift.

3.1.1 Uplift – case 1

Figure 5 shows a spread footing in which Corner 1 has become detached from the soil, where α and β are the percentages of detachment of the L and B dimensions, respectively.
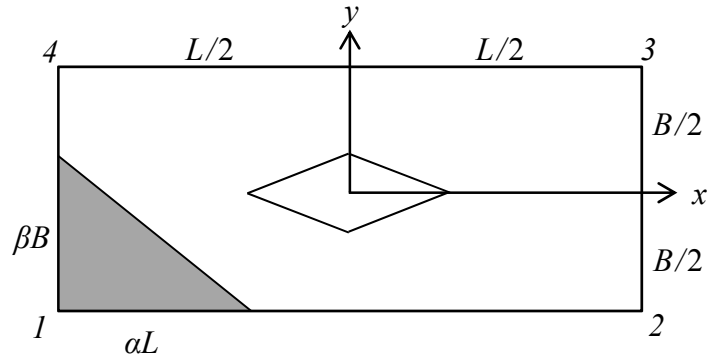
Figure 5. Footing with One Corner Detached.

Assuming that the intersection of the bearing pressure surface and the footing is linear, the line of zero bearing pressure can be expressed in two forms:

$$y(x) = \frac{-\beta B}{\alpha L}\left(x + \frac{L}{2} - \alpha L\right) - \frac{B}{2} \tag{11}$$

$$x(y) = \frac{-\alpha L}{\beta B}\left(y + \frac{B}{2}\right) - \frac{L}{2} + \alpha L \tag{12}$$

From this linear relationship, three boundary conditions are developed. Two of the boundary conditions are developed from the points of intersection of the line of zero bearing pressure and the sides of the footing:

$$q\left(\frac{-L}{2} + \alpha L, \frac{-B}{2}\right) = 0 \tag{13}$$

$$q\left(\frac{-L}{2}, \frac{-B}{2} + \beta B\right) = 0 \tag{14}$$

16

The third is developed from the line of zero bearing pressure itself:

$$q(x, y(x)) = 0 \tag{15}$$

By applying Equations (13), (14), and (15) to Equation (10); the following three relationships are derived:

$$q_2 = q_1\left(1 - \frac{1}{\alpha}\right) \tag{16}$$

$$q_4 = q_1\left(1 - \frac{1}{\beta}\right) \tag{17}$$

$$q_3 = q_1\left(1 - \frac{1}{\alpha} - \frac{1}{\beta}\right) \tag{18}$$

Substituting Equations (16), (17), and (18) into Equation (10) the bearing pressure surface becomes:

$$q(x, y) = \left(\frac{-q_1}{\alpha L}\right)x - \left(\frac{q_1}{\beta B}\right)y + \left(q_1 - \frac{q_1}{2\alpha} - \frac{q_1}{2\beta}\right) \tag{19}$$

From force equilibrium, the volume of the compressive bearing pressure distribution beneath the footing is equal to the applied load P. An expression for q_1 in terms of the footing dimensions, α and β, is derived from the following integration:

$$P = \int\limits_{\frac{-L}{2}}^{\frac{L}{2}} \int\limits_{\frac{-B}{2}}^{\frac{B}{2}} q(x,y)\, dy\, dx - \int\limits_{\frac{-L}{2}}^{\frac{-L}{2}+\alpha L} \int\limits_{\frac{-B}{2}}^{y(x)} q(x,y)\, dy\, dx \qquad (20)$$

Evaluating the integral in Equation (20) and rearranging terms yields:

$$q_1 = \frac{-6\alpha\beta P}{BL\left(\alpha^2\beta^2 - 6\alpha\beta + 3\alpha + 3\beta\right)} \qquad (21)$$

Integral equations are also written for moment equilibrium. The volume of the bearing pressure distribution which has become detached from the soil is subtracted from the total volume of the bearing pressure distribution. For a comparison to Irles and Irles (1994), moment equilibrium along the bottom and left edge of the footing is taken. This is satisfied by the following integral:

$$P\left(\frac{B}{2}+e_y\right) = \int\limits_{\frac{-L}{2}}^{\frac{L}{2}} \int\limits_{\frac{-B}{2}}^{\frac{B}{2}} q(x,y)\left(\frac{B}{2}+y\right) dy\, dx - \int\limits_{\frac{-L}{2}}^{\frac{-L}{2}+\alpha L} \int\limits_{\frac{-B}{2}}^{y(x)} q(x,y)\left(\frac{B}{2}+y\right) dy\, dx \qquad (22)$$

Evaluating the integral in Equation (22) and rearranging terms yields:

$$P\left(\frac{B}{2}+e_y\right) = \frac{-B^2 L q_1\left(\alpha^2\beta^3 - 12\alpha\beta + 8\alpha + 6\beta\right)}{24\alpha\beta} \qquad (23)$$

18

Moment equilibrium along the left edge of the footing is satisfied by the following integral:

$$P\left(\frac{L}{2}+e_x\right) = \int_{\frac{-L}{2}}^{\frac{L}{2}} \int_{\frac{-B}{2}}^{\frac{B}{2}} q(x,y)\left(\frac{L}{2}+x\right) dy\, dx - \int_{\frac{-L}{2}}^{\frac{-L}{2}+\alpha L} \int_{\frac{-B}{2}}^{y(x)} q(x,y)\left(\frac{L}{2}+x\right) dy\, dx \qquad (24)$$

Evaluating the integral in Equation (24) and rearranging terms yields:

$$P\left(\frac{L}{2}+e_x\right) = \frac{-BL^2 q_1\left(\alpha^3\beta^2 - 12\alpha\beta + 6\alpha + 8\beta\right)}{24\alpha\beta} \qquad (25)$$

Substituting Equation (21) into Equations (23) and (25) yields the following two relationships:

$$\frac{e_y}{B} = \frac{8\alpha + 6\beta - 12\alpha\beta + \alpha^2\beta^3}{4\left(3\alpha + 3\beta - 6\alpha\beta + \alpha^2\beta^2\right)} - \frac{1}{2} \qquad (26)$$

$$\frac{e_x}{L} = \frac{6\alpha + 8\beta - 12\alpha\beta + \alpha^3\beta^2}{4\left(3\alpha + 3\beta - 6\alpha\beta + \alpha^2\beta^2\right)} - \frac{1}{2} \qquad (27)$$

Equations (26) and (27) are a system of nonlinear equations and are identical to those presented by Irles and Irles (1994) who used only properties of tetrahedrons. Figure 6 shows a plot of Equations (26) and (27) for various values of α and β. If the load falls within this region, known as Region A; Corner 1 will become detached from the soil.
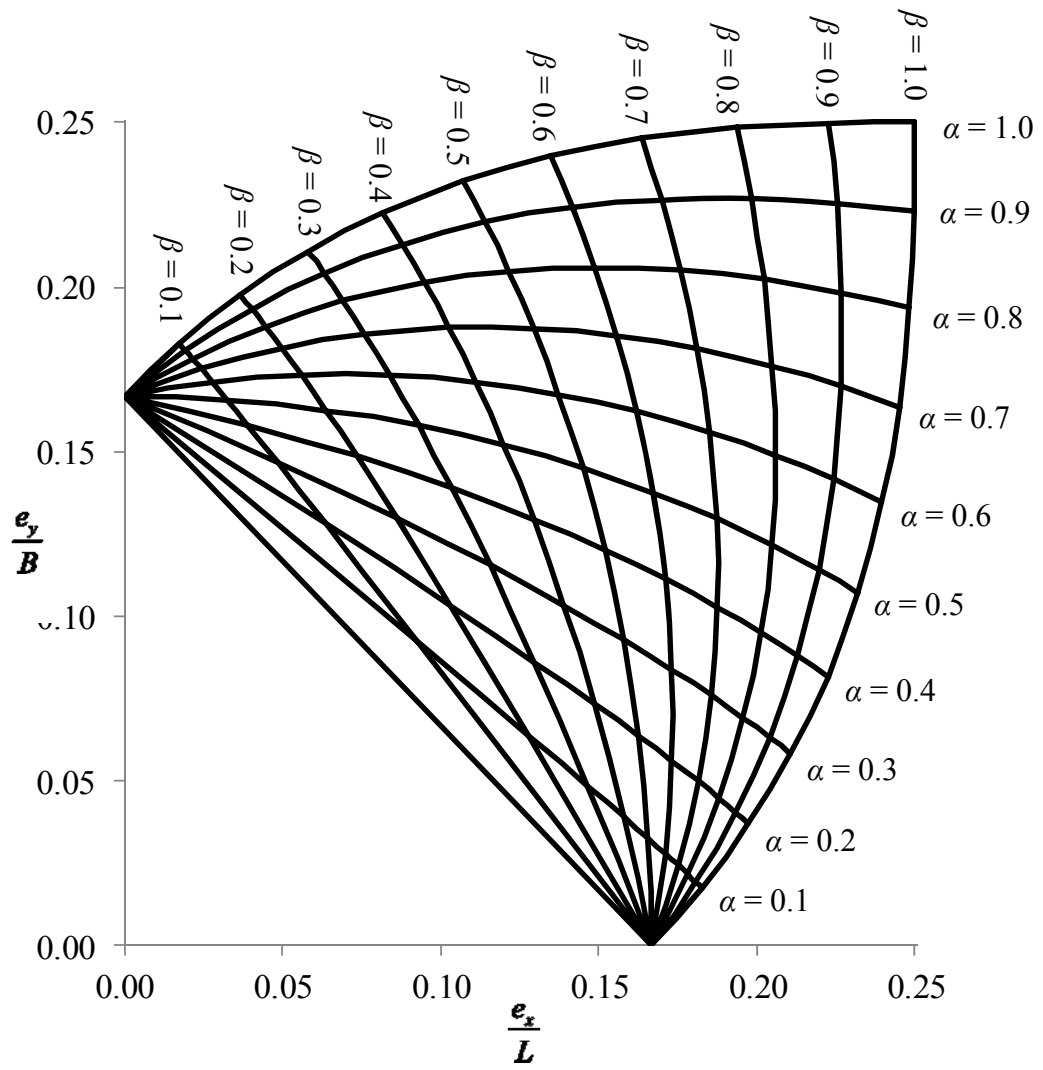
Figure 6. Biaxial Uplift – Region A.

By making some algebraic transformations, Equations (26) and (27) can be written as an eighth order polynomial $p_8(v)$ of a single variable v (Irles and Irles 1994). This is presented in this research as

$$\begin{aligned}
p_8(v) = {} & v\left(12A - 4v + 2Cv^3 + 2v^3 - 8Av - 4Cv - 6ACv^2 + ACv^3 + 6ACv\right) \\
& \left(4v + 6Av^2 - Av^3 - 2Cv^3 - 2v^3 - 12AC - 6Av + 4Cv + 8ACv\right) \\
& + (C+1)^2\left(v^2 - 3A + 2\right)^2\left(v^2 - 2\right)^2
\end{aligned} \tag{28}$$

where

$$A = 4\left(\frac{e_x}{L} + \frac{e_y}{B}\right) \tag{29}$$

$$C = \frac{e_x B}{e_y L} \tag{30}$$

$$v = \alpha\beta \tag{31}$$

Equation (28) is an eighth order polynomial with up to eight real roots for a unique combination of e_x/L and e_y/B. Equation (31) represents real roots of Equation (28). However, since the roots of Equation (28) represent the product of the percentages of detachment along each dimension of the footing, only real roots in the range [0, 1] are of interest. Once the desired root v is obtained, decimal values of α and β may be calculated using the following relationships (Irles and Irles 1994):

$$u = v\left(\frac{6A - (A+4)v}{3A - 2 - v^2}\right) \quad (32)$$

$$\beta = \frac{u(v^2 - 2C) + 2v^2(C-1)}{(C+1)(v^2 - 2)} \quad (33)$$

$$\alpha = u - \beta \quad (34)$$

Numerically finding the appropriate root for Equation (28) can be very cumbersome. The bisection method is applied to Equation (28) to determine the appropriate root in [0, 1], for a combination of e_x/L and e_y/B. Numerical studies have shown that for unique combinations of e_x/L and e_y/B, there may be either one or two real roots in [0, 1]. Figure 7 shows a plot of Equation (28) for a combination of e_x/L and e_y/B inside Region A, yielding one root at $v = 0.3$.

$$e_x/L = 0.137421$$

$$e_y/B = 0.167453$$
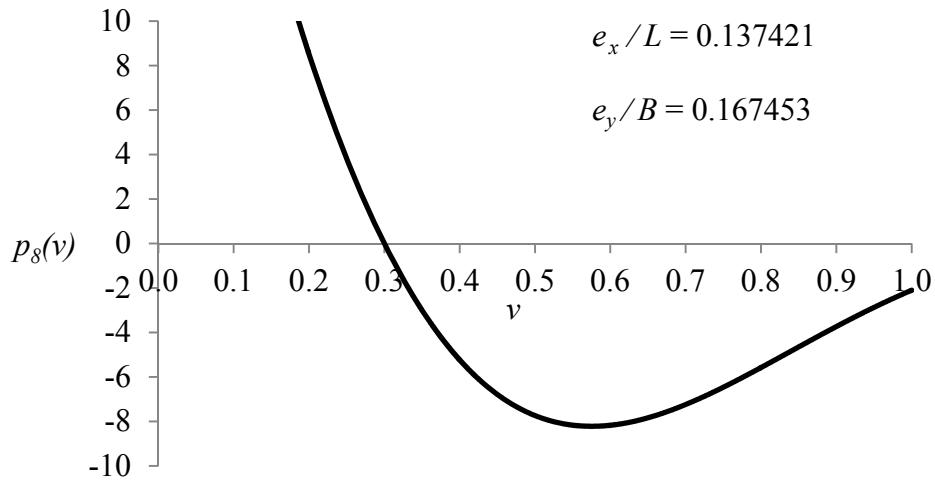
Figure 7. Polynomial $p_8(v)$ with One Root on [0,1].

22

For this combination of e_x/L and e_y/B; the value for A, given by Equation (29), is calculated as 1.2195. The value for C, given by Equation (30) is calculated as 0.82065. Utilizing Equation (32), the value for u is calculated as 1.1. The percentage of detachment along the B-face of the footing β is computed from Equation (33) as 48.4%. Using Equation (34), the percentage of detachment along the L-face of the footing α is 61.6%. Both α and β are between 0% and 100%, which makes physical sense for this application.

If there are two roots on the interval [0, 1], numerical studies have shown that the larger of the two roots produces a value for α or β that is larger than 1, which is meaningless for the application to spread footings. To show this, a combination of e_x/L and e_y/B inside Region A that produces two real roots on the interval [0, 1] will be evaluated. Figure 8 shows a plot of Equation (28) for a combination of e_x/L and e_y/B inside Region A, yielding two real roots. The first root is approximately $v = 0.18$ and the second is approximately $v = 0.72$.

$$e_x/L = 0.193314$$

$$e_y/B = 0.040441$$

$p_8(v)$
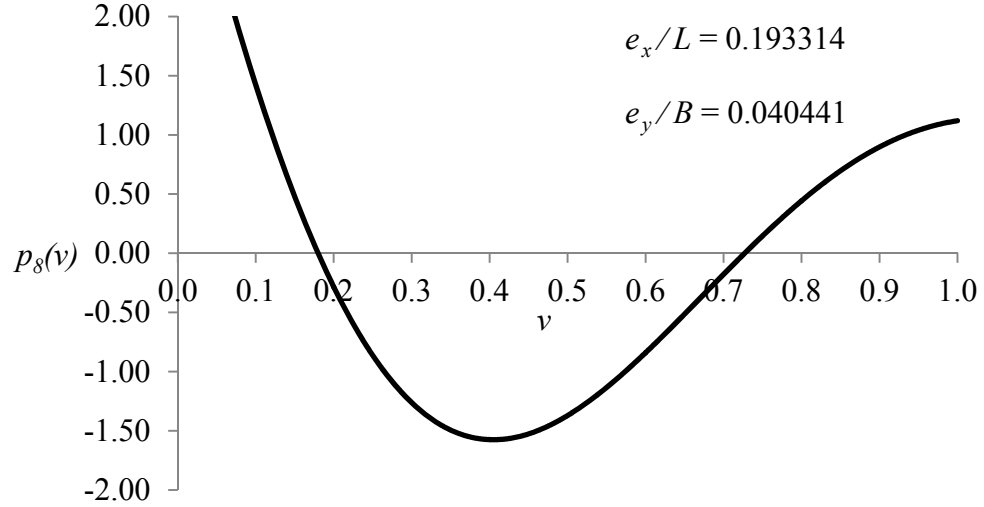
Figure 8. Polynomial $p_8(v)$ with Two Roots on [0,1].

First, the root $v = 0.18$ is considered. For this combination of e_x/L and e_y/B; the value for A, given by Equation (29), is calculated as 0.93502. The value for C, given by Equation (30) is calculated as 4.7801. Utilizing Equation (32), the value for u is calculated as 1.1. The percentage of detachment along the B-face of the footing β is computed from Equation (33) as 88.8%. Using Equation (34), the percentage of detachment along the L-face of the footing α is 21.1%. Both α and β are between 0% and 100%, which makes physical sense for this application.

Next, the root $v = 0.72$ is considered. Since the values of e_x/L and e_y/B have not changed, the value for A remains 0.93502. The value for C is also unchanged and remains 4.7801. Utilizing Equation (32), the value for u is calculated as 5.17. The percentage of detachment along the B-face of the footing β, computed from Equation (33) becomes 425%. There is no need to perform any further calculations as this value does not make physical sense for the spread footing application.

For the unique case when $e_x/L = e_y/B$; it can be shown that $\alpha = \beta$. Irles and Irles (1994) state that when Equations (26) and (27) are set equal, the resulting equation reduces to a fourth order, single variable polynomial. Irles and Irles (1994) do not present the fourth order polynomial but they discuss a general procedure for obtaining a closed form solution to this polynomial. By setting Equations (26) and (27) equal, a fourth order polynomial can be developed in terms of α only as:

$$\alpha^4 - \left(\frac{4e_x}{L} + 2\right)\alpha^3 + \left(\frac{24e_x}{L}\right)\alpha + \left(2 - \frac{24e_x}{L}\right) = 0 \qquad (35)$$

The analytical procedure that is presented by Irles and Irles (1994) is actually an incomplete combination of Ferrari's Method and Cardano's Method for solving third and fourth order polynomial equations. Although it is relatively easy to program the procedure for calculating the analytical solution of Equation (35), the analytical solution is extremely cumbersome to use in its general form for any e_x/L value. Therefore, a numerical root-finding method may be employed to find solutions to Equation (35) by varying the value of e_x/L. Figure 9 shows a plot of α versus e_x/L. The curve represents solutions to Equation (35) using the analytical procedure, while the scatter points represent solutions to Equation (35) obtained from the bisection method.
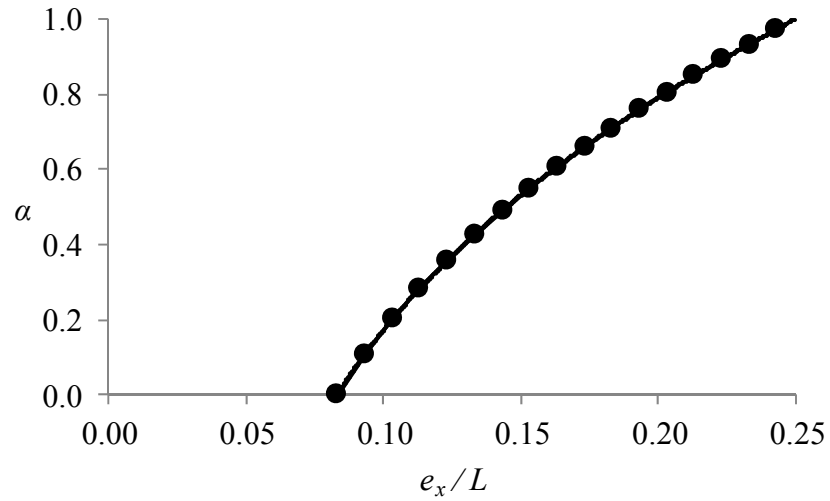
Figure 9. Percentage of Detachment α for Various Ratios e_x/L (Region A, $\alpha = \beta$).

The bisection method was chosen for its simplicity and because it will always locate the root of a function without using the function's derivative. Values obtained using the bisection method are calculated with a tolerance of 10^{-10}.

3.1.2 Uplift – case 2

Figure 10 shows a spread footing in which Corners 1 and 4 have become detached from the soil, where α and γ are the percentages of detachment of the lower L and upper L dimensions, respectively.

Figure 10. Footing with Corners 1 and 4 Detached.

Assuming that the intersection of the bearing pressure surface and the footing is linear, the line of zero bearing pressure can be expressed in two forms:

$$y(x) = \frac{B}{L(\gamma - \alpha)}\left(x + \frac{L}{2} - \gamma L\right) + \frac{B}{2}$$
(36)

$$x(y) = \frac{L(\gamma - \alpha)}{B}\left(y - \frac{B}{2}\right) - \frac{L}{2} + \gamma L$$
(37)

From this linear relationship, three boundary conditions are developed. Two of the boundary conditions are developed from the points of intersection of the line of zero bearing pressure and the sides of the footing:

$$q\left(\frac{-L}{2} + \gamma L, \frac{B}{2}\right) = 0$$
(38)

$$q\left(\frac{-L}{2}+\alpha L, \frac{-B}{2}\right)=0 \tag{39}$$

The third boundary condition is developed from the line of zero bearing pressure as:

$$q\big(x(y), y\big)=0 \tag{40}$$

By applying Equations (38), (39), and (40) to Equation (10), the following three relationships are derived:

$$q_3 = q_4\left(1-\frac{1}{\gamma}\right) \tag{41}$$

$$q_2 = q_1\left(1-\frac{1}{\alpha}\right) \tag{42}$$

$$q_1 = q_4\left(\frac{\alpha}{\gamma}\right) \tag{43}$$

Substituting Equations (41), (42), and (43) into Equation (10), the bearing pressure surface becomes:

$$q(x,y)=\frac{-q_4\left[2Bx+2L(\alpha-\gamma)y+BL(1-\alpha-\gamma)\right]}{2\gamma BL} \tag{44}$$

From force equilibrium, the volume of the compressive bearing pressure distribution beneath the footing is equal to the applied load P. An expression for q_4 in terms of the footing dimensions, α and γ, is derived from the following integration:

$$P = \int_{\frac{-B}{2}}^{\frac{B}{2}} \int_{x(y)}^{\frac{L}{2}} q(x,y)\,dx\,dy \tag{45}$$

Evaluating the integral in Equation (45) and rearranging yields:

$$q_4 = \frac{-6\gamma P}{BL\left(\gamma^2 - 3\alpha - 3\gamma + \alpha^2 + \alpha\gamma + 3\right)} \tag{46}$$

Integral equations are also written for moment equilibrium along the bottom and left edges of the footing. Moment equilibrium along the bottom edge of the footing is satisfied by the following integral:

$$P\left(\frac{B}{2} + e_y\right) = \int_{\frac{-B}{2}}^{\frac{B}{2}} \int_{x(y)}^{\frac{L}{2}} q(x,y)\left(\frac{B}{2} + y\right)dx\,dy \tag{47}$$

Evaluating the integral in Equation (47) and rearranging terms yields:

$$P\left(\frac{B}{2} + e_y\right) = \frac{-B^2 L q_4\left(3\gamma^2 - 4\alpha - 8\gamma + \alpha^2 + 2\alpha\gamma + 6\right)}{24\gamma} \tag{48}$$

Moment equilibrium along the left edge of the footing is satisfied by the following integral:

$$P\left(\frac{L}{2}+e_x\right)=\int\limits_{\frac{-B}{2}}^{\frac{B}{2}}\int\limits_{x(y)}^{\frac{L}{2}} q(x,y)\left(\frac{L}{2}+x\right)dx\,dy \tag{49}$$

Evaluating the integral in Equation (49) and rearranging terms yields:

$$P\left(\frac{L}{2}+e_x\right)=\frac{-BL^2 q_4\left(\alpha^2\gamma-6\alpha-6\gamma+\alpha\gamma^2+\alpha^3+\gamma^3+8\right)}{24\gamma} \tag{50}$$

Substituting Equation (46) into Equations (48) and (50) yields the following two relationships:

$$\frac{e_y}{B}=-\frac{\alpha^2-2\alpha+2\gamma-\gamma^2}{4\left(\gamma^2-3\alpha-3\gamma+\alpha^2+\alpha\gamma+3\right)} \tag{51}$$

$$\frac{e_x}{L}=\frac{\alpha^2\gamma+\alpha\gamma^2-2\gamma^2+\gamma^3-2\alpha^2+\alpha^3-2\alpha\gamma+2}{4\left(\gamma^2-3\alpha-3\gamma+\alpha^2+\alpha\gamma+3\right)} \tag{52}$$

Figure 11 shows Equations (51) and (52) plotted for various values of α and γ. If the load falls within this region, known as Region B; Corners 1 and 4 will become detached from the soil. Entering Figure 11 with e_x/L and e_y/B, α and γ may be obtained graphically.
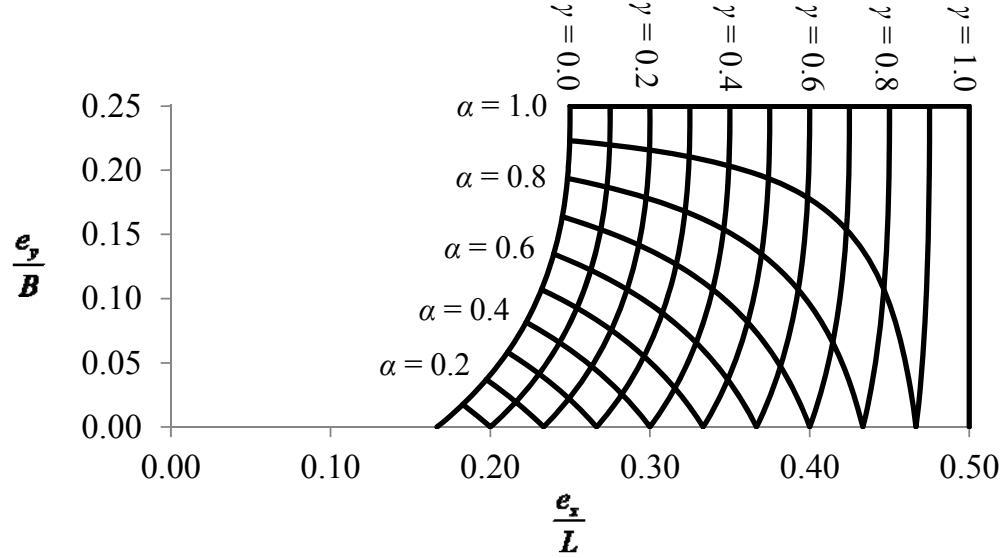
Figure 11. Biaxial Uplift – Region B.

Irles and Irles (1994) provide a procedure to solve for α and γ explicitly, knowing e_x/L and e_y/B. They define the variables μ and δ as:

$$\mu = 2 - 4\frac{e_y}{B} \tag{53}$$

$$\delta = \frac{8 - 3\mu + \sqrt{12\mu - 3\mu^2 - 8}}{12 - 6\mu} \tag{54}$$

Using Equation (54), the percentages of detachment γ and α are:

$$\gamma = 1 - 4\delta\left(\frac{1}{2} - \frac{e_x}{L}\right)\frac{\delta^3 - (\delta - 1)^3}{\delta^4 - (\delta - 1)^4} \tag{55}$$

$$\alpha = 1 - (1-\gamma)\left(1 - \frac{1}{\delta}\right) \tag{56}$$

Although the procedure presented by Irles and Irles (1994) to solve for α and γ is powerful, it is not applicable for the uniaxial case of $e_y / B = 0$, since this produces a zero value in the denominator of Equation (54). However, the graphical solution may be utilized for both the biaxial and uniaxial cases.

3.1.3 Uplift – case 3

Figure 12 shows a spread footing in which Corners 1 and 2 have become detached from the soil, where β and η are the percentages of detachment of the left B and right B dimensions, respectively.
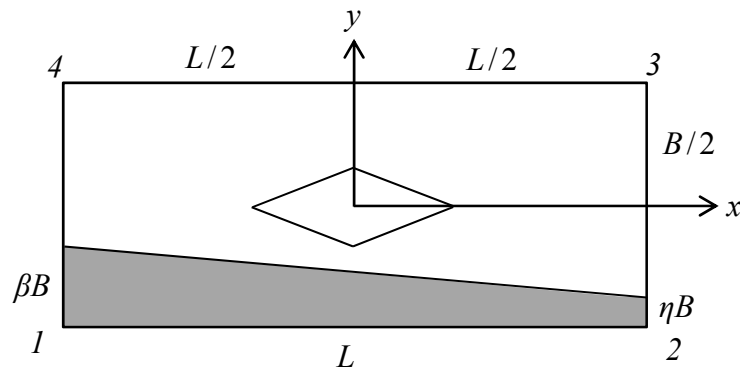
Figure 12. Footing with Corners 1 and 2 Detached.

Assuming that the intersection of the bearing pressure surface and the footing is linear, the line of zero bearing pressure can be expressed in two forms:

$$y(x) = \frac{B(\eta - \beta)}{L}\left(x + \frac{L}{2}\right) - \frac{B}{2} + \beta B \qquad (57)$$

$$x(y) = \frac{L}{B(\eta - \beta)}\left(y + \frac{B}{2} - \beta B\right) - \frac{L}{2} \qquad (58)$$

From this linear relationship, three boundary conditions are developed. Two of the boundary conditions are developed from the points of intersection of the line of zero bearing pressure and the sides of the footing:

$$q\left(\frac{-L}{2}, \frac{-B}{2} + \beta B\right) = 0 \qquad (59)$$

$$q\left(\frac{L}{2}, \frac{-B}{2} + \eta B\right) = 0 \qquad (60)$$

The third boundary condition is developed from the line of zero bearing pressure as:

$$q(x(y), y) = 0 \qquad (61)$$

By applying Equations (59), (60), and (61) to Equation (10), the following three relationships are derived:

$$q_4 = q_1\left(1 - \frac{1}{\beta}\right) \qquad (62)$$

33

$$q_3 = q_2 \left(1 - \frac{1}{\eta} \right) \tag{63}$$

$$q_1 = q_2 \left(\frac{\beta}{\eta} \right) \tag{64}$$

Substituting Equations (62), (63), and (64) into Equation (10), the bearing pressure

surface becomes:

$$q(x,y) = \frac{-q_2 \left[2B(\beta - \eta)x + 2Ly + BL(1 - \beta - \eta) \right]}{2\eta BL} \tag{65}$$

From force equilibrium, the volume of the compressive bearing pressure distribution

beneath the footing is equal to the applied load P. An expression for q_2 in terms of the

footing dimensions, α and γ, is derived from the following integration:

$$P = \int_{\frac{-L}{2}}^{\frac{L}{2}} \int_{y(x)}^{\frac{B}{2}} q(x,y)\, dy\, dx \tag{66}$$

Evaluating the integral in Equation (66) and rearranging terms yields:

$$q_2 = \frac{-6\eta P}{BL\left(\eta^2 - 3\beta - 3\eta + \beta^2 + \beta\eta + 3 \right)} \tag{67}$$

Integral equations are also written for moment equilibrium along the bottom and left edges of the footing. Moment equilibrium along the bottom edge of the footing is satisfied by the following integral:

$$P\left(\frac{B}{2}+e_y\right)=\int\limits_{\frac{-L}{2}}^{\frac{L}{2}}\int\limits_{y(x)}^{\frac{B}{2}}q(x,y)\left(\frac{B}{2}+y\right)dy\,dx \tag{68}$$

Evaluating the integral in Equation (68) and rearranging terms yields:

$$P\left(\frac{B}{2}+e_y\right)=\frac{-B^2Lq_2\left(\beta^2\eta-6\beta-6\eta+\beta\eta^2+\beta^3+\eta^3+8\right)}{24\eta} \tag{69}$$

Moment equilibrium along the left edge of the footing is satisfied by the following integral:

$$P\left(\frac{L}{2}+e_x\right)=\int\limits_{\frac{-L}{2}}^{\frac{L}{2}}\int\limits_{y(x)}^{\frac{B}{2}}q(x,y)\left(\frac{L}{2}+x\right)dy\,dx \tag{70}$$

Evaluating the integral in Equation (70) and rearranging terms yields:

$$P\left(\frac{L}{2}+e_x\right)=\frac{-BL^2q_2\left(3\eta^2-4\beta-8\eta+\beta^2+2\beta\eta+6\right)}{24\eta} \tag{71}$$

Substituting Equation (67) into Equations (69) and (71) yields the following two relationships:

$$\frac{e_y}{B} = \frac{\beta^2\eta + \beta\eta^2 - 2\eta^2 + \eta^3 - 2\beta^2 + \beta^3 - 2\beta\eta + 2}{4(\eta^2 - 3\beta - 3\eta + \beta^2 + \beta\eta + 3)} \tag{72}$$

$$\frac{e_x}{L} = -\frac{\beta^2 - 2\beta + 2\eta - \eta^2}{4(\eta^2 - 3\beta - 3\eta + \beta^2 + \beta\eta + 3)} \tag{73}$$

Figure 13 shows Equations (72) and (73) plotted for various values of β and η. If the load falls within this region, known as Region C, Corners 1 and 2 will become detached from the soil. Entering Figure 11 with e_x/L and e_y/B, β and η may be obtained graphically.
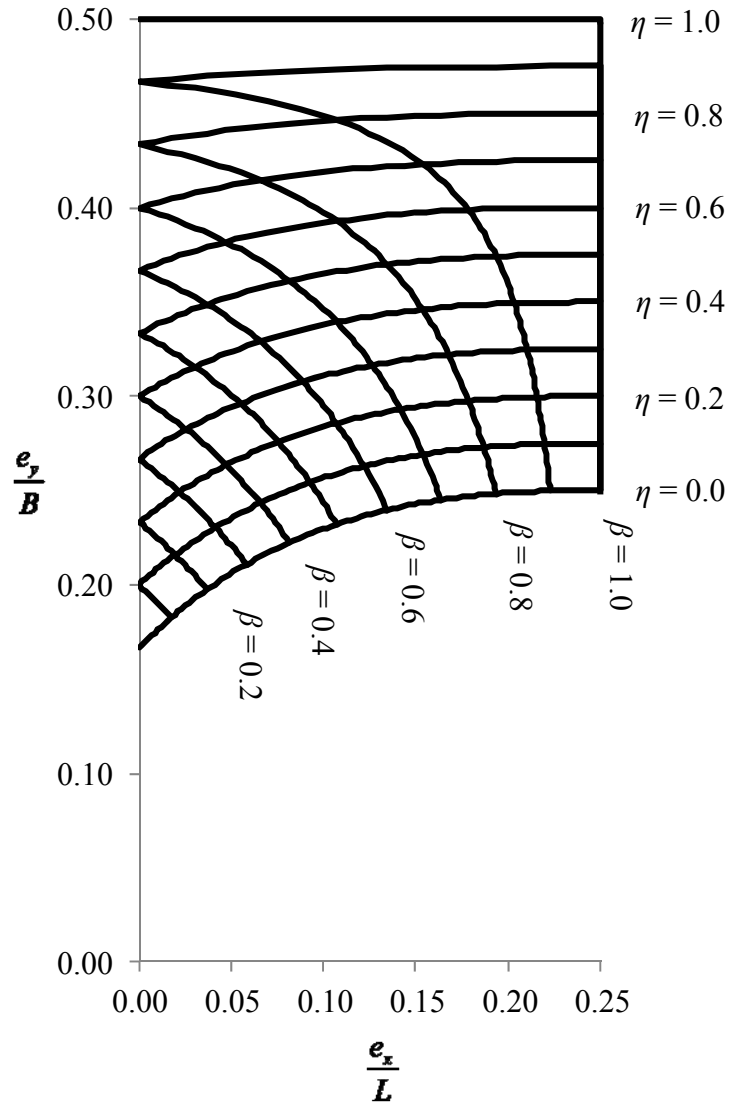
Figure 13. Biaxial Uplift – Region C.

Irles and Irles (1994) provide a procedure to solve for β and η explicitly, knowing e_x/L and e_y/B. They define the variables μ and δ as:

$$\mu = 2 - 4\frac{e_x}{L} \tag{74}$$

$$\delta = \frac{8 - 3\mu + \sqrt{12\mu - 3\mu^2 - 8}}{12 - 6\mu} \tag{75}$$

Using Equation (75), the percentages of detachment γ and β are:

$$\eta = 1 - \frac{4\delta}{B}\left(\frac{B}{2} - e_y\right)\frac{\delta^3 - (\delta - 1)^3}{\delta^4 - (\delta - 1)^4} \tag{76}$$

$$\beta = (B - \eta B)\left(1 - \frac{1}{\delta}\right) \tag{77}$$

Although the procedure presented by Irles and Irles (1994) to solve for β and η is powerful, it is not applicable for the uniaxial case of $e_x/L = 0$, since this produces a zero value in the denominator of Equation (75). However, the graphical solution may be utilized for both the biaxial and uniaxial cases.

3.1.4 Uplift – case 4

Figure 14 shows a spread footing in which Corners 1, 2, and 4 are detached from the soil, where γ and η are the percentages of detachment of the L and B dimensions, respectively.
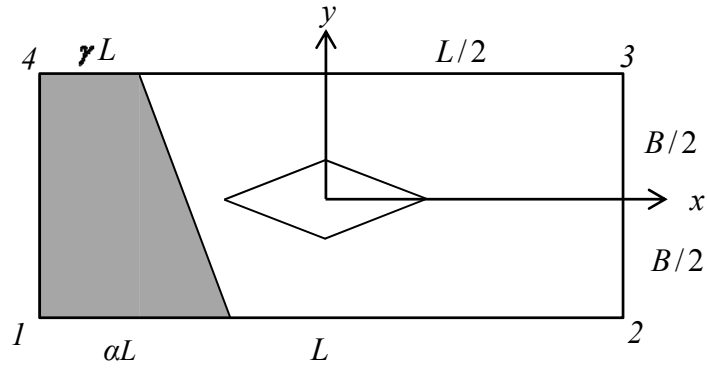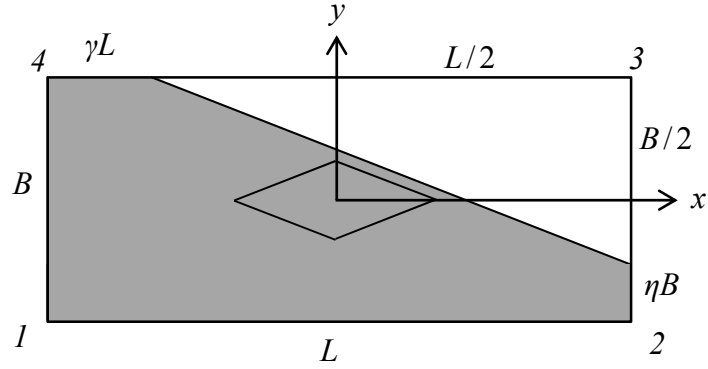
Figure 14. Footing with Corners 1, 2, and 4 Detached.

Assuming that the projection of zero bearing is linear, the line of zero bearing pressure can be expressed in two forms:

$$y(x) = -\frac{B-\eta B}{L-\gamma L}\left(x-\left(\frac{-L}{2}+\gamma L\right)\right)+\frac{B}{2} \tag{78}$$

$$x(y) = -\frac{L-\gamma L}{B-\eta B}\left(y-\frac{B}{2}\right)-\frac{L}{2}+\alpha L \tag{79}$$

Three boundary conditions are developed. Two of the boundary conditions define the points of intersection of the line of zero bearing pressure along the sides of the footing as:

$$q\left(\frac{-L}{2}-\gamma L,\frac{B}{2}\right)=0 \tag{80}$$

$$q\left(\frac{L}{2},\frac{-B}{2}+\eta B\right)=0 \tag{81}$$

The third boundary condition is developed from the line of zero bearing pressure as:

$$q(x, y(x)) = 0 \qquad (82)$$

By applying Equations (80), (81), and (82) to Equation (10), the following three relationships are derived:

$$q_4 = q_3 \left(\frac{\gamma}{\gamma - 1} \right) \qquad (83)$$

$$q_2 = q_3 \left(\frac{\eta}{\eta - 1} \right) \qquad (84)$$

$$q_1 = q_3 \left(\frac{\gamma\eta - 1}{1 + \gamma\eta - \gamma - \eta} \right) \qquad (85)$$

Substituting Equations (83), (84), and (85) into Equation (10), the bearing pressure surface becomes:

$$q(x, y) = \left(\frac{q_3}{L(1-\gamma)} \right) x + \left(\frac{q_3}{B(1-\eta)} \right) y + q_3 \left(\frac{2\gamma\eta - \gamma - \eta}{2(\gamma-1)(\eta-1)} \right) \qquad (86)$$

From force equilibrium, the volume of the compressive bearing pressure distribution

beneath the footing is equal to the applied load P. An expression for q_3 in terms of the

footing dimensions, α and β, is derived from the following integration:

$$P = \int_{\frac{-L}{2}+\gamma L}^{\frac{L}{2}} \int_{y(x)}^{\frac{B}{2}} q(x,y)\,dy\,dx \tag{87}$$

Evaluating the integral in Equation (87) and rearranging terms yields:

$$q_3 = \frac{6P}{(1-\gamma)L(1-\eta)B} \tag{88}$$

Integral equations are also written for moment equilibrium along the upper and right

edges of the footing. Moment equilibrium along the upper edge of the footing is satisfied

by the following integral:

$$P\left(\frac{B}{2}-e_y\right) = \int_{\frac{-L}{2}+\gamma L}^{\frac{L}{2}} \int_{y(x)}^{\frac{B}{2}} q(x,y)\left(\frac{B}{2}-y\right) dy\,dx \tag{89}$$

Evaluating the integral in Equation (89) and rearranging terms yields:

$$P\left(\frac{B}{2}-e_y\right) = \frac{(1-\gamma)L\left((1-\eta)B\right)^2 q_3}{24} \tag{90}$$

Moment equilibrium along the right edge of the footing is satisfied by the following integral:

$$P\left(\frac{L}{2}-e_x\right)=\int_{\frac{-L}{2}+\gamma L}^{\frac{L}{2}}\int_{y(x)}^{\frac{B}{2}}q(x,y)\left(\frac{L}{2}-x\right)dy\,dx \tag{91}$$

Evaluating the integral in Equation (91) and rearranging terms yields:

$$P\left(\frac{L}{2}-e_x\right)=\frac{\left((1-\gamma)L\right)^2(1-\eta)Bq_3}{24} \tag{92}$$

Substituting Equation (88) into Equations (90) and (92) yields the following two relationships:

$$\frac{e_y}{B}=\frac{1+\eta}{4} \tag{93}$$

$$\frac{e_x}{L}=\frac{1+\gamma}{4} \tag{94}$$

Figure 15 shows Equations (93) and (94) plotted for various values of γ and η. If the load falls within this region, known as Region D, Corners 1, 2, and 4 will become detached from the soil.
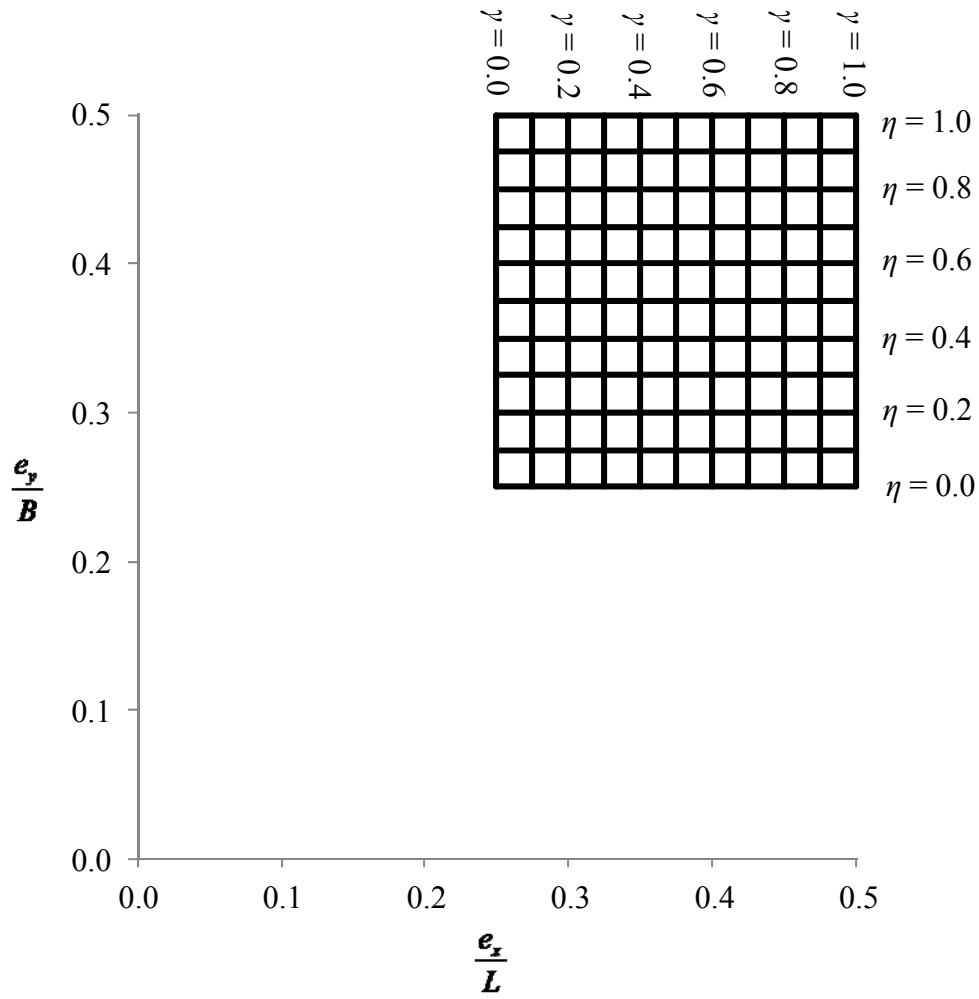
Figure 15. Biaxial Uplift – Region D.

Figure 16 shows Equations (26), (27), (51), (52), (72), (73), (93), and (94) plotted for various values of α, β, γ, and η. Teng (1962) produced a similar analysis chart with accompanying equations; however, there was little explanation of its usage and capabilities. In addition, Teng (1962) provides no explanation of how the chart was developed.
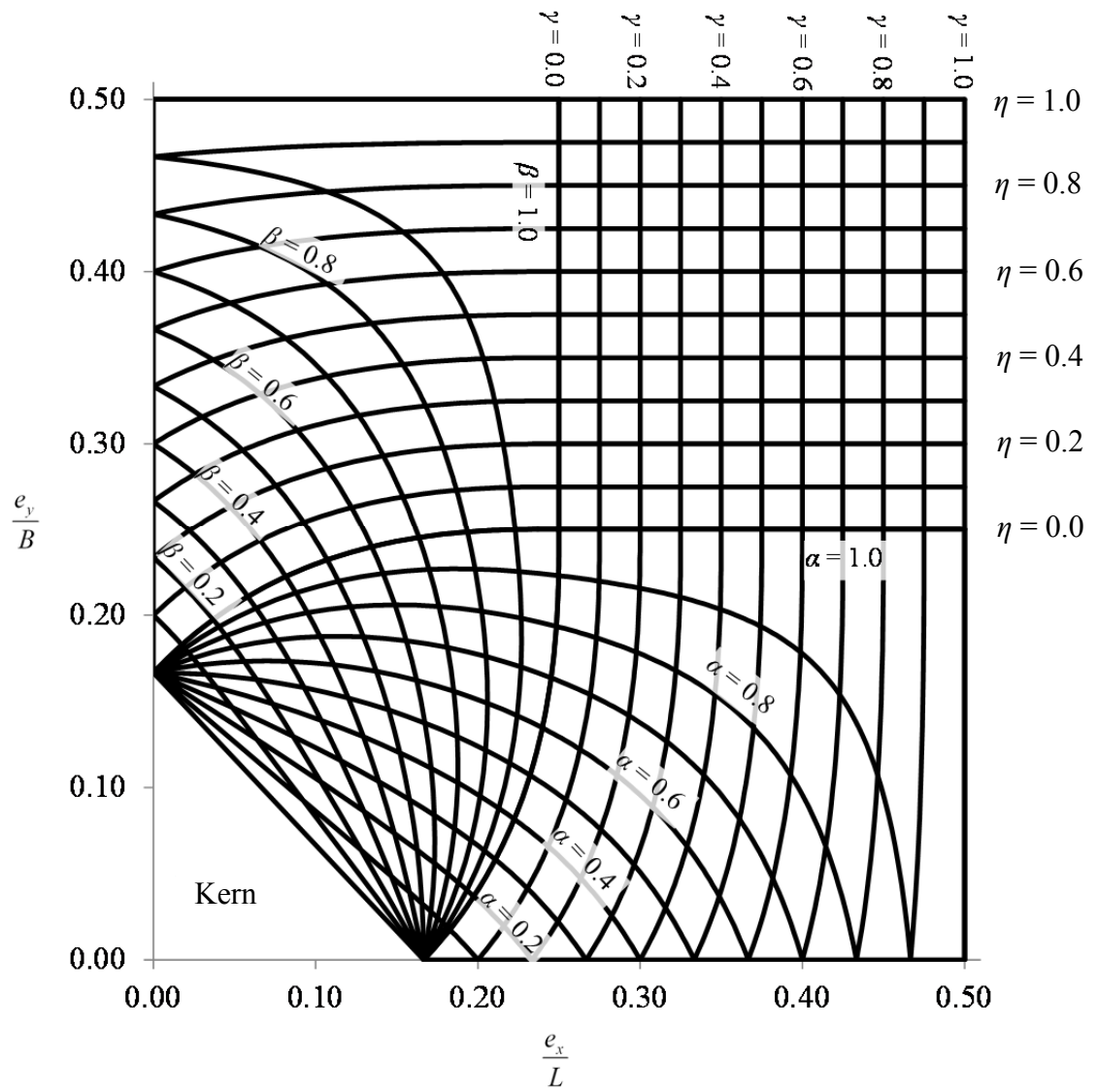
Figure 16. Analysis Chart for Biaxial Uplift.

When eccentricities are such that the values of e_x/L and e_y/B are within the kern area, no detachment of the footing from the soil will occur and Equation (1) is used to calculate the four corner stresses. When eccentricities are such that the values of e_x/L and e_y/B are within Region A, Corner 1 of the footing is detached from the soil.

Entering Figure 16 with e_x/L and e_y/B, the percentages of detachment, α and β, along the perpendicular dimensions of the footing are obtained. Equations (16), (17), and (18) are used to calculate the bearing pressure values beneath the three corners of the footing which are in compression. If e_x/L and e_y/B are within Region B, Corners 1 and 4 of the footing are detached from the soil. The percentages of detachment, α and γ, along the L-dimension are obtained. Equations (41) and (42) are used to calculate the compressive bearing pressures beneath Corners 2 and 3. If e_x/L and e_y/B are within Region C, Corners 1 and 2 of the footing are detached from the soil. The percentages of detachment, β and η, along the B-dimension are obtained. Equations (62) and (63) are used to calculate the compressive bearing pressures beneath Corners 3 and 4. If eccentricities are so large that e_x/L and e_y/B are within Region D, then Corners 1, 2, and 4 of the footing are detached from the soil. The percentages of detachment, γ and η, along the upper L-dimension and right B-dimension are obtained. Equation (88) is used to calculate the compressive bearing pressure beneath Corner 3.

3.2 Uniaxial Loading

Uniaxial loading occurs if a force acts through a point displaced from the center of the footing along only one of the principal directions or there is an applied moment about a principal axis. In this case, one of the eccentricity terms in Equation (2) will drop out, leaving

$$q_{min,max} = \frac{P}{BL}\left(1 \pm \frac{6e}{w}\right) \tag{95}$$

where w is either the B or L dimension, depending upon the axis on which the load is applied. Due to symmetry, only loading along the positive x and y-axes is considered. The kern boundary is defined as:

$$\frac{e}{w} = \frac{1}{6} \tag{96}$$

When the left side of Equation (96) exceeds 1/6, a portion of the footing will become detached from the soil (assuming that the soil cannot support tension) and Equation (95) is no longer applicable for determining the bearing pressure beneath the footing. Depending on the axis on which load is applied, either Corners 1 and 4 will become detached, or Corners 1 and 2 will become detached. For either of these cases, the area of detachment will be rectangular.

3.2.1 Corners 1 and 4 detached

If loading is on the positive x-axis, outside of the kern, then Corners 1 and 4 will become detached from the soil. Figure 17 shows a spread footing in which Corners 1 and

4 are detached from the soil, where α is the percentage of detachment along the L dimensions.
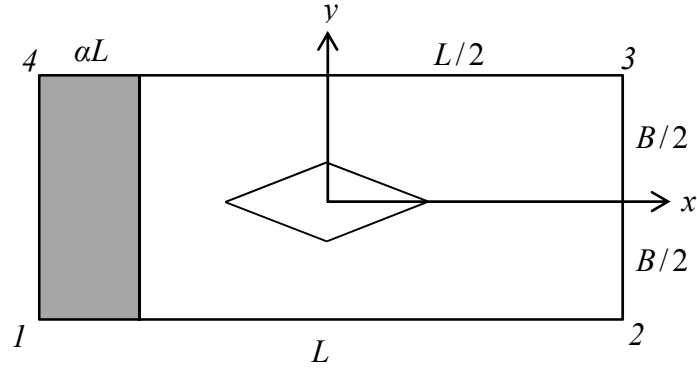
Figure 17. Footing with Corners 1 and 4 Detached.

For this scenario, Equation (41) simplifies and q_3 and q_2 are equal to the maximum compressive bearing pressure q_{max}, given by:

$$q_{max} = q_{min}\left(1 - \frac{1}{\alpha}\right) \tag{97}$$

Equation (46) also simplifies and q_1 and q_4 are equal to the minimum bearing pressure q_{min}, given by:

$$q_{min} = \frac{-2\alpha P}{BL\left(\alpha^2 - 2\alpha + 1\right)} \tag{98}$$

Equation (52) simplifies, giving the eccentricity ratio expressed in terms of α as:

$$\frac{e_x}{L} = \frac{2\alpha + 1}{6} \tag{99}$$

Solving for α in Equation (99) and substituting the resulting expression into Equations (97) and (98) yields the relationship given in Das (2008):

$$q_{max} = \frac{4P}{3B(L - 2e_x)} \tag{100}$$

3.2.2 Corners 1 and 2 detached

If loading is along the positive y-axis, outside of the kern, then Corners 1 and 2 will become detached from the soil. Figure 18 shows a spread footing in which Corners 1 and 2 are detached from the soil, where β is the percentage of detachment along the B dimensions.
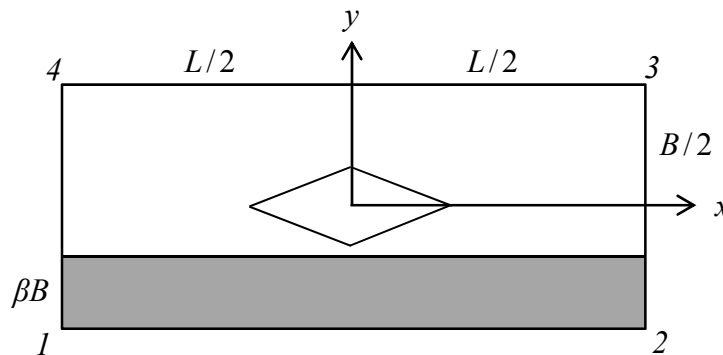
Figure 18. Footing with Corners 1 and 2 Detached.

For this scenario, Equation (62) simplifies and q_3 and q_4 are equal to the maximum compressive bearing pressure q_{max}, given by:

$$q_{max} = q_{min}\left(1 - \frac{1}{\beta}\right) \tag{101}$$

Equation (67) also simplifies and q_1 and q_2 are equal to the minimum bearing pressure q_{min}, given by:

$$q_{min} = \frac{-2\beta P}{BL\left(\beta^2 - 2\beta + 1\right)} \tag{102}$$

Equation (72) simplifies, giving the eccentricity ratio expressed in terms of β as:

$$\frac{e_y}{B} = \frac{2\beta + 1}{6} \tag{103}$$

Solving for β in Equation (103) and substituting the resulting expression into Equations (101) and (102) yields the relationship given in Das (2008):

$$q_{max} = \frac{4P}{3L\left(B - 2e_y\right)} \tag{104}$$

3.3 Concentric Loading

Concentric loading occurs if a force acts through the center of the footing. In this case, there are no eccentricities or applied moments. Equation (2) yields a constant bearing pressure q beneath the entire footing, becoming

$$q = \frac{P}{BL} \tag{105}$$

Under concentric loading, no detachment of the footing from the soil occurs.

3.4 Summary

Governing equations were developed to model the bearing pressure surface beneath a rigid spread footing subjected to biaxial uplift using a rectangular element with associated interpolation functions. The underlying soil was assumed to be linear-elastic, homogeneous, uniform, isotropic, and cohesionless. Depending on the magnitudes of the eccentricities and footing dimensions, the eccentricity ratios, e_x/L and e_y/B, will either fall within the kern area of the footing, or within one of four Regions: A, B, C, or D. An analysis chart, along with accompanying equations, was developed to determine the percentages of detachment from the soil along the footing dimensions, as well as the bearing pressure beneath the corners of the footing experiencing compression. During uniaxial loading, the governing equations simplify and are more easily used. The analysis chart is still applicable for determining the percentages of detachment and compressive bearing pressures at the footing corners during uniaxial uplift.

CHAPTER 4

STRUCTURAL MECHANICS

A reliable reinforced spread footing must provide adequate resistance against two-way (punching) shear failure, one-way shear failure, and flexural failure in both directions. Formulations for the analysis of two-way shear, one-way shear, and bending of rectangular spread footings are based on the magnitudes of the applied load and its eccentricities. Depending on whether the eccentricities of the applied load are within the kern area or in Region A, B, C, or D, different boundary conditions are applied to the governing equations to account for the orientation of the line of zero bearing pressure with respect to critical sections for two-way shear, one-way shear, and bending.

For structural analysis and design, factored loads are used in all formulations, as opposed to service loads. The factored column load P_u is calculated as

$$P_u = \phi\left(P + W_f\right) \tag{106}$$

where P is the applied service load and W_f is the weight of the footing. The applied load is taken as a dead load for all design examples, so $\phi = 1.4$ (ASCE 2010).

Two-way (punching) shear occurs in a footing when the column tends to punch through the footing due to the shear stresses that act in the footing around the perimeter of the column. It is generally calculated as the upward bearing pressure within the critical two-way shear perimeter subtracted from the factored column load. The critical two-way shear perimeter b_p is given as:

$$b_p = 4(b_{col} + d_a)$$

<div align="right">(107)</div>

where d_a is the average depth from the extreme compression fiber of the footing to the centroid of the reinforcement and b_{col} is the dimension of the column (which is assumed to be square). Figure 19 shows a spread footing with the two-way shear perimeter.
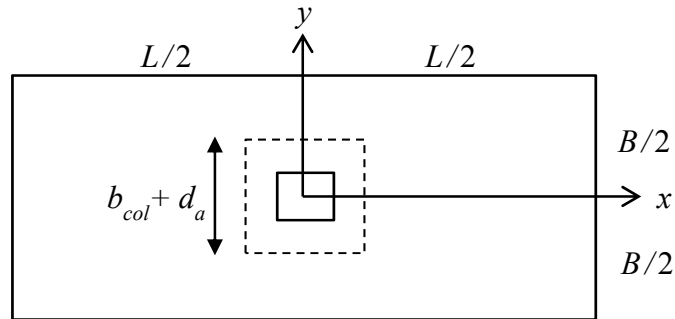
Figure 19. General Critical Section for Two-Way Shear.

The origin is taken as the center of the footing and only loading with positive eccentricities is considered, due to symmetry.

One-way shear may occur, as in beams and slabs, in either dimension of the footing. It is calculated as the upward bearing pressure acting on the footing from the critical one-way shear plane to the edge of the footing. The critical plane in which one-way shear occurs is at a distance d_a away from the face of the column. The origin is taken as the center of the footing and only loading with positive eccentricities is considered. Figure 20

shows the critical section for one-way shear parallel to the *B*-dimension in a spread footing.
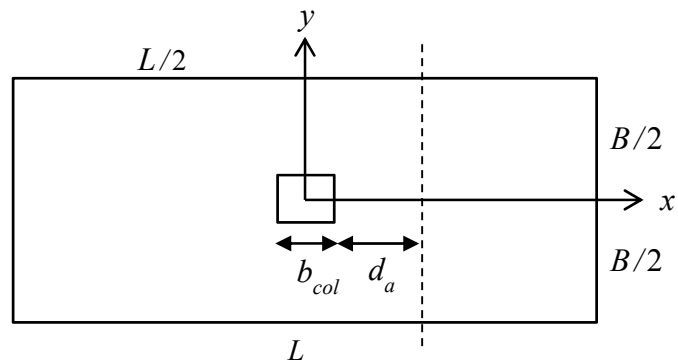
Figure 20. General Critical Section for One-Way Shear Parallel to the *B*-Dimension.

Figure 21 shows the critical section for one-way shear parallel to the *L*-dimension in a spread footing.
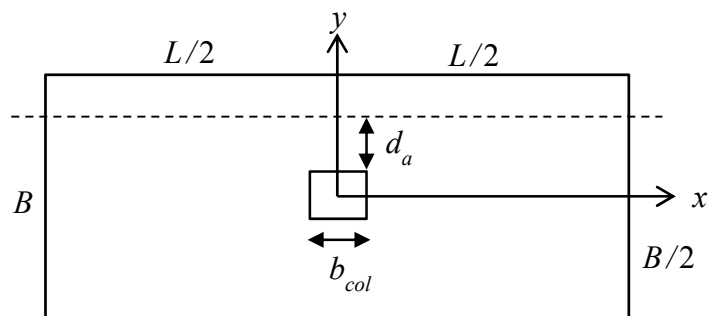
Figure 21. General Critical Section for One-Way Shear Parallel to the *L*-Dimension.

For bending, the critical moment is located at the face of the column and is calculated based on the upward bearing pressure acting on the footing from the face of the column to the edge of the footing. The origin is taken as the center of the footing and only loading with positive eccentricities is considered. Figure 22 shows the critical section for bending parallel to the *B*-dimension in a spread footing.
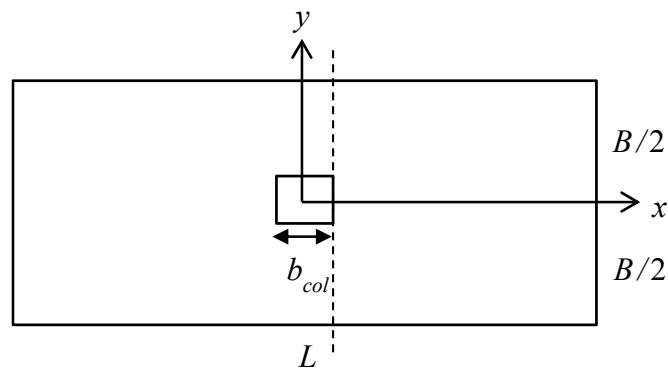
Figure 22. General Critical Section for Bending Parallel to the *B*-Dimension.

Figure 23 shows the critical section for bending parallel to the *L*-dimension in a spread footing.
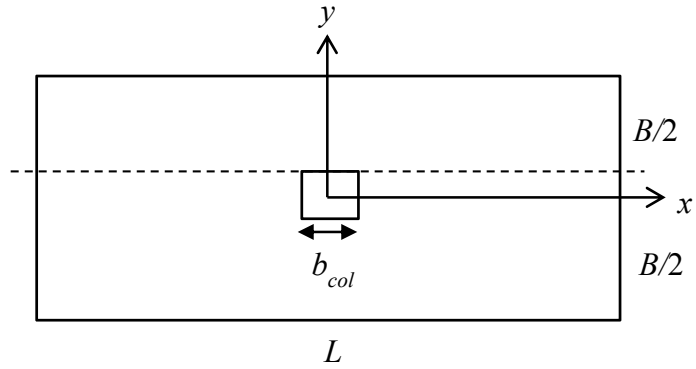
Figure 23. General Critical Section for Bending Parallel to the *L*-Dimension.

Expressions are derived to calculate two-way shear, one-way shear, and the critical moment for eccentricities within the kern area and Regions A, B, C, and D.

4.1 Biaxial Loading

For loading within the kern area, the bearing pressure surface $q(x,y)$ is given by Equation (10). The two-way shear force is

$$V_{punch} = P_u - \int_{L_{\text{limit}}}^{U_{\text{limit}}} \int_{L_{\text{limit}}}^{U_{\text{limit}}} q(x,y)\,dy\,dx \tag{108}$$

where the lower and upper limits for integration are based upon the critical two-way shear perimeter and are given, respectively as:

$$L_{\text{limit}} = -\left(\frac{b_{col} + d_a}{2}\right) \tag{109}$$

$$U_{\text{limit}} = \frac{b_{col} + d_a}{2} \tag{110}$$

Evaluating Equation (108) gives the two-way shear force as:

$$V_{punch} = P_u - \frac{\left(b_{col} + d_a\right)^2 \left(q_1 + q_2 + q_3 + q_4\right)}{4} \tag{111}$$

The one-way shear force on the critical section parallel to the L dimension of the footing is:

$$V_{one-way} = \int_{\frac{-L}{2}}^{\frac{L}{2}} \int_{\frac{b_{col}}{2}+d_a}^{\frac{B}{2}} q(x, y) \, dy \, dx \tag{112}$$

The evaluation of Equation (112) is listed in the Appendix as Equation (A1).

The one-way shear force on the critical section parallel to the B dimension of the footing is:

$$V_{one-way} = \int_{\frac{b_{col}}{2}+d_a}^{\frac{L}{2}} \int_{\frac{-B}{2}}^{\frac{B}{2}} q(x, y) \, dy \, dx \tag{113}$$

The evaluation of Equation (113) is listed in the Appendix as Equation (A2).

57

The bending moment on the critical section parallel to the *L* dimension of the footing is computed as:

$$M_L = \int_{\frac{-L}{2}}^{\frac{L}{2}} \int_{\frac{b_{col}}{2}}^{\frac{B}{2}} q(x,y)\left(y - \frac{b_{col}}{2}\right) dy\, dx \tag{114}$$

Evaluating Equation (114) gives the critical bending moment as:

$$M_L = \frac{L(B - b_{col})^2 (Bq_1 + Bq_2 + 5Bq_3 + 5Bq_4 - b_{col}q_1 - b_{col}q_2 + b_{col}q_3 + b_{col}q_4)}{96B} \tag{115}$$

The bending moment on the critical section parallel to the *B* dimension of the footing is computed as:

$$M_B = \int_{\frac{-B}{2}}^{\frac{B}{2}} \int_{\frac{b_{col}}{2}}^{\frac{L}{2}} q(x,y)\left(x - \frac{b_{col}}{2}\right) dx\, dy \tag{116}$$

Evaluating Equation (116) gives the critical bending moment as:

$$M_B = \frac{B(L - b_{col})^2 (Lq_1 + 5Lq_2 + 5Lq_3 + Lq_4 - b_{col}q_1 + b_{col}q_2 + b_{col}q_3 - b_{col}q_4)}{96L} \tag{117}$$

4.1.1 Uplift – region A

If the equivalent eccentricities are large enough to cause Corner 1 to become detached from the soil, shown in Figure 5, the eccentricities will be located in Region A and the

bearing pressure surface $q(x,y)$ is given by Equation (19), using factored loads. The line of zero bearing pressure can be expressed in two forms:

$$y(x) = \frac{-\beta B}{\alpha L}\left(x + \frac{L}{2} - \alpha L\right) - \frac{B}{2} \tag{118}$$

$$x(y) = \frac{-\alpha L}{\beta B}\left(y + \frac{B}{2}\right) - \frac{L}{2} + \alpha L \tag{119}$$

4.1.1.1 Region A: two-way shear. Figure 19 shows a spread footing with the two-way shear perimeter. There are four cases for which the two-way shear is calculated. Each case is represented by the amount of compressive bearing pressure within the two-way shear perimeter. Lower and Upper limits for integration are based upon the critical two-way shear perimeter and are given by Equations (109) and (110).

4.1.1.1.1 Case one. When the line of zero bearing pressure does not intersect the critical two-way shear perimeter, the two-way shear force V_{punch} is:

$$V_{punch} = P_u - \int_{L_{limit}}^{U_{limit}} \int_{L_{limit}}^{U_{limit}} q(x,y)\,dy\,dx \tag{120}$$

Evaluating the integral expression in Equation (120) gives:

$$V_{punch} = P_u - \frac{q_1\left(b_{col} + d_a\right)^2\left(\alpha + \beta - 2\alpha\beta\right)}{2\alpha\beta} \tag{121}$$

4.1.1.1.2 Case two. Figure 24 shows the critical two-way shear when a triangular

portion of the area becomes detached from the soil. The shaded area is the portion of the

two-way shear area that has become detached from the soil.
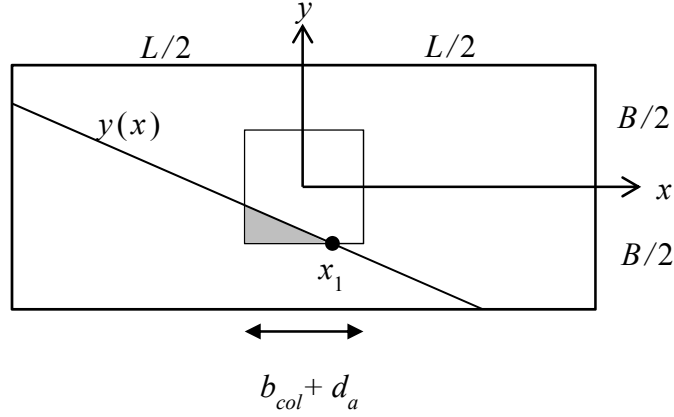
Figure 24. Critical Two-Way Shear Area for Region A, Case Two.

The point where the line of zero bearing pressure intersects the bottom of the two-way

shear perimeter x_1 is:

$$x_1 = \frac{\alpha L}{\beta B}\left(\frac{b_{col}+d_a}{2} - \frac{B}{2}\right) - \frac{L}{2} + \alpha L \tag{122}$$

The two-way shear force is computed as:

$$V_{punch} = P_u - \left(\int\limits_{L_{limit}}^{U_{limit}} \int\limits_{L_{limit}}^{U_{limit}} q(x,y)\,dy\,dx - \int\limits_{L_{limit}}^{x_1} \int\limits_{L_{limit}}^{y(x)} q(x,y)\,dy\,dx\right) \tag{123}$$

60

The evaluation of the integral in Equation (123) is listed in the Appendix as Equation (A3).

4.1.1.1.3 Case three. As the eccentricities become larger, more of the critical two-way shear area becomes detached from the soil beneath it. Figure 25 shows the critical two-way shear area where the trapezoidal shaded area is the portion of the two-way shear area that has become detached from the soil.
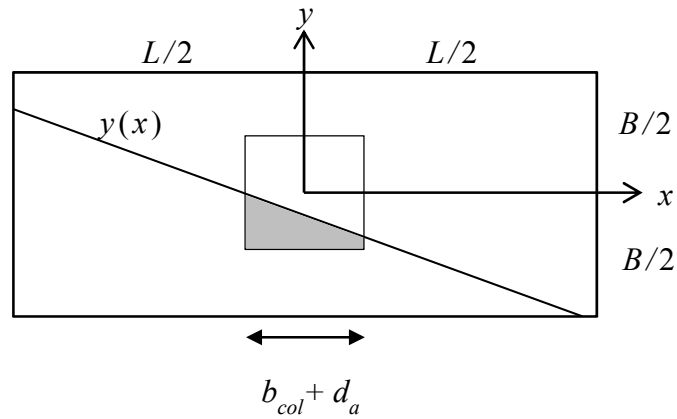
Figure 25. Critical Two-Way Shear Area for Region A, Case Three.

The two-way shear force is computed as:

$$V_{punch} = P_u - \int_{L_{limit}}^{U_{limit}} \int_{y(x)}^{U_{limit}} q(x,y)\, dy\, dx \tag{124}$$

Evaluating the integral in Equation (124) gives an expression for the two-way shear force listed in the Appendix as Equation (A4).

4.1.1.1.4 Case four. If the footing is such that the vertical dimension is significantly larger than the horizontal dimension, the line of zero bearing pressure may intersect the two-way shear area along both the top and bottom edges. Figure 26 shows the critical two-way shear area when the line of zero bearing pressure intersects the two-way shear area along both the top and bottom edges.
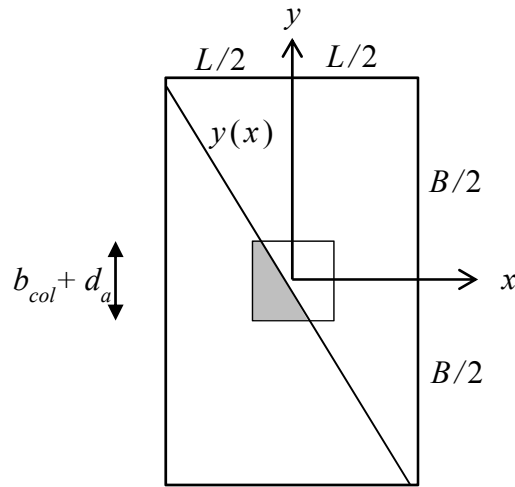
Figure 26. Critical Two-Way Shear Area for Region A, Case Four.

The two-way shear force is computed as:

$$V_{punch} = P_u - \int_{L_{limit}}^{U_{limit}} \int_{x(y)}^{U_{limit}} q(x,y)\, dx\, dy \tag{125}$$

Evaluating the integral in Equation (125) gives an expression for the two-way shear force listed in the Appendix as Equation (A5).

4.1.1.2 Region A: one-way shear. One-way shear may occur along either face of the spread footing. For each face of the footing, two cases should be considered: one, when the line of zero bearing pressure intersects the critical shear plane and two, when it does not.

4.1.1.2.1 B -Face: case one. Figure 27 shows a spread footing when the line of zero bearing pressure does not intersect the critical one-way shear plane.
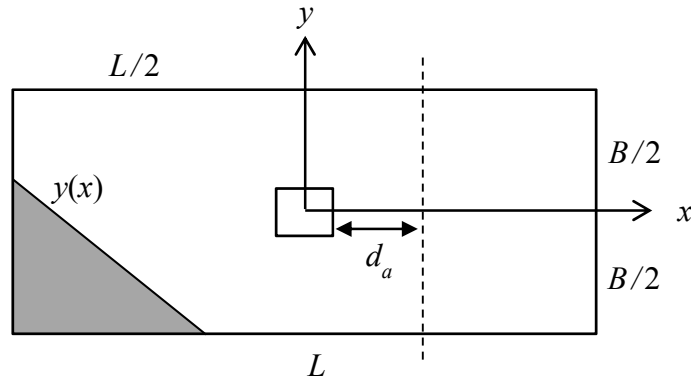
Figure 27. Critical One-Way Shear Section for Region A, *B*-Face: Case One.

In this case, the one-way shear force is computed as:

$$V_{one-way} = \int_{\frac{b_{col}}{2}+d_a}^{\frac{L}{2}} \int_{\frac{-B}{2}}^{\frac{B}{2}} q(x,y)\,dy\,dx \qquad (126)$$

Evaluating the integral in Equation (126) gives:

$$V_{one-way} = \frac{q_1 B (b_{col} - L + 2d_a)(3\beta L + 2\alpha L + \beta b_{col} + 2\beta d_a - 4\alpha\beta L)}{8\alpha\beta L} \qquad (127)$$

4.1.1.2.2 B-Face: case two. Figure 28 shows a spread footing when the line of zero bearing pressure intersects the critical one-way shear plane.
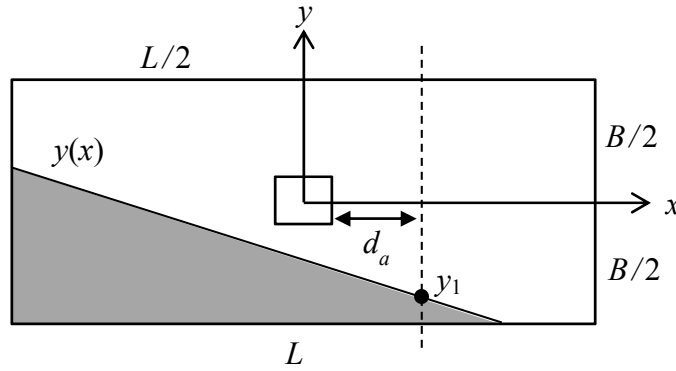
Figure 28. Critical One-Way Shear Section for Region A, *B*-Face: Case Two.

The point where the line of zero bearing pressure intersects the one-way shear section y_1 is

$$y_1 = \frac{-\beta B}{\alpha L}\left(\frac{b_{col}}{2} + d_a + \frac{L}{2} - \alpha L\right) - \frac{B}{2} \qquad (128)$$

In this case, the one-way shear force is computed as:

$$V_{one-way} = \int\limits_{\frac{b_{col}}{2}+d_a}^{\frac{L}{2}} \int\limits_{\frac{-B}{2}}^{\frac{B}{2}} q(x,y)\,dy\,dx - \int\limits_{-B/2}^{y_1} \int\limits_{\frac{b_{col}}{2}+d_a}^{x(y)} q(x,y)\,dx\,dy \tag{129}$$

Evaluating the integral in Equation (129) gives an expression for the one-way shear force and is listed in the Appendix as Equation (A6).

4.1.1.2.3 L-Face: case one. Figure 29 shows the critical section for one-way shear when the line of zero bearing pressure does not intersect the critical section.
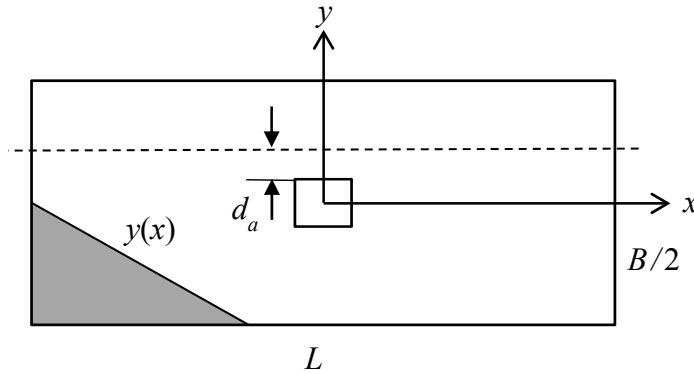
Figure 29. Critical One-Way Shear Section for Region A, *L*-Face: Case One.

In this case, the one-way shear force is computed as:

$$V_{one-way} = \int\limits_{\frac{-L}{2}}^{\frac{L}{2}} \int\limits_{\frac{b_{col}}{2}+d_a}^{\frac{B}{2}} q(x,y)\,dy\,dx \tag{130}$$

Evaluating the integral in Equation (130) gives:

$$V_{one-way} = \frac{q_1 L \left(b_{col} - B + 2d_a \right) \left(2\beta B + 3\alpha B + \alpha b_{col} + 2\alpha d_a - 4\alpha\beta B \right)}{8\alpha\beta B} \tag{131}$$

4.1.1.2.4 L-Face: case two. Figure 30 shows the critical section for one-way shear when the line of zero bearing pressure intersects the critical section.
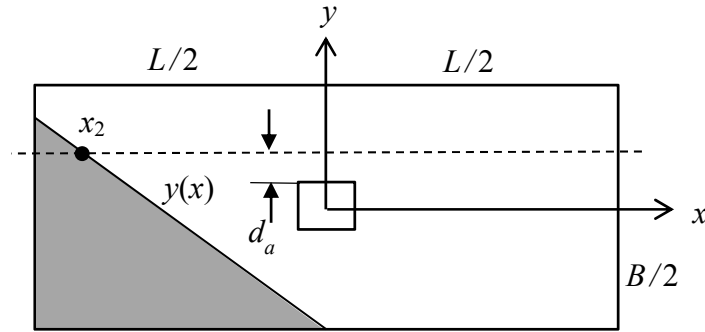
Figure 30. Critical One-Way Shear Section for Region A, *L*-Face: Case Two.

The point where the line of zero bearing pressure intersects the one-way shear section x_2 is:

$$x_2 = \frac{-\alpha L}{\beta B} \left(\frac{b_{col}}{2} + d_a + \frac{B}{2} \right) - \frac{L}{2} + \alpha L \tag{132}$$

In this case, the one-way shear force is computed as:

$$V_{one-way} = \int\limits_{\frac{-L}{2}}^{\frac{L}{2}} \int\limits_{\frac{b_{col}}{2}+d_a}^{\frac{B}{2}} q(x,y)\, dy\, dx - \int\limits_{\frac{-L}{2}}^{x_2} \int\limits_{\frac{b_{col}}{2}+d_a}^{y(x)} q(x,y)\, dy\, dx \qquad (133)$$

Evaluating the integral in Equation (133) gives an expression of the one-way shear force and is listed in the Appendix as Equation (A7).

4.1.1.3 Region A: flexure. The critical section for bending on a spread footing is at the column face. As with one-way shear, for each face of the footing, there are two cases for the calculation of moment.

4.1.1.3.1 B-Face: case one. Figure 31 shows the critical section for bending when the line of zero bearing pressure does not intersect the critical section.
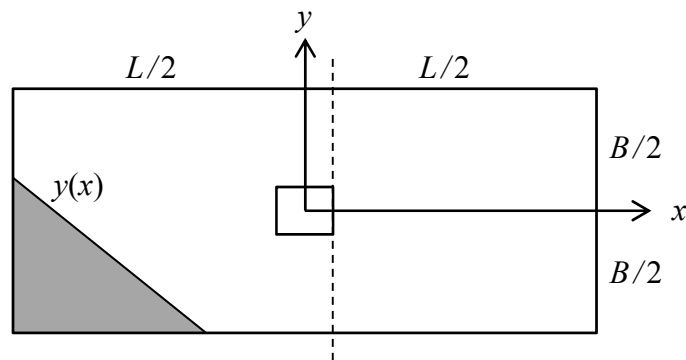
Figure 31. Critical Bending Section for Region A, *B*-Face: Case One.

In this case, the critical bending moment M_B is computed as:

$$M_B = \int\limits_{\frac{-B}{2}}^{\frac{B}{2}} \int\limits_{\frac{b_{col}}{2}}^{\frac{L}{2}} q(x,y) \left(x - \frac{b_{col}}{2} \right) dx\, dy \qquad (134)$$

Evaluating the integral in Equation (134) gives:

$$M_B = \frac{-q_1 B \left(L - b_{col} \right)^2 \left(5\beta L + 3\alpha L + \beta b_{col} - 6\alpha\beta L \right)}{48\alpha\beta L} \qquad (135)$$

4.1.1.3.2 B-Face: case two. Figure 32 shows the critical section for bending when the line of zero bearing pressure intersects the critical bending section.

Figure 32. Critical Bending Section for Region A, *B*-Face: Case Two.

The point where the line of zero bearing pressure intersects the critical bending section y_2 and is given as:

$$y_2 = \frac{-\beta B}{\alpha L}\left(\frac{b_{col}}{2} + \frac{L}{2} - \alpha L\right) - \frac{B}{2} \tag{136}$$

In this case, the critical bending moment M_B is computed as:

$$M_B = \int_{\frac{-B}{2}}^{\frac{B}{2}} \int_{\frac{b_{col}}{2}}^{\frac{L}{2}} q(x,y)\left(x - \frac{b_{col}}{2}\right) dx\,dy - \int_{\frac{-B}{2}}^{y_1} \int_{\frac{b_{col}}{2}}^{x(y)} q(x,y)\left(x - \frac{b_{col}}{2}\right) dx\,dy \tag{137}$$

Evaluating the integral in Equation (137) gives:

$$M_B = \frac{-q_1 \beta B\left(L + b_{col} - 2\alpha L\right)^4}{384\left(\alpha L\right)^2} - \frac{q_1 B\left(L - b_{col}\right)^2\left(5\beta L + 3\alpha L + \beta b_{col} - 6\alpha\beta L\right)}{48\alpha\beta L} \tag{138}$$

4.1.1.3.3 L-Face: case one. Figure 33 shows the critical section for bending when the line of zero bearing pressure does not intersect the critical section.

69
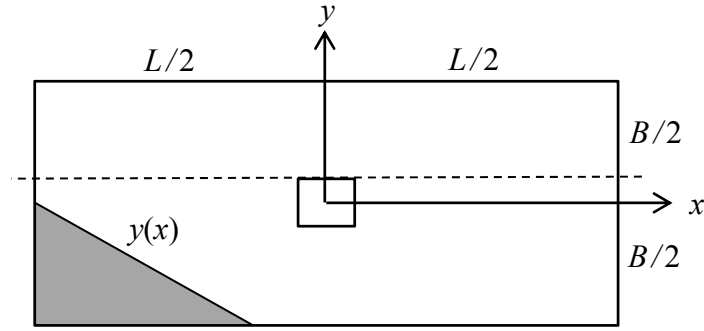
Figure 33. Critical Bending Section for Region A, *L*-Face: Case One.

In this case, the critical moment M_L is computed as:

$$M_L = \int_{\frac{-L}{2}}^{\frac{L}{2}} \int_{\frac{b_{col}}{2}}^{\frac{B}{2}} q(x,y)\left(y - \frac{b_{col}}{2}\right) dy\, dx \tag{139}$$

Evaluating the integral in Equation (139) gives:

$$M_L = \frac{-q_1 L (B - b_{col})^2 (5\alpha B + 3\beta B + \alpha b_{col} - 6\alpha\beta B)}{48\alpha\beta B} \tag{140}$$

4.1.1.3.4 L-Face: case two. Figure 34 shows the critical section for bending when the line of zero bearing pressure intersects the critical section.

.
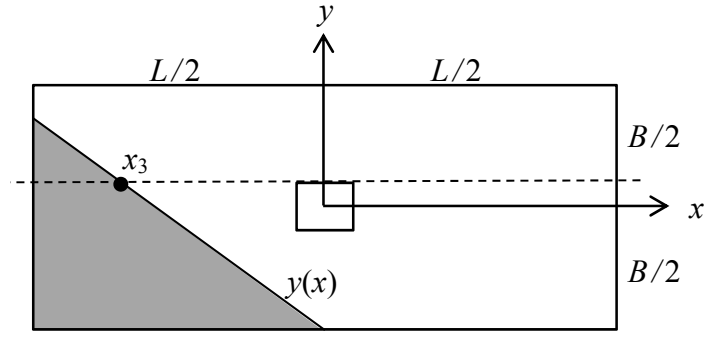
Figure 34. Critical Bending Section for Region A, *L*-Face: Case Two.

The point where the line of zero bearing pressure intersects the critical bending section x_3 is:

$$x_3 = \frac{-\alpha L}{\beta B}\left(\frac{b_{col}}{2} + \frac{B}{2}\right) - \frac{L}{2} + \alpha L \qquad (141)$$

In this case, the critical bending moment is M_L computed as:

$$M_L = \int_{\frac{-L}{2}}^{\frac{L}{2}} \int_{\frac{b_{col}}{2}}^{\frac{B}{2}} q(x,y)\left(y - \frac{b_{col}}{2}\right) dy\, dx - \int_{\frac{-L}{2}}^{x_3} \int_{\frac{b_{col}}{2}}^{y(x)} q(x,y)\left(y - \frac{b_{col}}{2}\right) dy\, dx \qquad (142)$$

Evaluating the integral in Equation (142) gives:

$$M_L = \frac{-q_1 \alpha L \left(B + b_{col} - 2\beta B\right)^4}{384\left(\beta B\right)^2} - \frac{q_1 L \left(B - b_{col}\right)^2 \left(5\alpha B + 3\beta B + \alpha b_{col} - 6\alpha\beta B\right)}{48\alpha\beta B} \qquad (143)$$

4.1.2 Uplift – region B

If the eccentricity ratios are such that the load is within Region B, shown in Figure 10, then Corners 1 and 4 are detached from the soil. The line of zero bearing pressure can be expressed in two forms:

$$y(x) = \frac{B}{L(\gamma - \alpha)}\left(x + \frac{L}{2} - \gamma L\right) + \frac{B}{2} \tag{144}$$

$$x(y) = \frac{L(\gamma - \alpha)}{B}\left(y - \frac{B}{2}\right) - \frac{L}{2} + \gamma L \tag{145}$$

4.1.2.1 Region B: two-way shear. There are six cases for which the two-way shear is calculated based upon how the line of zero bearing pressure intersects the critical two-way shear area. Lower and Upper limits for integration are based upon the critical two-way shear perimeter and are given by Equations (109) and (110).

4.1.2.1.1 Case one. When the line of zero bearing pressure does not intersect the critical punching shear perimeter, the two-way shear force V_{punch} is:

$$V_{punch} = P_u - \int_{L_{\text{limit}}}^{U_{\text{limit}}} \int_{L_{\text{limit}}}^{U_{\text{limit}}} q(x, y)\, dy\, dx \tag{146}$$

Evaluating the integral in Equation (146) gives:

$$V_{punch} = P_u - \frac{q_4\left(b_{col} + d_a\right)^2\left(\alpha + \gamma - 1\right)}{2\gamma} \tag{147}$$

4.1.2.1.2 Case two. Figure 35 shows the two-way shear area when a triangular portion of the two-way shear area becomes detached from the soil. The shaded area is the detached region beneath the critical two-way shear area.
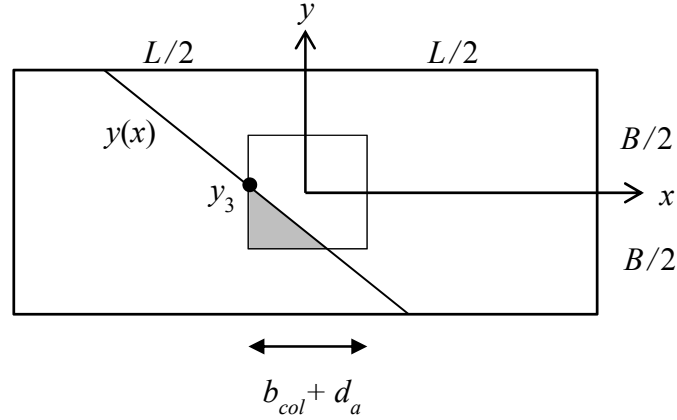
Figure 35. Critical Two-Way Shear Area for Region B, Case Two.

The point where the line of zero bearing pressure intersects left side of the two-way shear perimeter y_3 is:

$$y_3 = \frac{-B}{L(\gamma - \alpha)}\left(\frac{b_{col} + d_a}{2} - \frac{L}{2} + \gamma L\right) + \frac{B}{2} \tag{148}$$

The two-way shear force is computed as:

$$V_{punch} = P_u - \left(\int_{L_{limit}}^{U_{limit}} \int_{L_{limit}}^{U_{limit}} q(x,y)\,dy\,dx - \int_{L_{limit}}^{y_1} \int_{L_{limit}}^{x(y)} q(x,y)\,dx\,dy\right) \tag{149}$$

Evaluating the integral in Equation (149) gives an expression for the two-way shear force and is listed in the Appendix as Equation (A8).

4.1.2.1.3 Case three. The third case occurs when more of the two-way shear area becomes detached from the soil beneath it. Figure 36 shows the trapezoidal detached area beneath the critical two-way shear area.
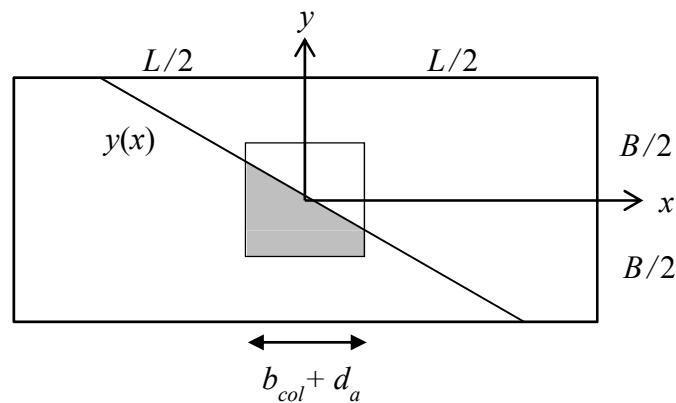
Figure 36. Critical Two-Way Shear Area for Region B, Case Three.

The two-way shear force is computed as:

$$V_{punch} = P_u - \int_{L_{limit}}^{U_{limit}} \int_{y(x)}^{U_{limit}} q(x,y)\, dy\, dx \qquad (150)$$

Evaluating the integral in Equation (150) gives an expression for the two-way shear force and is listed in the Appendix as Equation (A9).

4.1.2.1.4 Case four. Figure 37 shows the critical two-way shear area when the line of zero bearing pressure intersects it, causing the trapezoidal shaded area to become detached.

Figure 37. Critical Two-Way Shear Area for Region B, Case Four.

The two-way shear force is computed as:

$$V_{punch} = P_u - \int\limits_{L_{limit}}^{U_{limit}} \int\limits_{x(y)}^{U_{limit}} q(x,y)\,dx\,dy \tag{151}$$

Evaluating the integral in Equation (151) gives:

$$V_{punch} = P_u - \left(\frac{-q_4\left(\gamma L - \alpha L\right)^2 \left(b_{col} + d_a\right)^3}{24\gamma B^2 L} - \frac{q_4\left(b_{col} + d_a\right)\left(L + b_{col} + d_a - \gamma L - \alpha L\right)^2}{8\gamma L} \right) \tag{152}$$

75

4.1.2.1.5 Case five. Figure 38 shows the critical two-way shear area when only a triangular portion of the two-way shear area remains in contact with the soil.

Figure 38. Critical Two-Way Shear Area for Region B, Case Five.

The point that the line of zero bearing pressure intersects the right side of the two-way shear perimeter y_4 is:

$$y_4 = \frac{B}{L(\gamma-\alpha)}\left(\frac{b_{col}+d_a}{2}+\frac{L}{2}-\gamma L\right)+\frac{B}{2}$$

(153)

The two-way shear force is computed as:

$$V_{punch} = P_u - \int_{y_1}^{U_{limit}} \int_{x(y)}^{U_{limit}} q(x,y)\,dx\,dy$$

(154)

Evaluating the integral in Equation (154) gives:

$$V_{punch} = P_u - \frac{-q_4 \left(BL + b_{col}B + d_aB - \gamma BL - \alpha BL - \gamma b_{col}L - \gamma d_aL + \alpha b_{col}L + \alpha d_aL \right)^3}{48\gamma (\alpha - \gamma)(BL)^2} \quad (155)$$

4.1.2.1.6 Case six. The last case occurs when the line of zero bearing pressure is located to the right of the two-way shear area, causing the two-way shear area to be completely detached from the soil. In this case, the two-way shear force is computed as:

$$V_{punch} = P_u \quad (156)$$

4.1.2.2 Region B: one-way shear. For one-way shear on the *B*-face of the footing, there are three cases for which the line of zero bearing pressure may interact with the critical one-way shear section. For one-way shear on the *L*-face of the footing, there is only one case for which the line of zero bearing pressure may interact with the critical one-way shear section.

4.1.2.2.1 B-Face: case one. Figure 39 shows a spread footing when the line of zero bearing pressure does not intersect the critical section for one-way shear
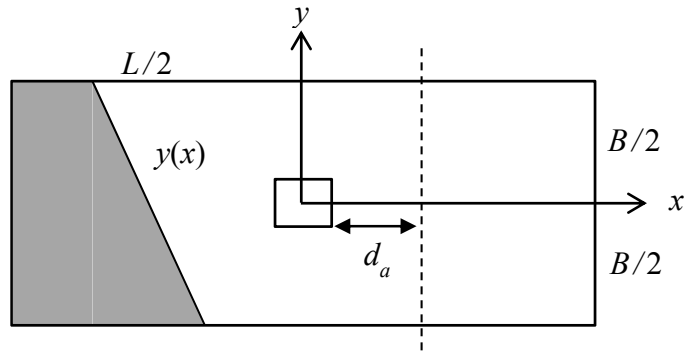
Figure 39. Critical One-Way Shear Section for Region B, *B*-Face: Case One.

The one-way shear force is computed as:

$$V_{one-way} = \int_{\frac{b_{col}}{2}+d_a}^{\frac{L}{2}} \int_{\frac{-B}{2}}^{\frac{B}{2}} q(x,y)\,dy\,dx \qquad (157)$$

Evaluating the integral in Equation (157) gives:

$$V_{one-way} = \frac{q_4 B \left(b_{col} - L + 2d_a\right)\left(3L + b_{col} + 2d_a - 2\gamma L - 2\alpha L\right)}{8\gamma L} \qquad (158)$$

4.1.2.2.2 B-Face: case two. Figure 40 shows a spread footing when the line of zero bearing pressure intersects the critical section of one-way shear.
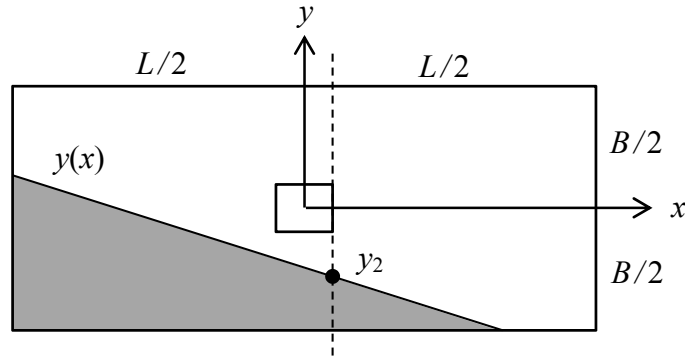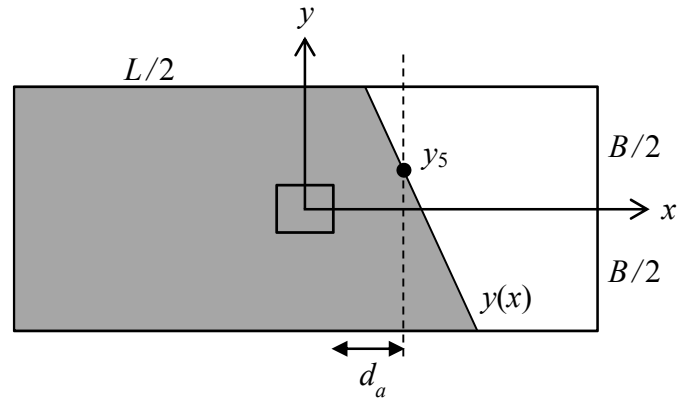
Figure 40. Critical One-Way Shear Section for Region B, *B*-Face: Case Two.

The point where the line of zero bearing pressure intersects the one-way shear section y_5

is:

$$y_5 = \frac{B}{L(\gamma-\alpha)}\left(\frac{b_{col}}{2}+d_a+\frac{L}{2}-\gamma L\right)+\frac{B}{2} \tag{159}$$

In this case, the one-way shear force is computed as:

$$V_{one-way} = \int_{\frac{b_{col}}{2}+d_a}^{\frac{L}{2}} \int_{\frac{-B}{2}}^{\frac{B}{2}} q(x,y)\,dy\,dx - \int_{\frac{-B}{2}}^{y_1} \int_{\frac{b_{col}}{2}+d_a}^{x(y)} q(x,y)\,dx\,dy \tag{160}$$

Evaluating the integral in Equation (160) gives an expression for the one-way shear and

is listed in the Appendix as Equation (A10).

4.1.2.2.3 B-Face: case three. Figure 41 shows a spread footing when the line of zero

bearing pressure is beyond the critical section for one-way shear.

Figure 41. Critical One-Way Shear Section for Region B, *B*-Face: Case Three.

In this case, the one-way shear force is compute as:

$$V_{one-way} = \int_{\frac{-B}{2}}^{\frac{B}{2}} \int_{x(y)}^{\frac{L}{2}} q(x, y)\, dx\, dy \tag{161}$$

Evaluating the integral in Equation (161) gives:

$$V_{one-way} = \frac{-q_4 BL\left(\gamma^2 - 3\alpha - 3\gamma + \alpha^2 + \alpha\gamma + 3\right)}{6\gamma} \tag{162}$$

4.1.2.2.4 L-Face. Figure 42 shows the critical section for one-way shear parallel to the *L*-face of the footing.

Figure 42. Critical One-Way Shear Section for Region B, *L*-Face.

In this case, the one-way shear force is computed as:

$$V_{one-way} = \int_{\frac{b_{col}}{2}+d_a}^{\frac{B}{2}} \int_{x(y)}^{\frac{L}{2}} q(x,y)\, dx\, dy \tag{163}$$

Evaluating the integral in Equation (163) gives an expression for the one-way shear and is listed in the Appendix as Equation (A11).

4.1.2.3 Region B: flexure. As with one-way shear, for each face of the footing, there are different cases for which the moment is calculated when eccentricities are in Region B. For the moment on the critical section parallel to the *B*-face of the footing, there are three cases based on where the line of zero bearing pressure is located with respect to the critical bending section. For bending on the *L*-face of the footing, there is only one case for which the line of zero bearing pressure may interact with the critical bending section.

4.1.2.3.1 B-Face: case one. This case occurs when the line of zero bearing pressure does not intersect the critical section for bending.

81
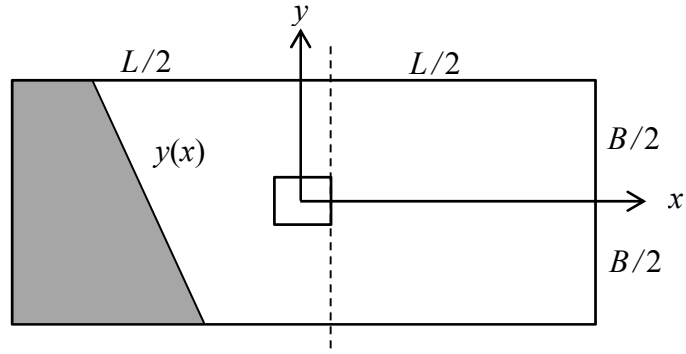
Figure 43. Critical Bending Section for Region B, *B*-Face: Case One.

The moment M_B is computed as:

$$M_B = \int\limits_{\frac{-B}{2}}^{\frac{B}{2}} \int\limits_{\frac{b_{col}}{2}}^{\frac{L}{2}} q(x,y)\left(x - \frac{b_{col}}{2}\right) dx\, dy \qquad (164)$$

Evaluating the integral in Equation (164) gives:

$$M_B = \frac{-q_4 B\left(L - b_{col}\right)^2 \left(5L + b_{col} - 3\alpha L - 3\gamma L\right)}{48\gamma L} \qquad (165)$$

4.1.2.3.2 B-Face: case two. Figure 44 shows the line of zero bearing pressure intersecting the critical section for bending.
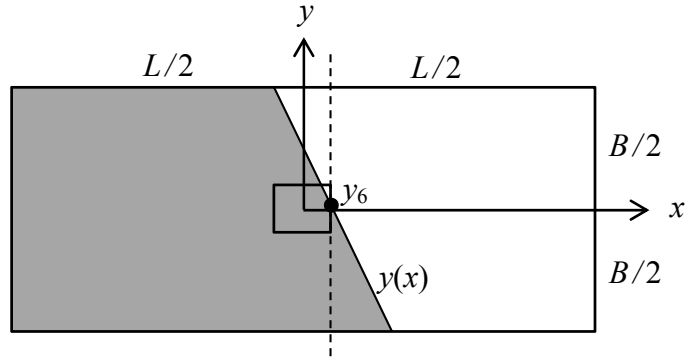
Figure 44. Critical Bending Section for Region B, *B*-Face: Case Two.

The point that the line of zero bearing pressure intersects the critical bending section y_6 is:

$$y_6 = \frac{B}{L(\gamma - \alpha)}\left(\frac{b_{col}}{2} + \frac{L}{2} - \gamma L\right) + \frac{B}{2}$$

(166)

The moment M_B is computed as:

$$M_B = \int\limits_{\frac{-B}{2}}^{\frac{B}{2}} \int\limits_{\frac{b_{col}}{2}}^{\frac{L}{2}} q(x,y)\left(x - \frac{b_{col}}{2}\right) dx\, dy - \int\limits_{\frac{-B}{2}}^{y_1} \int\limits_{\frac{b_{col}}{2}}^{x(y)} q(x,y)\left(x - \frac{b_{col}}{2}\right) dx\, dy$$

(167)

Evaluating the integral in Equation (167) gives:

$$M_B = \frac{-q_4 B\left(L - b_{col}\right)^2\left(5L + b_{col} - 3\alpha L - 3\gamma L\right)}{48\gamma L} - \frac{q_4 B\left(L + b_{col} - 2\alpha L\right)^4}{384\gamma(\alpha - \gamma)L^2}$$

(168)

4.1.2.3.3 B-Face: case three. This case occurs when the line of zero bearing pressure is beyond the critical section for bending. Figure 45 shows the line of zero bearing pressure beyond the critical bending section.
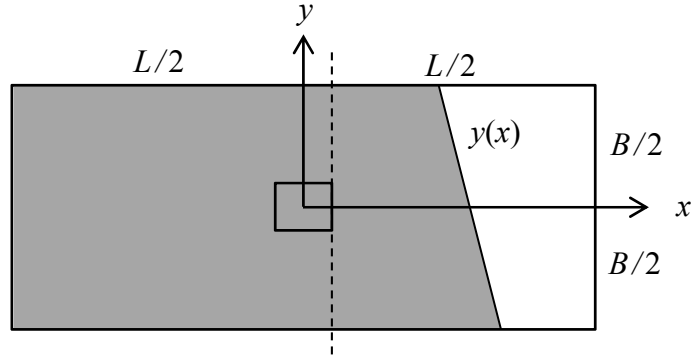
Figure 45. Critical Bending Section for Region B, *B*-Face: Case Three.

The moment M_B is computed as:

$$M_B = \int_{\frac{-B}{2}}^{\frac{B}{2}} \int_{x(y)}^{\frac{L}{2}} q(x,y)\left(x - \frac{b_{col}}{2}\right) dx\, dy \qquad (169)$$

Evaluating the integral in Equation (169) gives an expression for the moment and is listed in the Appendix as Equation (A12).

4.1.2.3.4 L-Face. Figure 46 shows the critical section for bending parallel to the *L*-face of the footing.

Figure 46. Critical Bending Section for Region B, *L*-Face.

In this case, the moment M_L is computed as:

$$M_L = \int\limits_{\frac{b_{col}}{2}}^{\frac{B}{2}} \int\limits_{x(y)}^{\frac{L}{2}} q(x,y)\left(y - \frac{b_{col}}{2}\right) dx\, dy \qquad (170)$$

Evaluating the integral in Equation (170) gives an expression for the moment and is listed in the Appendix as Equation (A13).

4.1.3 Uplift – region C

If the eccentricities are such that Corners 1 and 2 are detached from the soil, shown in Figure 12, then the line of zero bearing pressure can be expressed as:

$$y(x) = \frac{B(\eta - \beta)}{L}\left(x + \frac{L}{2}\right) - \frac{B}{2} + \beta B \qquad (171)$$

$$x(y) = \frac{L}{B(\eta - \beta)}\left(y + \frac{B}{2} - \beta B\right) - \frac{L}{2} \qquad (172)$$

4.1.3.1 Region C: two-way shear. There are six cases for which the two-way shear is calculated. Each case is represented by how the line of zero bearing pressure intersects the two-way shear area. Lower and Upper limits for integration are based upon the critical two-way shear perimeter and are given by Equations (109) and (110).

4.1.3.1.1 Case one. The first case occurs when the line of zero bearing pressure does not intersect the critical two-way shear perimeter. The two-way shear force is computed as:
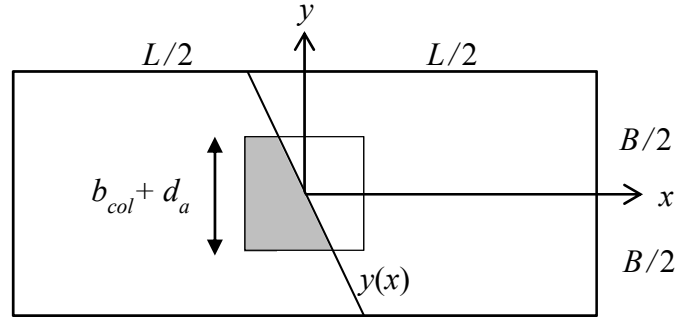
$$V_{punch} = P_u - \int_{L_{limit}}^{U_{limit}} \int_{L_{limit}}^{U_{limit}} q(x,y)\,dy\,dx \qquad (173)$$

Evaluating the integral in Equation (173) gives:

$$V_{punch} = P_u - \frac{q_2 \left(b_{col} + d_a\right)^2 \left(\beta + \eta - 1\right)}{2\eta} \qquad (174)$$

4.1.3.1.2 Case two. The second case occurs when a triangular portion of the two-way shear perimeter becomes detached from the soil. Figure 47 shows the triangular shaded area beneath the critical two-way shear area that has become detached from the soil.
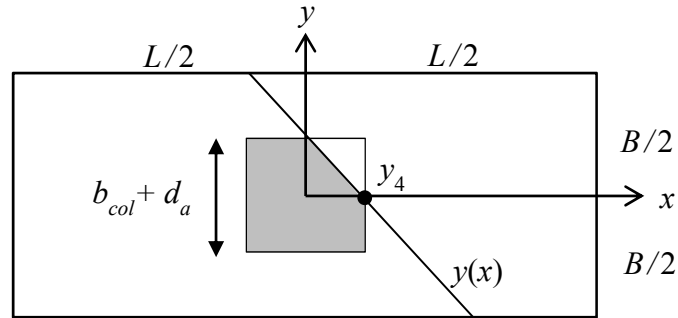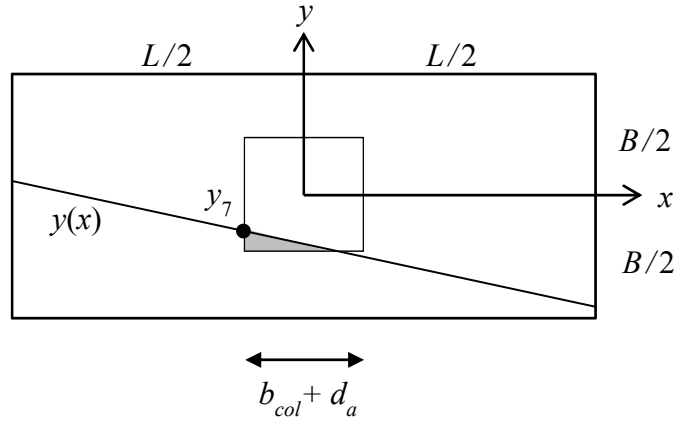
Figure 47. Critical Two-Way Shear Area for Region C, Case Two.

The point where the line of zero bearing pressure intersects the left side of the two-way shear perimeter y_7 is:

$$y_7 = \frac{B(\eta - \beta)}{L}\left(-\left(\frac{b_{col} + d_a}{2}\right) + \frac{L}{2}\right) - \frac{B}{2} + \beta B \qquad (175)$$

The two-way shear force is computed as:

$$V_{punch} = P_u - \left(\int_{L_{limit}}^{U_{limit}} \int_{L_{limit}}^{U_{limit}} q(x,y)\, dy\, dx - \int_{L_{limit}}^{y_1} \int_{L_{limit}}^{x(y)} q(x,y)\, dx\, dy\right) \qquad (176)$$

Evaluating the integral in Equation (176) gives an expression for the two-way shear force and is listed in the Appendix as Equation (A14).

87

4.1.3.1.3 Case three. The third case occurs when more of the critical two-way shear area becomes detached from the soil beneath it. Figure 48 shows the trapezoidal detached area.
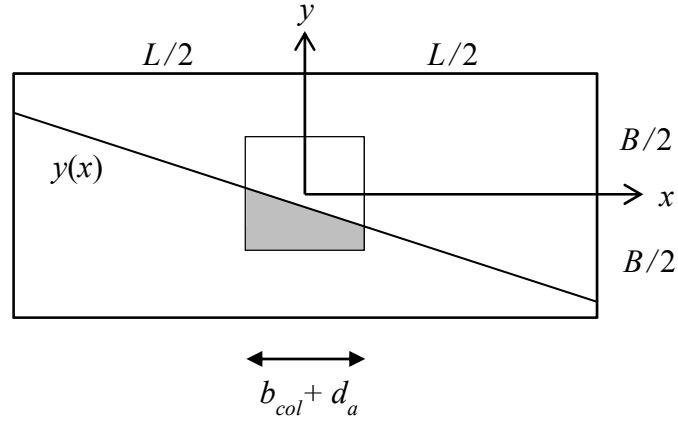
Figure 48. Critical Two-Way Shear Area for Region C, Case Three.

The two-way shear force is computed as:

$$V_{punch} = P_u - \int_{L_{limit}}^{U_{limit}} \int_{y(x)}^{U_{limit}} q(x,y)\,dy\,dx \tag{177}$$

Evaluating the integral in Equation (177) gives:

$$V_{punch} = P_u - \left(\frac{-q_2\left(b_{col}+d_a\right)\left(B+b_{col}+d_a-\eta B-\beta B\right)}{8\eta B} - \frac{q_2\left(b_{col}+d_a\right)^3\left(\eta B-\beta B\right)^2}{24\eta BL^2} \right) \tag{178}$$

4.1.3.1.4 Case four. The fourth case may occur when the vertical dimension of the footing is larger than the horizontal dimension. The line of zero bearing pressure intersects the two-way shear perimeter in an orientation causing a vertical trapezoidal area of detachment. Figure 49 shows the detached critical two-way shear area.
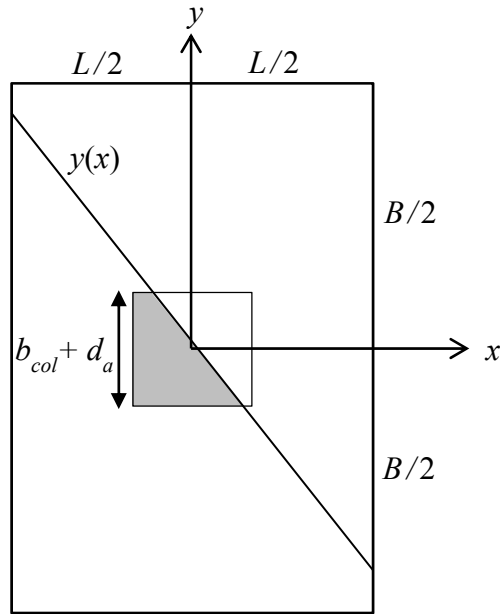
Figure 49. Critical Two-Way Shear Area for Region C, Case Four.

The two-way shear force is computed as:

$$V_{punch} = P_u - \int\limits_{L_{limit}}^{U_{limit}} \int\limits_{x(y)}^{U_{limit}} q(x,y)\, dx\, dy \qquad (179)$$

Evaluating the integral in Equation (179) gives an expression for the two-way shear force and is listed in the Appendix as Equation (A15).

4.1.3.1.5 Case five. This case occurs when only a triangular portion of the two-way shear perimeter remains attached to the soil. Figure 50 shows the triangular shaded area beneath the critical two-way shear area that is attached to the soil.

Figure 50. Critical Two-Way Shear Area for Region C, Case Five.

The point where the line of zero bearing pressure intersects the top of the critical two-way shear perimeter x_4 is calculated as:

$$x_4 = \frac{L}{B(\eta - \beta)} \left(\frac{b_{col} + d_a}{2} + \frac{B}{2} - \beta B \right) - \frac{L}{2} \qquad (180)$$

The two-way shear force is computed as:

$$V_{punch} = P_u - \int_{x_4}^{U_{limit}} \int_{y(x)}^{U_{limit}} q(x,y)\,dy\,dx$$

(181)

Evaluating the integral in Equation (181) gives:

$$V_{punch} = P_u - \frac{-q_2\left(BL + b_{col}L + d_aL - \eta BL - \beta BL - \eta b_{col}B - \eta d_aB + \beta b_{col}B + \beta d_aB\right)^3}{48\eta(\beta - \eta)(BL)^2}$$

(182)

4.1.3.1.6 Case six. The last case occurs when the line of zero bearing pressure is located to the right the critical two-way shear area. In this case, the critical two-way shear area is completely detached from the soil. The two-way shear force is computed as:

$$V_{punch} = P_u$$

(183)

4.1.3.2 Region C: one-way shear. For one-way shear on the critical section parallel to the *L*-face of the footing, there are three cases for which the line of zero bearing pressure may interact with the critical one-way shear section. For one-way shear on the critical section parallel to the *B*-face of the footing, there is only one case for which the line of zero bearing pressure may interact with the critical one-way shear section.

4.1.3.2.1 B –Face. Figure 51 shows the critical one-way shear section parallel the *B*-face of the footing.
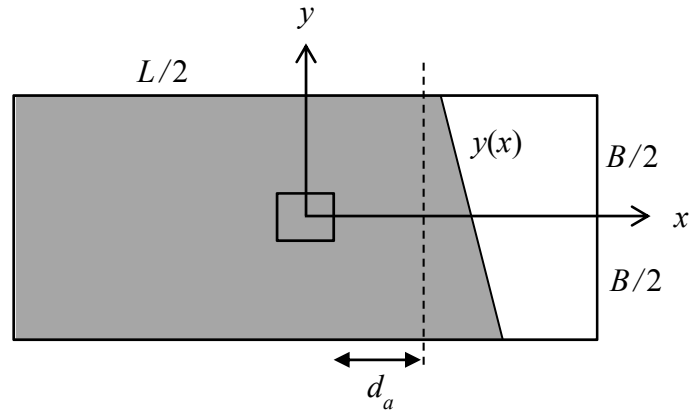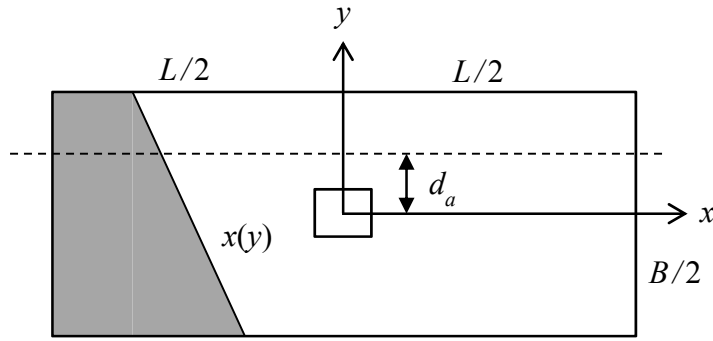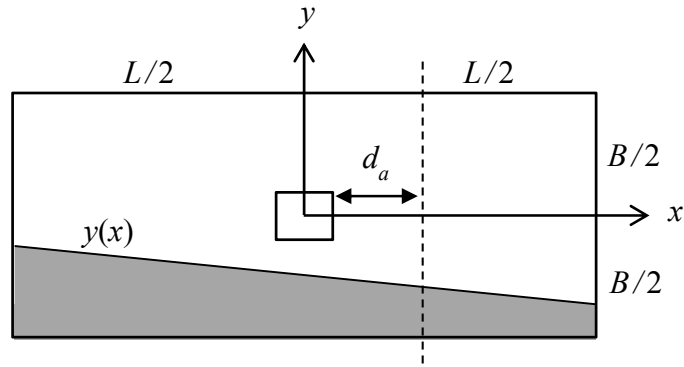
Figure 51. Critical One-Way Shear Section for Region C, *B*-Face.

In this case, the one-way shear force is computed as:

$$V_{one-way} = \int\limits_{\frac{b_{col}}{2}+d_a}^{\frac{L}{2}} \int\limits_{y(x)}^{\frac{B}{2}} q(x,y)\,dy\,dx \qquad (184)$$

Evaluating the integral in Equation (184) gives an expression for the one-way shear force and is listed in the Appendix as Equation (A15).

For one-way shear on the *L*-face of the footing, there are three cases for which the line of zero bearing pressure may interact with the critical one-way shear section.

4.1.3.2.2 L-Face: case one. Figure 52 shows the case when the line of zero bearing pressure does not intersect the critical section for one-way shear.

Figure 52. Critical One-Way Shear Section for Region C, *L*-Face: Case One.

In this case, the one-way shear force is computed as:

$$V_{one-way} = \int\limits_{\frac{-L}{2}}^{\frac{L}{2}} \int\limits_{\frac{b_{col}}{2}+d_a}^{\frac{B}{2}} q(x,y)\, dy\, dx \tag{185}$$

Evaluating the integral in Equation (185) gives:

$$V_{one-way} = \frac{q_2 L\left(b_{col} - B + 2d_a\right)\left(3B + b_{col} + 2d_a - 2\eta B - 2\beta B\right)}{8\eta B} \tag{186}$$

*4.1.3.2.3 L -Face: case two.* Figure 53 shows the line of zero bearing pressure intersecting the critical section for one-way shear.
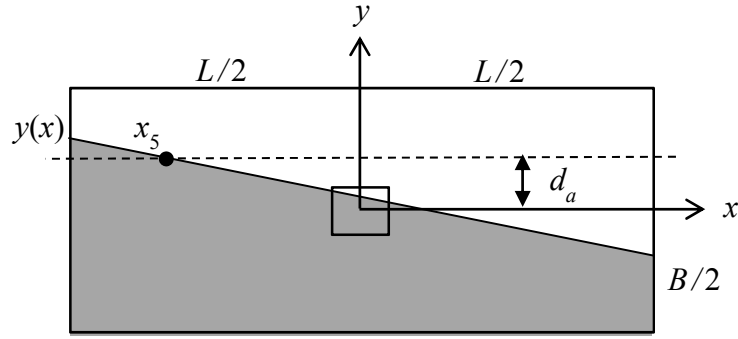
Figure 53. Critical One-Way Shear Section for Region C, *L*-Face: Case Two.

The point where the line of zero bearing pressure intersects the one-way shear section x_5

is:

$$x_5 = \frac{L}{B(\eta-\beta)}\left(\frac{b_{col}}{2}+d_a+\frac{B}{2}-\beta B\right)-\frac{L}{2} \tag{187}$$

In this case, the one-way shear force is computed as:

$$V_{one-way} = \int_{\frac{-L}{2}}^{\frac{L}{2}} \int_{\frac{b_{col}}{2}+d_a}^{\frac{B}{2}} q(x,y)\,dy\,dx - \int_{\frac{-L}{2}}^{x_5} \int_{\frac{b_{col}}{2}+d_a}^{y(x)} q(x,y)\,dy\,dx \tag{188}$$

Evaluating the integral in Equation (188) gives an expression for the one-way shear force

and is listed in the Appendix as Equation (A17).

4.1.3.2.4 L-Face: case three. This case occurs when the line of zero bearing pressure

is beyond the critical section for one-way shear. Figure 54 shows the line of zero bearing

pressure beyond the critical section for one-way shear.
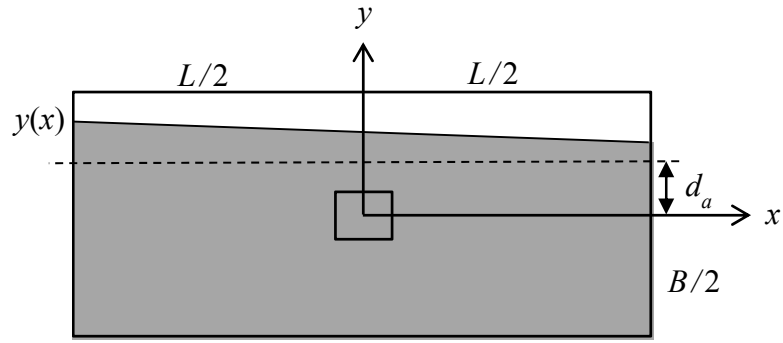
Figure 54. Critical One-Way Shear Section for Region C, *L*-Face: Case Three.

In this case, the one-way shear force is computed as:

$$V_{one-way} = \int\limits_{\frac{-L}{2}}^{\frac{L}{2}} \int\limits_{y(x)}^{\frac{B}{2}} q(x,y)\, dy\, dx \qquad (189)$$

Evaluating the integral in Equation (189) gives:

$$V_{one-way} = \frac{-q_2 BL\left(\eta^2 - 3\beta - 3\eta + \beta^2 + \eta\beta + 3\right)}{6\eta} \qquad (190)$$

4.1.3.3 Region C: flexure. As with one-way shear, for each face of the footing, there are different cases for which the moment is calculated when eccentricities are in Region C. For the moment on the critical section parallel to the *B*-face of the footing, there is one case that is based on the location of the line zero bearing pressure with respect to the critical bending section.

4.1.3.3.1 B-Face. Figure 55 shows the critical bending section parallel to the *B*-face of the footing.
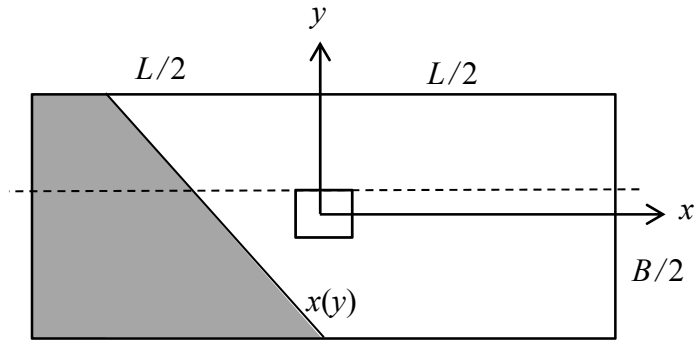

Figure 55. Critical Bending Section for Region C, *B*-Face.

In this case, the moment M_B is computed as:

$$M_B = \int\limits_{\frac{b_{col}}{2}}^{\frac{L}{2}} \int\limits_{y(x)}^{\frac{B}{2}} q(x,y)\left(x - \frac{b_{col}}{2}\right) dy\, dx \qquad (191)$$

Evaluation of the integral in Equation (191) gives an expression for the moment and is listed in the Appendix as Equation (A18).

For bending on the *L*-face of the footing, there are three cases for which the line of zero bearing pressure may interact with the critical bending section.

4.1.3.3.2 L-Face: case one. This case occurs when the line of zero bearing pressure does not intersect the critical section for bending. Figure 56 shows the case when the line of zero bearing pressure does not intersect the critical section for bending.
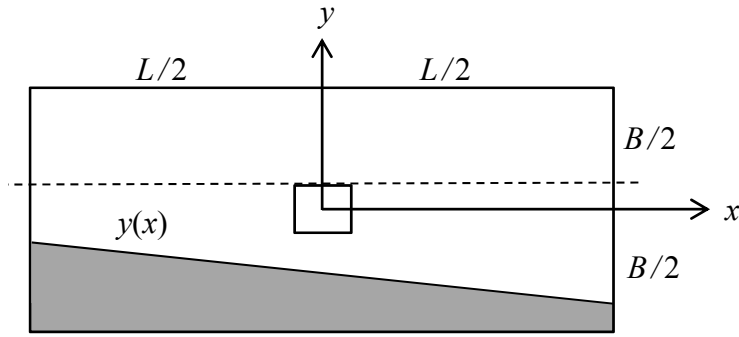
Figure 56. Critical Bending Section for Region C, *L*-Face: Case One.

In this case, the moment M_L is computed as:

$$M_L = \int\limits_{\frac{-L}{2}}^{\frac{L}{2}} \int\limits_{\frac{b_{col}}{2}}^{\frac{B}{2}} q(x,y)\left(y - \frac{b_{col}}{2}\right) dy\, dx \tag{192}$$

Evaluation of the integral in Equation (192) gives:

$$M_L = \frac{-q_2 L\left(B - b_{col}\right)^2\left(5B + b_{col} - 3\eta B - 3\beta B\right)}{48\eta B} \tag{193}$$

4.1.3.3.3 L-Face: case two. This case occurs when the line of zero bearing pressure intersects the critical section for bending. Figure 57 shows the line of zero bearing pressure intersecting the critical bending section.
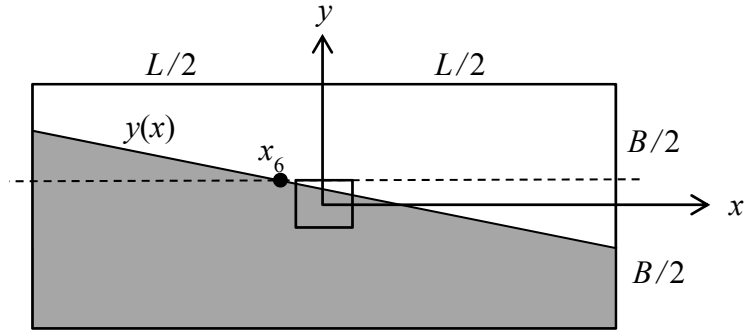
Figure 57. Critical Bending Section for Region C, *L*-Face: Case Two.

The point where the line of zero bearing pressure intersects the critical bending section x_6 is:

$$x_6 = \frac{L}{B(\eta - \beta)}\left(\frac{b_{col}}{2} + \frac{B}{2} - \beta B\right) - \frac{L}{2} \tag{194}$$

In this case, the moment M_L is given computed as:

$$M_L = \int_{\frac{-L}{2}}^{\frac{L}{2}} \int_{\frac{b_{col}}{2}}^{\frac{B}{2}} q(x,y)\left(y - \frac{b_{col}}{2}\right) dy\, dx - \int_{\frac{-L}{2}}^{x_6} \int_{\frac{b_{col}}{2}}^{y(x)} q(x,y)\left(y - \frac{b_{col}}{2}\right) dy\, dx \tag{195}$$

Evaluating the integral in Equation (195) gives:

$$M_L = \frac{-q_2 L (B - b_{col})^2 (5B + b_{col} - 3\eta B - 3\beta B)}{48 \eta B} - \frac{q_2 L (B + b_{col} - 2\beta B)^4}{384 \eta (\beta - \eta) B^2} \tag{196}$$

4.1.3.3.4 L-Face: case three. This case occurs when the line of zero bearing pressure is beyond the critical section for bending. Figure 58 shows the line of zero bearing pressure beyond the critical bending section.
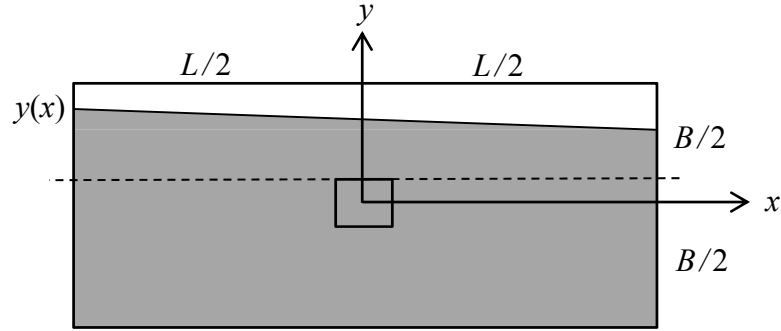
Figure 58. Critical Bending Section for Region C, *L*-Face: Case Three.

In this case, the moment M_L is computed as:

$$M_L = \int_{\frac{-L}{2}}^{\frac{L}{2}} \int_{y(x)}^{\frac{B}{2}} \sigma(x,y)\left(y - \frac{b_{col}}{2}\right) dy\, dx \tag{197}$$

Evaluating the integral in Equation (197) gives an expression for the moment and is listed in the Appendix as Equation (A19).

4.1.4 Uplift – region D

When the eccentricities increase to values that cause Corners 1, 2 and 4 to become

detached, shown in Figure 14, the load will be in Region D and the line of zero bearing

pressure can be expressed in two forms:

$$y(x) = -\frac{B - \eta B}{L - \gamma L}\left(x - \left(\frac{-L}{2} + \gamma L\right)\right) + \frac{B}{2} \tag{198}$$

$$x(y) = -\frac{L - \gamma L}{B - \eta B}\left(y - \frac{B}{2}\right) - \frac{L}{2} + \alpha L \tag{199}$$

4.1.4.1 Region D: two-way shear. There are five cases for which the two-way shear

is calculated. Each case is represented by how the line of zero bearing pressure intersects

the two-way shear area. For all of the integrations, the lower and upper limits are given

by Equations (109) and (110).

4.1.4.1.1 case one. The first case occurs when a triangular portion of the two-way

shear perimeter becomes detached from the soil. This may occur if the spread footing is

nearly square in the plan view. The triangular shaded area is the area beneath the two-

way shear area that has become detached from the soil and is shown in Figure 59.
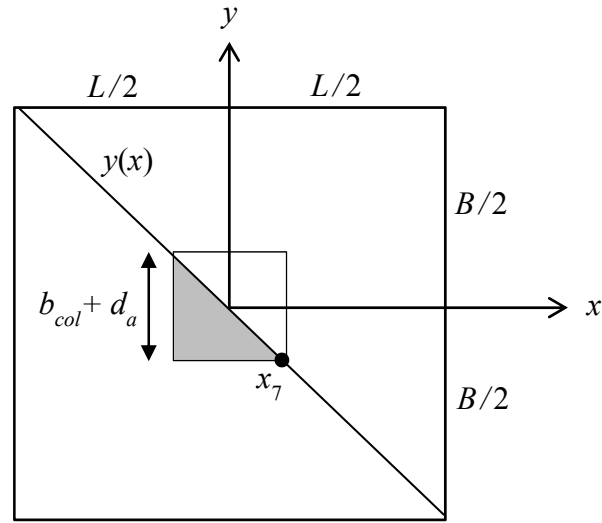
Figure 59. Critical Two-Way Shear Area for Region D, Case One.

The point where the line of zero bearing pressure intersects the bottom side of the two-way shear perimeter x_7 is:

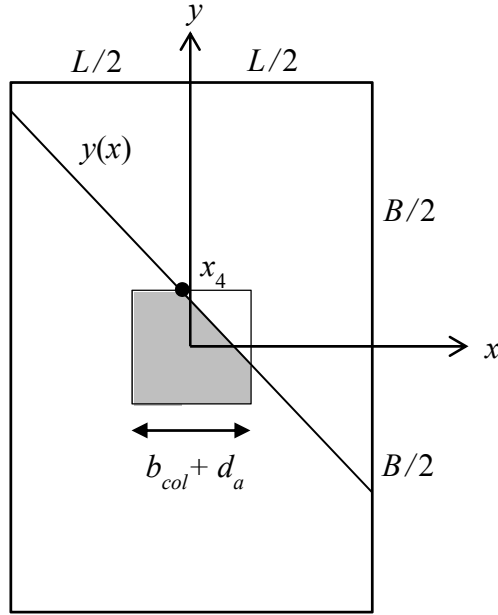$$x_7 = -\frac{L - \gamma L}{B - \eta B}\left(-\left(\frac{b_{col} + d_a}{2}\right) - \frac{B}{2}\right) - \frac{L}{2} + \alpha L \qquad (200)$$

The two-way shear force is computed as:

$$V_{punch} = P_u - \left(\int_{L_{limit}}^{U_{limit}} \int_{L_{limit}}^{U_{limit}} q(x,y)\,dy\,dx - \int_{L_{limit}}^{x_7} \int_{L_{limit}}^{y(x)} q(x,y)\,dy\,dx\right) \qquad (201)$$

Evaluating the integral in Equation (201) gives an expression for the two-way shear force and is listed in the Appendix as Equation (A20).

4.1.4.1.2 case two. The second case occurs when more of the two-way shear area becomes detached from the soil beneath it. This trapezoidal detached area is shown as the shaded portion of Figure 60.
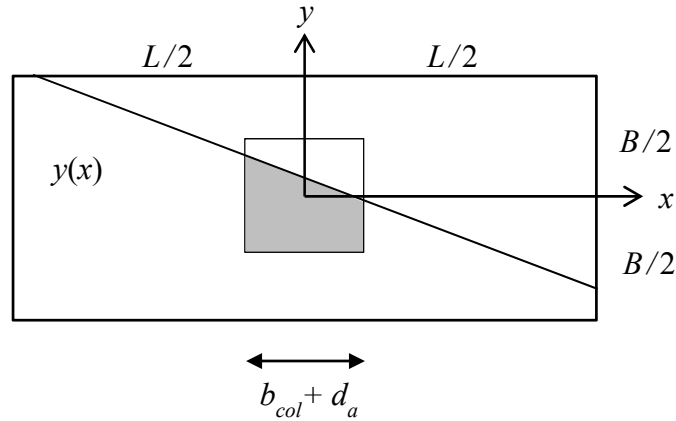
Figure 60. Critical Two-Way Shear Area for Region D, Case Two.

The two-way shear force is computed as:

$$V_{punch} = P_u - \int_{L_{limit}}^{U_{limit}} \int_{y(x)}^{U_{limit}} q(x, y) \, dy \, dx \tag{202}$$

Evaluating the integral in Equation (202) gives an expression for the two-way shear force and is listed in the Appendix as Equation (A21).

4.1.4.1.3 case three. The third case occurs when if the line of zero bearing pressure intersects the two-way shear perimeter in the orientation shown in Figure 61.
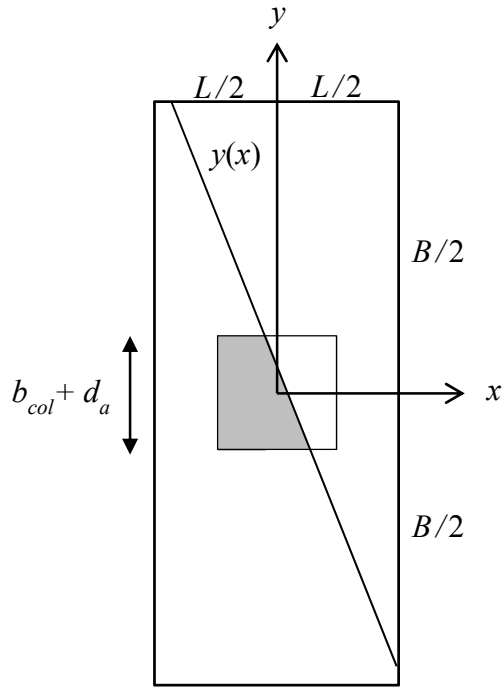
Figure 61. Critical Two-Way Shear Area for Region D, Case Three.

The two-way shear force is computed as:

$$V_{punch} = P_u - \int_{L_{limit}}^{U_{limit}} \int_{x(y)}^{U_{limit}} q(x,y)\,dx\,dy \qquad (203)$$

Evaluating the integral in Equation (203) gives an expression for the two-way shear force and is listed in the Appendix as Equation (A22).

4.1.4.1.4 Case Four. This case occurs when only a triangular portion of the two-way shear perimeter remains attached to the soil. The triangular area is the area beneath the two-way shear area that remains attached to the soil and is shown in Figure 62.
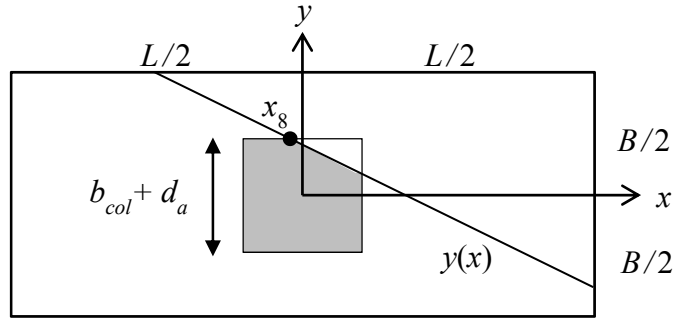
Figure 62. Critical Two-Way Shear Area for Region D, Case Four.

The point where the line of zero bearing pressure intersects the top of the two-way shear perimeter x_8 is:

$$x_8 = -\frac{L - \gamma L}{B - \eta B}\left(\frac{b_{col} + d_a}{2} - \frac{B}{2}\right) - \frac{L}{2} + \alpha L \qquad (204)$$

The two-way shear force is computed as:

$$V_{punch} = P_u - \int_{x_8}^{U_{limit}} \int_{y(x)}^{U_{limit}} q(x, y)\, dy\, dx \qquad (205)$$

Evaluating the integral in Equation (205) gives an expression for the two-way shear force and is listed in the Appendix as Equation (A23).

4.1.4.1.5 case five. The last case occurs when the line of zero bearing pressure is located past the two-way shear perimeter, causing the two-way shear area to be completely detached from the soil. In this case, the two-way shear force is computed as:

$$V_{punch} = P_u \qquad (206)$$

4.1.4.2 One-Way Shear. One-way shear may occur on either face of the spread footing. The one-way shear on the critical section parallel to the *B*-face of the footing is shown in Figure 63.
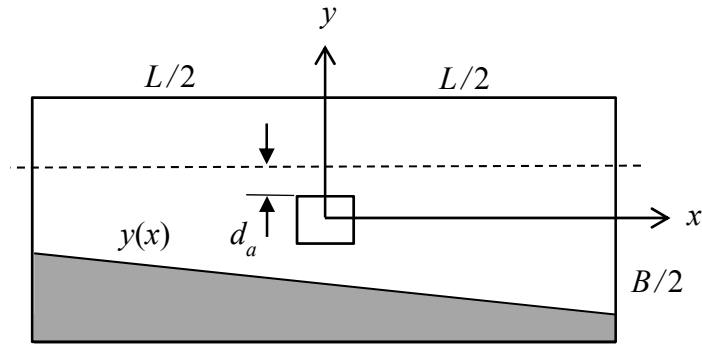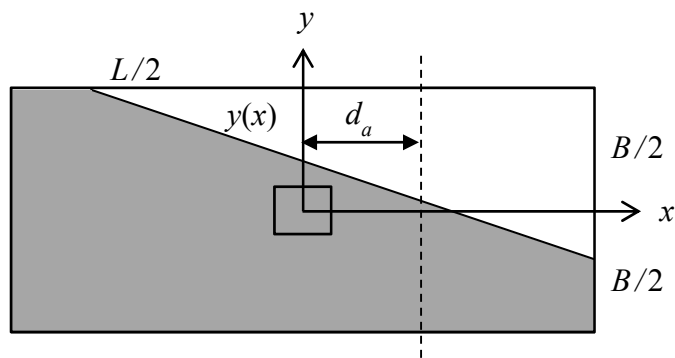

Figure 63. Critical One-Way Shear Section for Region D, *B*-Face.

In this case, the one-way shear force is computed as:

$$V_{one-way} = \int_{\frac{b_{col}}{2}+d_{ave}}^{\frac{L}{2}} \int_{y(x)}^{\frac{B}{2}} q(x,y)\,dy\,dx \qquad (207)$$

Evaluating the integral in Equation (207) gives an expression for the one-way shear force and is listed in the Appendix as Equation (A24).

The one-way shear on the critical section parallel to the *L*-face of the footing is shown in Figure 64.
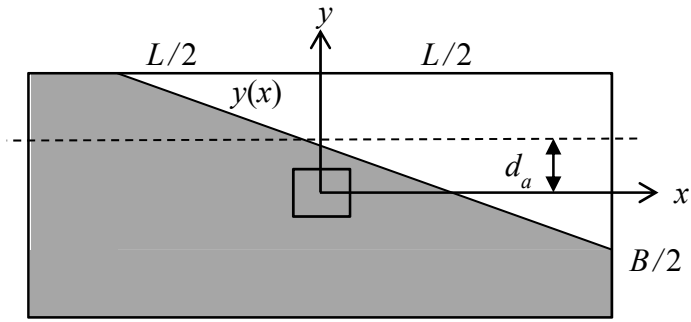
Figure 64. Critical One-Way Shear Section for Region D, *L*-Face.

In this case, the one-way shear force is computed as:

$$V_{one-way} = \int_{\frac{b_{col}}{2}+d_a}^{\frac{B}{2}} \int_{x(y)}^{\frac{L}{2}} \sigma(x,y)\,dx\,dy \qquad (208)$$

Evaluating the integral in Equation (208) gives an expression for the one-way shear force and is listed in the Appendix as Equation (A25).

4.1.4.3 flexure. Bending may occur on either face of the spread footing. The bending on the critical section parallel to the *B*-face of the footing is shown in Figure 65.

106
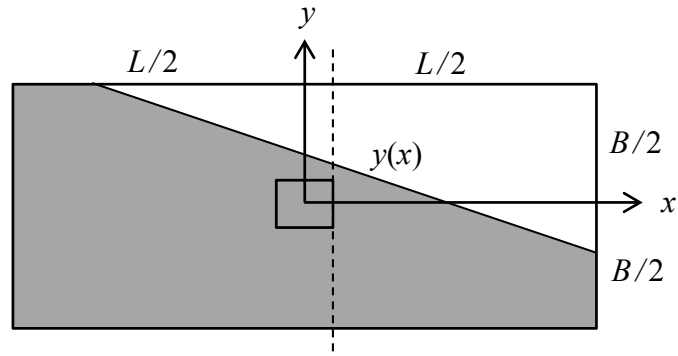
Figure 65. Critical Bending Section for Region D, B-Face.

In this case, the moment is computed as:

$$M_B = \int_{\frac{b_{col}}{2}}^{\frac{L}{2}} \int_{y(x)}^{\frac{B}{2}} q(x,y)\left(x - \frac{b_{col}}{2}\right) dy\, dx \tag{209}$$

Evaluating the integral in Equation (209) gives:

$$M_B = \frac{-q_3 B(\eta-1)(L-b_{col})^2 \left(24(\gamma L)^2 - 40\gamma L^2 + 17L^2 - 8\gamma b_{col}L + 6b_{col}L + b_{col}^2\right)}{384(\gamma-1)^2 L^2} \tag{210}$$

The moment on the critical section parallel to the L-face of the footing is shown in Figure 66.
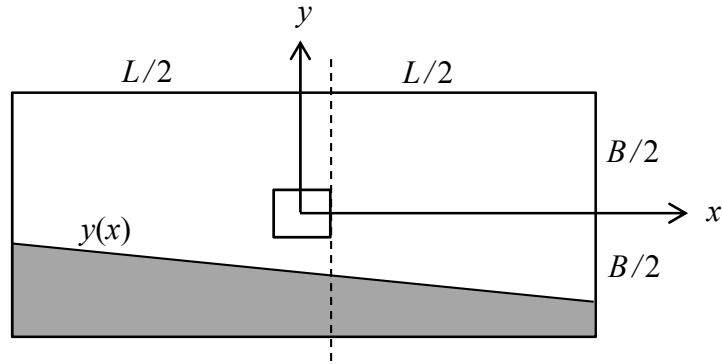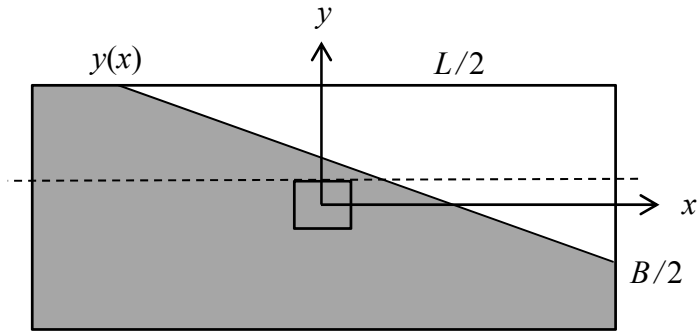
Figure 66. Critical Bending Section for Region D, *L*-Face.

In this case, the moment is computed as:

$$M_L = \int\limits_{\frac{b_{col}}{2}}^{\frac{B}{2}} \int\limits_{x(y)}^{\frac{L}{2}} q(x,y)\left(y - \frac{b_{col}}{2}\right) dx\, dy \tag{211}$$

Evaluating the integral in Equation (211) gives:

$$M_B = \frac{-q_3 L(\gamma-1)(B-b_{col})^2 \left(24(\eta B)^2 - 40\eta B^2 + 17B^2 - 8\eta b_{col}B + 6b_{col}B + b_{col}^2\right)}{384(\eta-1)^2 B^2} \tag{212}$$

4.2 Uniaxial Loading

If one of the eccentricities is zero, or there is only one applied moment along one of the principle axes; the spread footing is subjected to uniaxial loading and the biaxial loading formulations for structural mechanics simplify. For an eccentric loading condition where the eccentricity is within the kern and along the positive *x*-axis, the bearing pressures at Corners 1 and 4 will be equal and the bearing pressures at Corners 2

and 3 will be equal; that is, $q_1 = q_4$ will be the minimum compressive bearing pressure $q_{\min}$ and $q_2 = q_3$ will be the maximum compressive bearing pressure $q_{\max}$.

For an eccentric loading condition where the eccentricity is within the kern and along the positive x-axis, the two-way shear force in Equation (111) reduces to:

$$V_{punch} = P_u - \left(\frac{q_{max} + q_{min}}{2} \right)(b_{col} + d_a)^2 \tag{213}$$

The one-way shear force on the critical section parallel to the L-face of the footing in Equation (A1) reduces to

$$V_{one-way} = \left(\frac{q_{min} + q_{max}}{2} \right)L\left(\frac{B}{2} - \frac{b_{col}}{2} - d_a \right) \tag{214}$$

The one-way shear force on the critical section parallel to the B-face of the footing in Equation (A2) reduces to

$$V_{one-way} = \left(\frac{q_{d_a} + q_{max}}{2} \right)B\left(\frac{L}{2} - \frac{b_{col}}{2} - d_a \right) \tag{215}$$

where q_{d_a} is the value of the bearing pressure at the location d_a distance away from the face of the column in the L-direction, defined as:

$$q_{d_a} = q_{min} + \left(\frac{q_{max} - q_{min}}{L} \right)\left(\frac{L}{2} + \frac{b_{col}}{2} + d_a \right) \tag{216}$$

The moment on the critical section parallel to the *L*-face of the footing in Equation (115) can be expressed as

$$M_L = \frac{q_{min}L}{2}\left(\frac{B}{2} - \frac{b_{col}}{2}\right)^2 + \frac{(q_{max} - q_{min})L}{4}\left(\frac{B}{2} - \frac{b_{col}}{2}\right)^2 \qquad (217)$$

The moment on the critical section parallel to the *B*-face of the footing in Equation (117) can be expressed as

$$M_B = \frac{q_{col}B}{2}\left(\frac{L}{2} - \frac{b_{col}}{2}\right)^2 + \frac{(q_{max} - q_{col})B}{3}\left(\frac{L}{2} - \frac{b_{col}}{2}\right)^2 \qquad (218)$$

where q_{col} is the value of the bearing pressure at the face of the column parallel to the *B* direction:

$$q_{col} = q_{min} + \left(\frac{q_{max} - q_{min}}{L}\right)\left(\frac{L}{2} + \frac{b_{col}}{2}\right) \qquad (219)$$

For an eccentric loading condition where the eccentricity is within the kern and along the positive *y*-axis, the bearing pressures at Corners 1 and 2 will be equal and the bearing pressures at Corners 3 and 4 will be equal; that is, $q_1 = q_2$ will be the minimum compressive bearing pressure q_{min} and $q_3 = q_4$ will be the maximum compressive bearing pressure q_{max}.

For an eccentric loading condition where the eccentricity is within the kern and along the positive *y*-axis, the two-way shear force is given by Equation (213). Due to symmetry,

the one-way shear force on the critical section parallel to the *L*-face of the footing becomes

$$V_{one-way} = \left(\frac{q_{d_a} + q_{max}}{2}\right) L \left(\frac{B}{2} - \frac{b_{col}}{2} - d_a\right) \tag{220}$$

where q_{d_a} is the value of the bearing pressure at the location d_a distance away from the face of the column in the *B* direction, defined as:

$$q_{d_a} = q_{min} + \left(\frac{q_{max} - q_{min}}{B}\right)\left(\frac{B}{2} + \frac{b_{col}}{2} + d_a\right) \tag{221}$$

The one-way shear force on the critical section parallel to the *B*-face of the footing becomes

$$V_{one-way} = \left(\frac{q_{min} + q_{max}}{2}\right) B \left(\frac{L}{2} - \frac{b_{col}}{2} - d_a\right) \tag{222}$$

The moment on the critical section parallel to the *L*-face of the footing becomes

$$M_L = \frac{q_{col} L}{2}\left(\frac{B}{2} - \frac{b_{col}}{2}\right)^2 + \frac{(q_{max} - q_{col}) L}{3}\left(\frac{B}{2} - \frac{b_{col}}{2}\right)^2 \tag{223}$$

where q_{col} is the value of the bearing pressure at the face of the column, expressed as:

$$q_{col} = q_{min} + \left(\frac{q_{max} - q_{min}}{B} \right) \left(\frac{B}{2} + \frac{b_{col}}{2} \right) \tag{224}$$

The moment on the critical section parallel to the B dimension of the footing becomes:

$$M_B = \frac{q_{min}B}{2} \left(\frac{L}{2} - \frac{b_{col}}{2} \right)^2 + \frac{(q_{max} - q_{min})B}{4} \left(\frac{L}{2} - \frac{b_{col}}{2} \right)^2 \tag{225}$$

4.2.1 Corners 1 and 4 detached

If loading is on the positive x-axis, outside of the kern, then Corners 1 and 4 will become detached from the soil. The bearing pressures at Corners 2 and 3 are equal and they are the maximum bearing pressure q_{max} beneath the footing. When this occurs, the formulations for two-way shear, one-way shear, and moment at the critical sections within Region B will simplify since the percentage of detachments will be equal on the upper and lower L dimensions of the footing. Referring to Figure 17, the line of zero bearing pressure is vertical and α is the percentage of detachment along the L dimensions.

4.2.1.1 two-way shear. There are two cases of two-way shear that a spread footing may experience if detachment occurs when the load is along the positive x-axis. Both cases are simplifications of the two-way shear formulations for biaxial loading. If the line of zero bearing pressure does not intersect the critical two-way shear perimeter, Equation (147) simplifies to

$$V_{punch} = P_u - \frac{q_4 \left(b_{col} + d_a\right)^2 \left(2\alpha - 1\right)}{2\alpha} \qquad (226)$$

where q_4 represents the minimum bearing pressure q_{min} given in Equation (98).

Rearranging Equation (97) and substituting it into Equation (226) gives

$$V_{punch} = P_u - \frac{q_{max} \left(2\alpha - 1\right)\left(b_{col} + d_a\right)^2}{2\left(\alpha - 1\right)} \qquad (227)$$

If the line of zero bearing pressure intersects the critical two-way shear perimeter, Equation (152) simplifies to

$$V_{punch} = P_u + \frac{q_4 \left(b_{col} + d_a\right)\left(L + b_{col} + d_a - 2\alpha L\right)^2}{8\alpha L} \qquad (228)$$

where q_4 represents the minimum bearing pressure q_{min} given in Equation (98).

Rearranging Equation (97) and substituting it into Equation (228) gives:

$$V_{punch} = P_u - \frac{q_{max} \left(b_{col} + d_a\right)\left(L + b_{col} + d_a - 2\alpha L\right)^2}{8\left(1 - \alpha\right)L} \qquad (229)$$

4.2.1.2 one-way shear. For one-way shear on the *B*-face of the footing, there are two cases for which the line of zero bearing pressure may interact with the critical one-way shear section. If the line of zero bearing pressure does not intersect the critical section for one-way shear, Equation (158) simplifies to

$$V_{one-way} = \frac{q_4 B \left(b_{col} - L + 2d_a\right)\left(3L + b_{col} + 2d_a - 4\alpha L\right)}{8\alpha L} \tag{230}$$

where q_4 represents the minimum bearing pressure q_{min} given in Equation (98).

Rearranging Equation (97) and substituting it into Equation (230) gives:

$$V_{one-way} = \frac{q_{max} B \left(b_{col} - L + 2d_a\right)\left(3L + b_{col} + 2d_a - 4\alpha L\right)}{8\left(\alpha - 1\right)L} \tag{231}$$

If the line of zero bearing pressure is beyond the critical section for one-way shear, Equation (162) simplifies to:

$$V_{one-way} = \frac{-q_4 BL \left(\alpha^2 - 2\alpha + 1\right)}{2\alpha} \tag{232}$$

Rearranging Equation (97) and substituting it into Equation (232) gives:

$$V_{one-way} = \frac{q_{max} BL \left(1 - \alpha\right)}{2} \tag{233}$$

For one-way shear on the L-face of the footing, there is only one case for which the line of zero bearing pressure may interact with the critical one-way shear section. Equation (A11) simplifies to:

$$V_{one-way} = \frac{q_4 L \left(\alpha - 1\right)^2 \left(b_{col} - B + 2d_a\right)}{4\alpha} \tag{234}$$

114

Rearranging Equation (97) and substituting it into Equation (234) gives:

$$V_{one-way} = \frac{q_{max}L(\alpha-1)(b_{col}-B+2d_a)}{4} \tag{235}$$

4.2.1.3 flexure. As with one-way shear, there are two cases for which the line of zero bearing pressure may interact with the critical one-way shear section on the B-face of the footing. If the line of zero bearing pressure does not intersect the critical section for bending, Equation (165) simplifies to:

$$M_B = \frac{-q_4 B(L-b_{col})^2(5L+b_{col}-6\alpha L)}{48\alpha L} \tag{236}$$

Rearranging Equation (97) and substituting it into Equation (236) gives:

$$M_B = \frac{q_{max}B(L-b_{col})^2(5L+b_{col}-6\alpha L)}{48(1-\alpha)L} \tag{237}$$

If the line of zero bearing pressure is beyond the critical section for bending, Equation (A12) simplifies to:

$$M_B = \frac{-q_4 BL(\alpha-1)^2(L-3b_{col}+2\alpha L)}{12\alpha} \tag{238}$$

Rearranging Equation (97) and substituting it into Equation (238) gives:

$$M_B = \frac{q_{max}BL(1-\alpha)(L-3b_{col}+2\alpha L)}{12}$$

(239)

For bending on the *L*-face of the footing, there is only one case for which the line of zero bearing pressure may interact with the critical one-way shear section. Equation (A13) simplifies to:

$$M_L = \frac{-q_4 L(\alpha-1)^2 (B-b_{col})^2}{16\alpha}$$

(240)

Rearranging Equation (97) and substituting it into Equation (240) gives:

$$M_L = \frac{q_{max}L(1-\alpha)(B-b_{col})^2}{16}$$

(241)

4.2.2 Corners 1 and 2 detached

If loading is on the positive *y*-axis, outside of the kern, then Corners 1 and 2 will become detached from the soil. The bearing pressures at Corners 3 and 4 are equal and they are the maximum bearing pressure q_{max} beneath the footing. When this occurs, the formulations for two-way shear, one-way shear, and moment at the critical sections within Region C will simplify since the percentage of detachments will be equal on the left and right *B* dimensions of the footing. Referring to Figure 18, the line of zero bearing pressure is horizontal and β is the percentage of detachment along the *B* dimensions.

4.2.2.1 two-way shear. There are two cases of two-way shear that a spread footing may experience if detachment occurs when the load is along the positive *y*-axis. Both cases are simplifications of the two-way shear formulations for biaxial loading. If the line of zero bearing pressure does not intersect the critical two-way shear perimeter, Equation (174) simplifies to

$$V_{punch} = P_u - \frac{q_2 \left(b_{col} + d_a\right)^2 \left(2\beta - 1\right)}{2\beta} \tag{242}$$

where q_2 represents the minimum bearing pressure q_{min} given in Equation (102). Rearranging Equation (101) and substituting it into Equation (242) gives:

$$V_{punch} = P_u - \frac{q_{max} \left(2\beta - 1\right)\left(b_{col} + d_a\right)^2}{2\left(\beta - 1\right)} \tag{243}$$

If the line of zero bearing pressure intersects the critical two-way shear perimeter, Equation (178) simplifies to

$$V_{punch} = P_u + \frac{q_2 \left(b_{col} + d_a\right)\left(B + b_{col} + d_a - 2\beta B\right)^2}{8\beta B} \tag{244}$$

where q_2 represents the minimum bearing pressure q_{min} given in Equation (102). Rearranging Equation (101) and substituting it into Equation (244) gives:

$$V_{punch} = P_u - \frac{q_{max}(b_{col} + d_a)(B + b_{col} + d_a - 2\beta B)^2}{8(1-\beta)L} \tag{245}$$

4.2.2.2 one-way shear. For one-way shear on the *L*-face of the footing, there are two

cases for which the line of zero bearing pressure may interact with the critical one-way

shear section. If the line of zero bearing pressure does not intersect the critical section for

one-way shear, Equation (186) simplifies to

$$V_{one-way} = \frac{q_2 L(b_{col} - B + 2d_a)(3B + b_{col} + 2d_a - 4\beta B)}{8\beta B} \tag{246}$$

where q_2 represents the minimum bearing pressure q_{min} given in Equation (102).

Rearranging Equation (101) and substituting it into Equation (246) gives:

$$V_{one-way} = \frac{q_{max} L(b_{col} - B + 2d_a)(3B + b_{col} + 2d_a - 4\beta B)}{8(\beta - 1)B} \tag{247}$$

If the line of zero bearing pressure is beyond the critical section for one-way shear,

Equation (190) simplifies to:

$$V_{one-way} = \frac{-q_2 BL(\beta^2 - 2\beta + 1)}{2\beta} \tag{248}$$

Rearranging Equation (101) and substituting it into Equation (248) gives:

$$V_{one-way} = \frac{q_{max}BL(1-\beta)}{2} \tag{249}$$

For one-way shear on the B-face of the footing, there is only one case for which the line of zero bearing pressure may interact with the critical one-way shear section. Equation (A15) simplifies to:

$$V_{one-way} = \frac{q_2 B(\beta-1)^2 (b_{col} - L + 2d_a)}{4\beta} \tag{250}$$

Rearranging Equation (101) and substituting it into Equation (250) gives:

$$V_{one-way} = \frac{q_{max}B(\beta-1)(b_{col} - L + 2d_a)}{4} \tag{251}$$

4.2.2.3 flexure. As with one-way shear, there are two cases for which the line of zero bearing pressure may interact with the critical bending section on the L-face of the footing. If the line of zero bearing pressure does not intersect the critical section for bending, Equation (193) simplifies to:

$$M_L = \frac{-q_2 L(B - b_{col})^2 (5B + b_{col} - 6\beta B)}{48\beta B} \tag{252}$$

Rearranging Equation (101) and substituting it into Equation (252) gives:

$$M_B = \frac{q_{max}L(B-b_{col})^2(5B+b_{col}-6\beta B)}{48(1-\beta)B} \tag{253}$$

If the line of zero bearing pressure is beyond the critical section for bending, Equation (A19) simplifies to:

$$M_L = \frac{-q_2BL(\beta-1)^2(B-3b_{col}+2\beta B)}{12\beta} \tag{254}$$

Rearranging Equation (101) and substituting it into Equation (254) gives:

$$M_L = \frac{q_{max}BL(1-\beta)(B-3b_{col}+2\beta B)}{12} \tag{255}$$

For bending on the B-face of the footing, there is only one case for which the line of zero bearing pressure may interact with the critical one-way shear section. Equation (A18) simplifies to:

$$M_B = \frac{-q_2B(\beta-1)^2(L-b_{col})^2}{16\beta} \tag{256}$$

Rearranging Equation (101) and substituting it into Equation (256) gives:

$$M_B = \frac{q_{max}B(1-\beta)(L-b_{col})^2}{16}$$

(257)

4.3 Concentric Loading

During concentric loading, an applied force acts through the center of the footing. A constant, compressive bearing pressure q is developed beneath the footing, given by Equation (105). The two-way shear force in Equation (213) further reduces to:

$$V_{punch} = P_u - q(b_{col} + d_a)^2$$

(258)

The one-way shear force on the L face of the footing in Equation (214) further reduces to:

$$V_{one-way} = qL\left(\frac{B}{2} - \frac{b_{col}}{2} - d_a\right)$$

(259)

The one-way shear force on the B face of the footing in Equation (215) reduces to:

$$V_{one-way} = qB\left(\frac{L}{2} - \frac{b_{col}}{2} - d_a\right)$$

(260)

The moment on the critical section parallel to the *L*-face of the footing in Equation (217) reduces to:

$$M_L = \frac{qL}{2}\left(\frac{B}{2} - \frac{b_{col}}{2}\right)^2 \qquad (261)$$

The moment on the critical section parallel to the *B*-face of the footing in Equation (218) reduces to:

$$M_B = \frac{qB}{2}\left(\frac{L}{2} - \frac{b_{col}}{2}\right)^2 \qquad (262)$$

4.4 Summary

Governing equations are developed to calculate the two-way shear force, one-way shear force, and bending moments at critical sections in a reinforced concrete spread footing. The spread footing may be subjected to biaxial, or uniaxial uplift, as well as concentric loading. The bearing pressure surface beneath a spread footing was developed using a rectangular element with associated interpolation functions.

CHAPTER 5

DESIGN METHODOLOGY

Economical design has always been central in the practice of engineering. More recently, sustainable design has gained interest in engineering practice. As the annual emissions of carbon dioxide (CO_2) have grown by about 80% since 1970 and were estimated to be 77% of total anthropogenic greenhouse gas emissions in 2004 (UNIPCC 2007), the consideration of CO_2 emissions in structural concrete design has become a prudent area of research. Large emissions of CO_2 are produced during the manufacturing of Portland cement, the principal binder used in concrete. Due to these large CO_2 productions, efforts have been made to design concrete structures that are more sustainable. A detailed method for developing low-cost and low-CO_2-emission designs of reinforced concrete spread footings is relatively new (Wang and Kulhawy 2008, Wang 2009, Khajehzadeh et al. 2011, and Camp and Assadollahi 2013). In addition, there has been no investigation into the comparison of footing designs based on simplified analysis procedures with theoretical analysis procedures for low-cost and low-CO_2 emissions, subjected to biaxial bending, which consider all of the geotechnical and structural limit states.

In practice, there are many simplified analysis procedures that yield conservative design results. If cost or CO_2 emissions are not of significant concern to the design engineer, then applying simplified analysis procedures is acceptable. However; if the material and construction costs or CO_2 emissions of the spread footing are of significant concern, using simplified analysis procedures that yield over-designed footings and result in increased costs and CO_2 emissions may not be desired. The theoretical analysis

123

procedures presented in Chapters 3 and 4 for the analysis of spread footings subjected to biaxial bending more accurately describe the bearing pressure distribution beneath the footing and do not yield over-designed spread footings that result in increased costs and CO_2 emissions.

When designing a reinforced spread footing, both geotechnical and structural limit states must be considered. Geotechnical limit states are evaluated using service loads and include the bearing capacity of the surrounding geomaterial and the allowable settlement of the footing. Allowable Stress Design (ASD) is used for the evaluation of the geotechnical limit states. Structural limit states are evaluated based on Load Resistance Factor Design (LRFD) and include the shear capacity of the footing (one-way shear and two-way shear); the flexural capacity; the bearing capacity of the column, dowels, and footing; and development length requirements for the reinforcing. Structural limit states conform to the specifications prescribed by the American Concrete Institute building code 318-11 (ACI 2011) for structural concrete.

5.1 Simplified Analysis Procedures

In practice, several simplified structural analysis procedures can be implemented for footings subjected to eccentric loading that will yield over-designed footings. For the purposes of this research, five of these simplified analysis procedures are considered:

1) The two-way (punching) shear force through the footing is taken as the applied factored axial load,

2) The one-way shear force through the footing due to the soil pressure is calculated by assuming that the maximum bearing pressure is constant across the entire footing and is computed using Equation (1),

3) The moment produced at the face of the column due to the soil pressure is calculated by assuming that the maximum bearing pressure is constant,

4) The development length of the flexural steel is the entire length of each direction of the footing less the clear cover distance,

5) Eccentricities outside of the kern area are not permitted.

Taking the two-way shear force V_{punch} as the factored column load, the two-way shear force through the footing is

$$V_{punch} = P_u \tag{263}$$

where P_u is the factored column load given by Equation (106). The shear stress v_{punch} transferred to the footing by the combined two-way shear force and moment is computed as

$$v_{punch} = \frac{V_{punch}}{b_p d_a} + \frac{\gamma_v M_u \left(\dfrac{b_{col} + d_a}{2} \right)}{J_c} \tag{264}$$

where γ_v is the fraction of the moment that is transferred by shear stress on the critical shear perimeter, given in ACI 318-11, M_u is the factored moment transmitted from the column, and J_c is the polar moment of inertia of the critical shear perimeter. For biaxial loading, v_{punch} calculations are made for each principal direction and superimposed.

Recall that the critical plane in which one-way shear occurs is at a distance d_a away from the face of the column. By assuming that the bearing pressure distribution is

constant, with a value of q_{max}, the one-way shear on the critical plane parallel to the L-face is computed as:

$$V_{one-way} = q_{max} L \left(\frac{B}{2} - \frac{b_{col}}{2} - d_a \right)$$

(265)

The one-way shear on the critical plane and parallel to the B-face of the footing is computed as:

$$V_{one-way} = q_{max} B \left(\frac{L}{2} - \frac{b_{col}}{2} - d_a \right)$$

(266)

The critical sections for bending are located along the face of the column in both of the dimensions L and B. By assuming that the bearing pressure distribution is constant, with a value of q_{max}, the moment on the critical section parallel to the L-face of the footing is computed as:

$$M_L = q_{max} \frac{L}{2} \left(\frac{B}{2} - \frac{b_{col}}{2} \right)^2$$

(267)

The moment on the critical section parallel to the B-face of the footing is computed as:

$$M_B = q_{max} \frac{B}{2} \left(\frac{L}{2} - \frac{b_{col}}{2} \right)^2$$

(268)

Based on the calculated shear and moment values from these simplified analysis procedures, the size of the footing and reinforcement requirements are determined. While a conservatively-designed foundation provides additional safety against ultimate limit state and service limit state failures, there is an associated increase in both cost and CO_2 emissions for the extra materials and labor. Depending on the overall cost or acceptable CO_2 emissions of the project, the extra cost and emissions of CO_2 may not be of consequence; however, for projects with small budgets or ones striving to be environmentally friendly, the additional cost and emissions might be undesirable

5.2 Geotechnical Limit States

For a spread footing of length L, width B (where L > B), thickness H, and depth of penetration D, the bearing capacity limit state of the soil is defined by the factor of safety. For bearing capacity analysis on an eccentrically loaded spread footing, the effective area method is used (Meyerhof 1953), in which effective footing dimensions are calculated such that the applied load will act through the center of the equivalent footing area, producing a uniform bearing pressure distribution over the equivalent footing area. The equivalent dimensions B' and L' are defined, respectively, as:

$$B' = \min(L - 2e_x, \ B - 2e_y) \tag{269}$$

$$L' = \max(L - 2e_x, \ B - 2e_y) \tag{270}$$

If the footing is subjected to concentric loading, then e_x and e_y are zero and the effective dimensions are equal to the actual footing dimensions. The equivalent bearing pressure q_{equiv} is:

$$q_{equiv} = \frac{P+W_f}{B'L'} \tag{271}$$

The factor of safety against soil bearing capacity failure FS_B is

$$FS_B = \frac{q_{ult}}{q_{equiv}} \tag{272}$$

where q_{ult} is the ultimate bearing capacity of the footing. For a cohesionless soil with no ground slope and an internal angle of friction ϕ', the bearing capacity is calculated as (Vesic 1975)

$$q_{ult} = \gamma D N_q F_{qs} F_{qd} + 0.5 \gamma B' N_\gamma F_{\gamma s} F_{\gamma d} \tag{273}$$

where γ is the unit weight of the soil. The bearing capacity factors N_q and N_γ, as well as the shape and depth factors F_{qs}, $F_{\gamma s}$, F_{qd}, and $F_{\gamma d}$ are given as:

$$N_q = e^{\pi \tan(\phi')} \tan^2\left(\frac{\pi}{4} + \frac{\phi'}{2}\right) \tag{274}$$

$$N_\gamma = 2(N_q + 1)\tan\phi' \tag{275}$$

$$F_{qs} = 1 + \frac{B'}{L'}\tan\phi' \tag{276}$$

$$F_{\gamma s} = 1 - 0.4\frac{B'}{L'} \tag{277}$$

$$F_{qd} = \begin{cases} 1+2\tan\phi'\left(1-\sin\phi'\right)^2\left[\arctan\left(\dfrac{D}{\min(B_1,\ B_2)}\right)\right] & \text{if} \quad D > \min(B_1,\ B_2) \\[4mm] 1+2\tan\phi'\left(1-\sin\phi'\right)^2\left(\dfrac{D}{\min(B_1,\ B_2)}\right) & \text{if} \quad \text{otherwise} \end{cases} \tag{278}$$

$$F_{\gamma d} = 1.0 \tag{279}$$

The second geotechnical limit state to be considered is settlement of the spread footing. For a cohesionless soil with a sufficiently deep ground water level, only the immediate settlement is considered. The settlement δ is calculated using the elastic solution given by Poulos and Davis (1974)

$$\delta = \frac{(P+W_f)(1-\mu^2)}{\beta_z E\sqrt{BL}} \tag{280}$$

where μ is the Poisson ratio and E is the modulus of elasticity of the soil. The shape factor β_z was developed by Whitman and Richart (1967) as:

$$\beta_z = -0.0017\left(\frac{L}{B}\right)^2 + 0.0597\left(\frac{L}{B}\right) + 0.9843 \tag{281}$$

Immediate rotational settlement also occurs due to the moment loading. The angle of rotation that the column-footing connection experiences is calculated using the elastic solution given by Poulos and Davis (1974) due to the moment M applied in either the L or B direction. For moment loading in the L direction, the angle of rotation is given as

$$\phi = \frac{M(1-\mu^2)}{L^2 BE} I_\theta \qquad (282)$$

where I_θ is an influence factor developed by Whitman and Richart (1967) and interpreted in this study as:

$$I_\theta = \begin{cases} 0.9411 \ \ln\left(\dfrac{B}{L}\right) + 3.7937 & \text{if} \quad 4L > B \\ 5.1 & \text{if} \quad \text{otherwise} \end{cases} \qquad (283)$$

Corresponding formulations are used to compute rotational settlement for moment loading in the *B*-direction.

5.3 Structural Limit States

Structural limit states include the shear capacity of the footing (one-way shear and two-way shear); the flexural capacity; the bearing capacity of the column, dowels, and footing; and development length requirements for the reinforcing. The structural limit states conform to the specifications prescribed by the American Concrete Institute building code 318-11 (ACI 2011) for structural concrete.

For spread footing design, ACI 318-11 provides capacity equations for two-way shear, one-way shear, flexure, and bearing. The two-way shear strength $v_{n,punch}$ is calculated as

$$v_{n,punch} = \phi \min \begin{cases} 0.17\left(1+\dfrac{2}{\beta}\right)\kappa\sqrt{f_c'} \\[2em] 0.083\left(\dfrac{40d_a}{b_p}+2\right)\kappa\sqrt{f_c'} \\[2em] 0.33\kappa\sqrt{f_c'} \end{cases} \tag{284}$$

where β is the ratio of the long side to the short side of the column (ACI 318-11, 11.11.2.1), ϕ is the nominal strength coefficient ($\phi = 0.75$ per ACI 318-11), κ is a factor representing the type of concrete ($\kappa = 1.0$ for normal weight concrete), and f_c' is the compressive strength of the concrete.

The one-way shear strength $V_{n,one-way}$ in either the long or short dimension is

$$V_{n,one-way} = \phi\left(0.17\,w\,d_a\,\kappa\sqrt{f_c'}\right) \tag{285}$$

where w is either B for the short dimension or L for the long dimension of the footing.

The flexural strength M_n is calculated for reinforcing steel in both the L-direction and B-direction. For reinforcing steel in the L-direction, the flexural strength is

$$M_n = \phi A_{s,L} f_y\left(d_L - 0.59\frac{A_{s,L} f_y}{B f_c'}\right) \tag{286}$$

where ϕ is the nominal strength coefficient (defined in section 9.3.2.2 of ACI 318-11), $A_{s,L}$ is the area of reinforcing steel in the L-direction, f_y is the tensile strength of the reinforcement, and d_L is the depth from the compression face of the footing to the

centroid of the reinforcement in the *L*-direction. For reinforcing steel in the *B*-direction, the flexural strength is

$$M_n = \phi A_{s,B} f_y \left(d_B - 0.59 \frac{A_{s,B} f_y}{L f_c'} \right) \tag{287}$$

where $A_{s,B}$ is the area of reinforcing steel in the *B*-direction and d_B is the depth from the compression face of the footing to the centroid of the reinforcement in the *B*-direction.

The reinforcement steel should be spaced appropriately in both directions of the footing. Minimum and maximum spacing requirements in the long and short directions of the footing conform to sections 7.6 and 13.3.2 of ACI 318-11. In addition, spacing in the short direction should conform to section 15.4.4.2 of ACI 318-11. The minimum amount of reinforcing steel defined by section 10.5.4 of ACI 318-11 is:

$$A_{s,min} = 0.0018wH \tag{288}$$

There is no required maximum steel reinforcing in ACI 318-11; however, there is a limitation that ensures the section be tension-controlled based upon the developed strain in the tension steel in both the *L* and *B* directions. The strain in the tension steel $\varepsilon_{s,L}$ in the *L*-direction is calculated as

$$\varepsilon_{s,L} = 0.003 \left(\frac{d_L - c_L}{c_L} \right) \tag{289}$$

where c_L is:

$$c_L = \frac{A_{s,L} f_y}{0.85 f'_c B \beta_1}$$

(290)

and β_1 is a factor relating the depth of the equivalent rectangular compressive stress block to the neutral axis depth given by section 10.2.7.3 of ACI 318-11. The strain in the tension steel $\varepsilon_{s,B}$ in the B-direction is calculated as

$$\varepsilon_{s,B} = 0.003 \left(\frac{d_B - c_B}{c_B} \right)$$

(291)

where c_B is:

$$c_B = \frac{A_{s,B} f_y}{0.85 f'_c L \beta_1}$$

(292)

The minimum development length l_d for all flexural steel reinforcing is defined as:

$$l_d = \frac{f_y \psi_s \psi_t \psi_e}{1.1 \lambda \sqrt{f'_c} \left(\frac{c_b + K_{tr}}{d_{bar}} \right)} d_{bar}$$

(293)

where ψ_s is the size factor, ψ_t is the traditional reinforcement location factor, ψ_e is a coating factor reflecting the effects of epoxy coating, λ is a factor reflecting the lower tensile strength of lightweight concrete, and d_{bar} is the diameter of the reinforcement bar. In this study, ψ_t, ψ_e, and λ are 1.0 and ψ_s is 0.8 for #6 bars and smaller and 1.0 for bars larger than #6. The c_b factor is the smaller of the distance from the center of a bar to the nearest concrete surface and one-half the center-to-center spacing of the bars being developed. The K_{tr} factor represents the contribution of confining reinforcement across potential splitting planes and is taken as zero.

The bearing strength of the concrete is also calculated for the base of the column and top of the footing based on sections 10.14 and 15.7 of ACI 318-11. The bearing strength P_b of the dowels and footing are calculated respectively as

$$P_{b,dowel} = \phi A_{s,dowel} f_y \tag{294}$$

$$P_{b,footing} = \phi 0.85 \, f_c'\left(b_{col}\right)^2 \sqrt{\frac{A_{proj}}{b^2_{col}}} \le \phi 1.7 \, f_c'\left(b_{col}\right)^2 \tag{295}$$

where ϕ is the nominal strength coefficient ($\phi = 0.65$ per ACI 318-11) and A_{proj} is the area of the lower base of the largest frustum of a pyramid, defined in section 10.14 of ACI 318-11. The minimum amount of steel required for the dowels is given in section 15.8.2.1 of ACI 318-11 as $0.005(b_{col})^2$.

The total bearing strength provided is:

$$P_b = P_{b,footing} + P_{b,dowel} \tag{296}$$

The development length of the dowels conforms to sections 12.3, 12.5, 12.16, and 15.8 of ACI 318-11. The development length of the dowels into the column $l_{d,dowel,col}$ is calculated as

$$l_{d,dowel,col} = \max(0.0005 f_y d_{dowel}, l_{d,col}) \tag{297}$$

where d_{dowel} is the diameter of the dowels. The development length of the column reinforcement $l_{d,col}$ is defined in ACI 318-11 as

$$l_{d,col} = \max\left(\frac{0.24 d_{col} f_y}{\sqrt{f_c'}}, \ 0.043 d_{col} f_y, \ 200\, mm \right) \tag{298}$$

where d_{col} is the diameter of the column bars. The development length of the dowels into the footing $l_{d,dowel}$ is defined by ACI 318-11 as:

$$l_{d,dowel} = \max\left(\frac{0.24 d_{dowel} f_y}{\sqrt{f_c'}}, \ 0.043 d_{dowel} f_y, \ 200\, mm \right) \tag{299}$$

Standard hooking of the dowels is provided based upon Sections 7.1 and 7.2 of ACI 318-11 and the added material cost of the bend diameters and extensions of the dowel hooks is computed. Placement of the dowels is not considered in this research.

5.4 Summary

In order for a spread footing to provide safety and stability for a superstructure, it must meet all geotechnical and structural limit states. Service loads are used for the geotechnical limit state analysis while factored loads are used for the structural limit state analysis. In order to provide added safety against structural limit state failure, simplified analysis procedures are commonly employed in practice. However, simplifications typically lead to increases in cost and CO_2 emissions. Theoretical analysis procedures presented in earlier chapters use a more realistic distribution of the bearing pressure surface and may be used to analyze a spread footing subjected to biaxial loading, without leading to increases in cost and CO_2 emissions.

CHAPTER 6

OPTIMIZATION

Mathematical optimization involves selecting the best value from a set of available alternatives. An optimization problem typically consists of minimizing or maximizing a function by systematically choosing input values from a set and computing the value of the function. Big Bang-Big Crunch (BB-BC) has been shown to be a computationally efficient heuristic method to solve a variety of mathematical and engineering optimization problems. Erol and Eksin (2006) proposed the original BB-BC algorithm, which involved exploiting the power of the mean using an abstract model of the lifecycle of the universe. In each "Big Bang" stage, a set of normally distributed solutions is generated about the weighted mean of the current solution population. After the solutions are evaluated, a "Big Crunch" stage computes a new center for the next "Big Bang" based on the fitness of the various solutions. Over successive cycles of Big Bangs and Big Crunches, the standard derivation of the normal distribution of new solutions decreases and the search tends to become more localized in the neighborhood of the best solution. When the average and/or the best solution cease to improve over a number of cycles, the optimization is assumed to have converged. Erol and Eksin (2006) established that a simple BB-BC algorithm can outperform enhanced and classic genetic algorithms (GA) for many benchmark optimization functions.

6.1 Objective Functions

Three objective functions are utilized in this research. The forms of the first two objective functions for this optimization are consistent with those presented by Wang and Kulhawy (2008). Both the cost objective function and the CO_2 emission objective

function include the cost of excavation, formwork, reinforcing steel, concrete, and compacted backfill. The values include material cost and associated cost for labor and installation.

The general form of the optimization problem is

$$\textit{Minimize:} \quad f_{cost} = \sum_{i=1}^{R} C_i u_i \left(x_1, x_2, ..., x_n \right) \quad \textit{or} \quad f_{CO_2} = \sum_{i=1}^{R} E_i u_i \left(x_1, x_2, ..., x_n \right) \tag{300}$$

$$\textit{Subject to:} \quad \sum_{j=1}^{N} p_j \left(x_1, x_2, ..., x_n \right) \le 0 \tag{301}$$

where f_{cost} is the cost function, f_{CO_2} is the CO_2 emission function, C_i are the unit costs, u_i is the amount of material and construction units, x_i are the design variables, n is the number of design variables, R is the number of material and construction units, E_i are the unit CO_2 emissions, p_j are penalty functions, and N is the number of penalty functions.

For all examples, cost and CO_2 fitness functions are defined, respectively, as

$$f_{cost} = C_e V_e + C_f A_f + \xi C_r M_r + \frac{f_c'}{f_{cmin}'} C_c V_c + C_b V_b \tag{302}$$

$$f_{CO_2} = E_e V_e + E_f A_f + \xi E_r M_r + \frac{f_c'}{f_{cmin}'} E_c V_c + E_b V_b \tag{303}$$

where C_e is the unit cost of excavation, C_f is the unit cost of formwork, C_r is the unit cost of reinforcement, C_c is the unit cost of concrete, C_b is the unit cost of backfill, E_e is the unit emission of excavation, E_f is the unit emission of formwork, E_r is the unit emission

of reinforcement, E_c is the unit emission of concrete, E_b is the unit emission of backfill, V_e is the volume of excavation, V_c is the volume of concrete, and V_b the volume of backfill. A_f is the area of formwork, and M_r is the mass of reinforcement. To help keep the cost and CO_2 emissions of concrete and steel comparable, a scale factor ξ is introduced. In addition, the impact of the strength of concrete is scaled using the minimum allowable strength of concrete f'_{cmin}.

Scale factors on the unit values for steel reinforcing and concrete help reflect the impact of design variables more equitably on related terms in the optimization fitness function. Three factors account for applying a scale factor to the unit values for concrete strength: (1) at moderate values of the applied load, the footing design is controlled by geotechnical considerations, where concrete strength is not influential; (2) calculations for flexural strength, shear strength, and development length are related to both reciprocal and square root functions of concrete strength; and (3) in the optimization formulation, the concrete strength design variable space is very small. A scale factor on concrete unit values that artificially increases the associated fitness value as concrete strength increases significantly improves the quality and reliability of the optimization. Numerical studies have shown that a scaling factor of $\xi = 10$ is adequate to artificially increase the magnitude of the fitness function term associated with unit values for steel reinforcement to the same order of magnitude as unit values for concrete and, more importantly, results in more consistent structural designs in terms of the size and number of rebars.

To gain better insight on the relationship between low-cost and low-CO_2 emission design, a multi-objective optimization is applied using the weighted aggregation (sum) approach. In general, this approach consists of adding all the single-objective functions

together using different weighting coefficients. Many applications of this method can be found in the literature. Coello (1999) presented a comprehensive survey of multi-objective optimization techniques, which includes a summary of the weighted aggregation approach, its applications, strengths, and weaknesses. Parsopoulos and Vrahatis (2002) present a detailed description of the weighted aggregation approach. Marler and Arora (2004) also present a survey of multi-objective optimization methods.

The general form of the weighted aggregation approach is given as

$$\textit{Minimize:} \quad f_{multi} = \sum_{h=1}^{m} \zeta_h f_h \left(x_1, x_2, \ldots, x_n \right) \tag{304}$$

$$\textit{Assuming:} \quad \sum_{h=1}^{m} \zeta_h = 1 \tag{305}$$

where f_{multi} is the multi-objective fitness function, ζ_h are non-negative weights, f_h are the single-objective fitness functions, and m is the number of weights.

For the multi-objective study, the fitness function is defined as

$$f_{multi} = \zeta f_{cost} + \left(1 - \zeta \right) f_{CO_2} \tag{306}$$

where ζ is a weighting factor that varies from 0 to 1.

6.2 Design Variables

Figure 67 shows the dimensions and design variables for a rectangular spread footing. In general, there are four geometric design variables representing the dimensions of the

footing: the long dimension of the footing is $L = x_{min, L} + X_1$ (the minimum dimension of the footing is assumed to be the larger of the column width b_{col} and $3e_x$), the short dimension is $B = x_{min, B} + X_2$ (the minimum dimension of the footing is assumed to be the larger of the column width b_{col} and $3e_y$), the depth from the ground surface to the bottom of the footing is $D = X_3$, and the thickness of the footing is $H = T_{min} + X_4$ (the minimum thickness of the footing is assumed to be T_{min} and is specified as the sum of 76.2 mm concrete cover below the reinforcement and 152.4 mm concrete cover above the reinforcement). There are six design variables related to the steel reinforcement of the various sections of the footing: R_1 is the bar number in the long direction of the footing, R_2 is the number of bars in the long direction of the footing, R_3 is the bar number in the short direction of the footing, R_4 is the number of bars in the short direction of the footing, R_5 is the bar number of the dowels, and R_6 is the number of dowels. One additional design variable S_1 represents the compressive strength of the concrete.
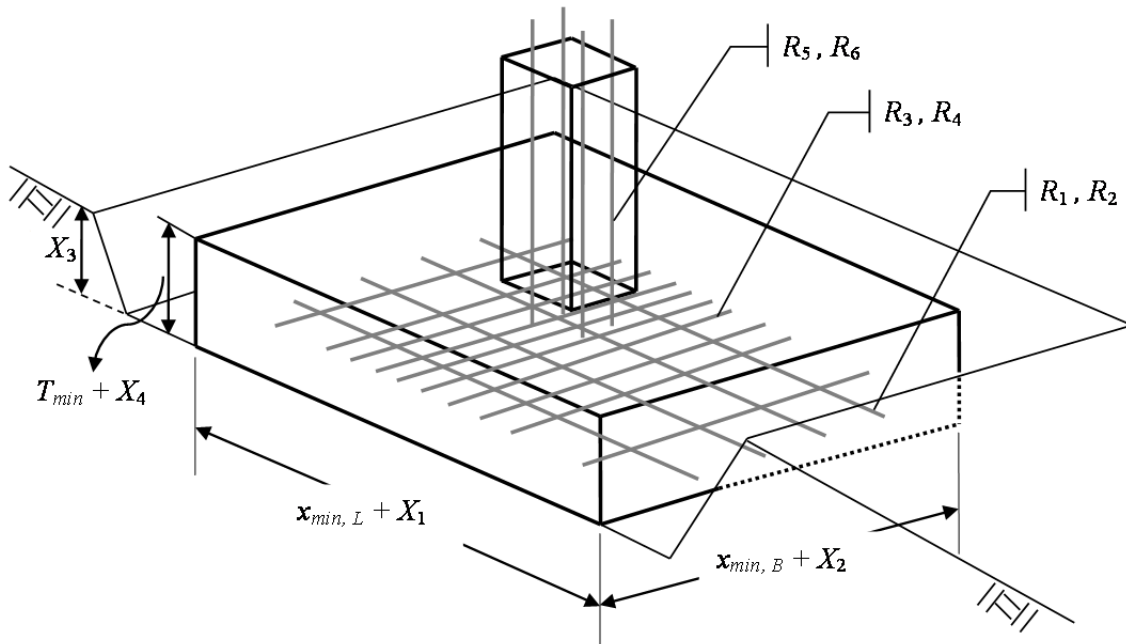
Figure 67. Reinforced Spread Footing Design Variables

6.3 Constraints

The typical design philosophy of shallow foundations seeks designs that provide safety and stability against geotechnical limit state failure and structural limit state failure. These requirements include stability of the geomaterial, concrete capacity, reinforcement configuration, and geometric limitations. Each design constraint is posed as a penalty on the objective function of the design and is non-zero only when violated. In other words, if the design is feasible, the sum of the constraint penalties will be zero. The general form of a penalty equation for minimum constraint values is:

$$p_{\min} = 1 - \frac{\text{constraint}}{\text{constraint}_{\min}} > 0 \tag{307}$$

The general form of a penalty equation for maximum constraint values is:

$$p_{max} = 1 - \frac{constraint_{max}}{constraint} > 0 \qquad (308)$$

Penalties are imposed for violations of: soil bearing capacity; vertical settlement; rotational settlement; two-way shear capacity; one-way shear capacity in both directions of the footing; moment capacity in both directions of the footing; minimum area of steel in both directions; tension steel strain in both directions; development length in both directions; development length of dowels; minimum and maximum dimensions based on spacing requirements; concrete bearing strength; and minimum and maximum depth of embedment of the footing in the soil.

The geotechnical limit state penalties are defined as

$$p_1 = 1 - \frac{FS_B}{FS_{min}} > 0 \qquad (309)$$

$$p_2 = 1 - \frac{\delta_{max}}{\delta} > 0 \qquad (310)$$

where FS_{min} is the minimum prescribed safety factor for bearing capacity and δ_{max} is the maximum allowable settlement.

The shear capacity of any reinforced concrete foundation should be greater than the ultimate shear force in the foundation. In the same way, moment capacities of footing sections should be greater than the design moments. The two-way shear capacity penalty

and the one-way shear capacity penalties for each of the footing dimensions B and L are summarized as:

$$p_{[3-5]} = 1 - \left(\frac{V_n}{V_u} \right) > 0 \qquad (311)$$

Moment capacity penalties in both dimensions of the footing may be summarized as:

$$p_{[6-7]} = 1 - \left(\frac{M_n}{M_u} \right) > 0 \qquad (312)$$

The amount of steel reinforcement in each direction of the footing must satisfy minimum limits required by ACI 318-11. Minimum reinforcement area penalties for each direction and for the dowels are defined as:

$$p_{[8-10]} = 1 - \left(\frac{A_s}{A_{s,min}} \right) > 0 \qquad (313)$$

For flexural design, if failure is to occur, it is desired that it be in tension. When the strain in the tension steel is less than 0.005, the section is no longer tension controlled. To ensure a tension-controlled section, tension steel strain penalties in each direction are defined as:

$$p_{[11-12]} = 1 - \left(\frac{\varepsilon_s}{0.005} \right) > 0 \qquad (314)$$

All footing sections must satisfy minimum requirements for the development length of steel reinforcement bars within the dimensions of the structure. The minimum basic development length is checked against the allowable space in the appropriate footing dimension (accounting for rebar size and concrete cover). All appropriate footing dimensions should accommodate the required development lengths for the reinforcement. The reinforcement development length penalties are summarized for each dimension of the footing; for the short dimension, the development length penalty is:

$$p_{13} = 1 - \frac{\left(\dfrac{B}{2} - \dfrac{b_{col}}{2} - cover\right)}{l_{d,short}} > 0 \tag{315}$$

For the long dimension, the development length penalty is:

$$p_{14} = 1 - \frac{\left(\dfrac{L}{2} - \dfrac{b_{col}}{2} - cover\right)}{l_{d,long}} > 0 \tag{316}$$

For the development length of dowels into the footing, a minimum footing thickness penalty is established as

$$p_{15} = 1 - \left(\frac{H}{2\,cover + d_{b,long} + d_{b,short} + d_{bend}/2 + d_{dowel} + l_{d,dowel}}\right) > 0 \tag{317}$$

where d_{bend} is the bend diameter of the hooked dowels, defined in section 7.2 of ACI 318-11.

In general, the spacing of the reinforcing bars must meet minimum and maximum requirements s_{min} and s_{max} in the long direction, the center band of the short direction, and the outer bands of the short direction. To address spacing criteria, additional geometric penalties are established to prevent infeasible footing dimensions. The minimum dimension penalty for the B-dimension is defined as

$$p_{16} = 1 - \left(\frac{B}{2\,cover + n_{bars,L}\,d_L + \left(n_{bars,L} - 1\right)s_{min,L}} \right) > 0 \qquad (318)$$

where $n_{bars,L}$ and $s_{min,L}$ are the number of bars and minimum bar spacing in the L-direction, respectively. The minimum dimension penalty for the L-dimension is defined as

$$p_{17} = 1 - \left(\frac{L}{2\,cover + n_{bars,B}\,d_B + \left(n_{bars,B} - 1\right)s_{min,B}} \right) > 0 \qquad (319)$$

where $n_{bars,B}$ and $s_{min,B}$ are the number of bars and minimum bar spacing in the B-direction, respectively.

The maximum dimension penalty for the B-dimension is defined as

$$p_{18} = 1 - \left(\frac{2\,cover + d_L + \left(n_{bars,L} - 1\right)s_{max.L}}{B} \right) > 0 \qquad (320)$$

146

where $s_{max,L}$ is the maximum bar spacing in the L-direction. The maximum dimension penalty for the L-dimension is defined as

$$p_{19} = 1 - \left(\frac{2\,cover + d_B + \left(n_{bars,B} - 1\right)s_{max,B}}{L} \right) > 0 \qquad (321)$$

where $s_{max,B}$ is the maximum bar spacing in the B-direction.

The concrete bearing strength penalty is:

$$p_{20} = 1 - \frac{P_b}{P_u} > 0 \qquad (322)$$

The depth of the footing must not be less than a minimum value defined by the frost depth and must not be greater than a maximum value that delineates a shallow foundation. The footing depth penalties are given as

$$p_{21} = 1 - \frac{D_{max}}{D} > 0 \qquad (323)$$

$$p_{22} = 1 - \frac{D}{D_{min}} > 0 \qquad (324)$$

where D_{max} is the maximum allowable depth of the footing to be considered a shallow foundation (equal to four times the shorter plan dimension) and D_{min} is equal to the depth of frost, taken as 0.3 m for this study. Additional geometric constraints are developed to

147

prevent infeasible footing designs due to the calculation of negative punching shear, one-way shear, and development lengths.

An additional penalty is developed for footing designs using the simplified analysis procedures. This penalty does not allow for footing detachment from the soil, as this is typically not allowed in practice. Based upon the kern, this penalty is given as:

$$p_{23} = 1 - \frac{BL}{6\left(Le_y + Be_x\right)} > 0$$ (325)

A penalty function is used to enforce each penalty p_j on the objective function. The penalty Φ_k for a candidate low-cost or low-CO_2 emission design k is a function of the summation of the all of the penalties and is defined as

$$\Phi_k = \left(1 + \sum_{j=1}^{m} p_j\right)^{\Omega}$$ (326)

where m is the total number of penalties and Ω is a positive penalty exponent (typically > 1). The penalized objective function F_k is a product of either the cost or the CO_2 objective function of candidate design k and its total penalty:

$$F_k = \Phi_k f_k$$ (327)

The penalty function imposes a numerical penalty on the value of the objective function that tends to reflect the degree to which the constraints are violated by a candidate set of design variables.

6.4 Big Bang-Big Crunch Optimization

Erol and Eksin (2006) developed BB-BC optimization from an abstract model of the lifespan of the universe. In their model, each Big Bang stage of the process simulates the dissipation of energy by transforming ordered space to a randomly distributed space. This is followed by a Big Crunch stage where space contracts about a center of mass. Over successive cycles of Big Bangs and Big Crunches, the overall search space decreases and becomes localized about the best solution.

In the initial Big Bang stage, solution variables are uniformly randomly distributed throughout the search space; this step is nearly identical to other evolutionary methods in that an initial population of candidate solutions is generated randomly over the range of the search space. Next, during the contraction of the Big Crunch stage, a center of mass $\vec{x}_{cm}$ is computed from the initial population using penalized objective function values

$$\vec{x}_{cm} = \frac{\sum_{k=1}^{NC} \frac{\vec{x}_k}{F_k}}{\sum_{k=1}^{NC} \frac{1}{F_k}} \tag{328}$$

where $\vec{x}_k$ is the position of candidate k in an n-dimensional search space and NC is the candidate population size.

For the subsequent iterations of the Big Bang stage, new candidate solution positions $\vec{x}_k^{new}$ are normally distributed around the center of mass by

$$\vec{x}_k^{new} = \vec{x}_{cm} + \vec{\sigma} \tag{329}$$

where $\vec{\sigma}$ is a vector of standard deviations for each normal distribution computed as

$$\vec{\sigma} = \frac{r\,\tau\left(\vec{x}_{max} - \vec{x}_{min}\right)}{n_{cycle}} \tag{330}$$

where r is a random number from a standard normal distribution, τ is a parameter limiting the size of the search space, $\vec{x}_{max}$ and $\vec{x}_{min}$ are the upper and lower limits on the values of the design variables, and n_{cycle} is the number of Big Bang iterations. The size of the search space available for new candidate $\vec{x}_k^{new}$ positions decreases inversely with the number of completed Big Bang iterations.

For discrete variables, the continuous values maybe rounded to the nearest integer value:

$$\vec{x}_k^{new} = ROUND\left(\vec{x}_{cm} + \frac{r\,\tau\left(\vec{x}_{max} - \vec{x}_{min}\right)}{n_{cycle}}\right) \tag{331}$$

Depending on where the center of mass is located in the search space, especially during early cycles of the algorithm, it is possible to generate a design variable value that is

150

outside the prescribed range. In this case, values that lie outside the search space limits are reset to the appropriate minimum/maximum values (Erol and Eksin 2006).

Both Camp (2007) and Kaveh and Talatahari (2010) developed hybrid formulations that not only use the center of mass, but weighted values of the local best solution and the global best solution to compute the mean of the Big Bang. The local best solution is the best solution in a given cycle. The global best solution is the overall best unpenalized solution found from all previous cycles. A modified version of Equation (329) is given as:

$$\vec{x}_k^{new} = \omega_1 \vec{x}_{cm} + (1 - \omega_1) \left[\omega_2 \vec{x}_l^{best} + (1 - \omega_2) \vec{x}_g^{best} \right] + \frac{r\tau (\vec{x}_{max} - \vec{x}_{min})}{n_{cycle}} \qquad (332)$$

where ω_1 and ω_2 are values in the range [0, 1] that weight the influence of the local best solution $\vec{x}_l^{best}$ and the global best solution $\vec{x}_g^{best}$ on the center of mass of new population positions. Since normally distributed numbers can exceed ±1, it is necessary to limit candidate positions to the prescribed search space boundaries. As a result of this contraction, there may be an accumulation of candidate solutions at the search space boundaries (Erol and Eksin 2006).

For structural optimization, Camp (2007) and Kaveh and Talatahari (2009 and 2010) have shown that there is a significant improvement in the quality of the solution and the computational efficiency of the BB-BC algorithm using formulations similar to Equation (332) over the original model developed by Erol and Eksin (2006).

The BB-BC method used here also employs a two-phase search procedure. Unlike traditional BB-BC algorithms, during Phase 1 the initial random search Big Bang stage is

repeated until the local best solution $\vec{x}_l^{best}$ has an acceptable minimum penalty. Once a pseudo-feasible solution is found, the Big Crunch stage is initiated. Phase 1 is completed when the global best solution $\vec{x}_g^{best}$ has not improved over a number of consecutive Big Bang cycles; with this condition reached, the algorithm is considered to have converged to a solution. The global best solution $\vec{x}_g^{best}$ is limited to candidates that are feasible, in other words, designs that have no penalty applied to their objective function values. In Phase 2, a local search space is defined in the immediate neighborhood around $\vec{x}_g^{best}$ from Phase 1 and a new search is initiated. A new set of candidate solutions $\vec{x}_k^{new}$ are randomly generated within the local search space with $\vec{x}_g^{best}$ from Phase 1 either being retained or reset. Phase 2 uses the same convergence criteria as Phase 1. The BB-BC optimization parameters include the size of the candidate solution population; values of τ, ω_1 and ω_2 required for Equation (332); the penalty function exponent; the search space reduction factor used for a multi-phase search; and the algorithm stopping criteria.

6.5 Summary

A modified BB-BC algorithm is applied to the analysis and design of spread footings subjected to biaxial, uniaxial, or concentric loading. Cost and CO_2 emission functions are considered as single objective functions, while the weighted aggregate of the cost and CO_2 emission functions is considered as a multi-objective function to gain better insight on the relationship between cost and CO_2 emissions.

CHAPTER 7

OPTIMIZATION DESIGN EXAMPLES

Design examples are presented to investigate the impacts of cost and CO_2 emissions on spread footing designs. The first set of design examples considers concentric loading, the second set considers uniaxial loading, and the third set considers biaxial loading. The BB-BC optimization procedure is applied to find the best low-cost and low-CO_2 emission footing designs, subjected to geotechnical and structural limit states, using the formulations developed in Chapters 3 and 4.

Table 1 and Table 2 list the unit costs and unit CO_2 emissions used in Equation (302), the cost fitness function, and Equation (303), the CO_2 fitness function. Table 1 lists unit cost values, based on costs for raw material and labor (Wang and Kulhawy 2008), and unit emission values, based on extraction and the transportation of raw materials; processing, manufacturing, and fabrication of products and machinery; and the emissions of equipment involved in the construction process (Yepes et al. 2012). Concrete unit cost values are scaled to match the costs presented by Wang and Kulhawy (2008) at $f'_c = 27.6$ MPa. CO_2 emissions are estimated from concrete proportions and emissions data on cement works, crushed rock, sand, and ready-mixed concrete production (MPA 2010). Table 2 lists the unit cost and CO_2 emission values for concrete based upon compressive strength, estimated by Camp and Assadollahi (2013).

For all design examples, the volume of excavation V_e, area of formwork A_f, volume of concrete V_c, and volume of backfill V_b, used in Equations (302) and (303), are computed in the same manner. The volume of excavation V_e is calculated as

$$V_e = (B + B_0)(L + L_0)D \qquad (333)$$

where B_0 and L_0 are the over-excavation lengths long the B and L dimensions of the footing. The area of formwork A_f is calculated as:

$$A_f = 2H(B + L) \qquad (334)$$

The volume of concrete V_c is calculated as

$$V_c = BLH - V_r \qquad (335)$$

where V_r is the volume of reinforcement. If $H \geq D$, there is no backfill above the footing and the volume of compacted backfill V_b is

$$V_b = \left[(B + B_0)(L + L_0) - BL \right] D \qquad (336)$$

otherwise:

$$V_b = V_e - \left[BLH + b_{col}^2 (D - H) \right] \qquad (337)$$

154

Unless otherwise specified, the mass of reinforcement M_r is calculated based on the total volume of reinforcement and the density of steel, which is taken as 7,850 kg/m^3.

As the value of the penalty function exponent Ω increases in Equation (326), the penalty for a given candidate design increases. In Phase 1 of the BB-BC algorithm, if $\Omega > 2$, the search tends to be more exploitive and less explorative, generating solutions that, while feasible, are too costly to be considered good designs. For all the spread footing design examples, $\Omega = 2$ in both Phase 1 and Phase 2.

Table 1. Unit Cost and CO_2 Values

Input parameter	Unit	Symbol	Value
Cost of excavation	$/m^3	C_e	25.16
Cost of concrete formwork	$/m^2	C_f	51.97
Cost of reinforcement	$/kg	C_r	2.16
Cost of compacted backfill	$/m^3	C_b	3.97
CO_2 emission for excavation	kg/m^3	E_e	13.16
CO_2 emission for concrete formwork	kg/m^2	E_f	14.55
CO_2 emission for reinforcement	kg/kg	E_r	3.02
CO_2 emission for compacted backfill	kg/m^3	E_b	27.20

Table 2. Unit Cost and CO_2 Values for Concrete

Compressive Strength of Concrete (MPa)	Unit Cost Value ($/m^3$)	Unit CO_2 Value (kg/m^3)
20	169.13	214.09
25	173.14	240.33
30	177.42	268.36
35	182.41	301.01
40	188.53	341.09
45	196.23	391.43
50	205.92	454.86
55	218.05	534.21

7.1 Concentric Loading

Two design examples considering concentric loading are presented. The first example, originally developed by Wang and Kulhawy (2008), did not consider the ACI 318-11 requirements for structural concrete (i.e. one-way and two-way shear capacity of the footing; the flexural capacity; the bearing capacity of the column, dowels, and footing; and development length requirements). The objective in presenting the first example is to compare the low-cost designs of the BB-BC algorithm, using both continuous-variable and discrete-variable formulations, to those of Wang and Kulhawy (2008) and develop companion low-CO_2-emission designs. The purpose of using both continuous-variable and discrete-variable formulations is to show how the designs from both formulations using BB-BC algorithm compare to those of Wang and Kulhawy (2008), who used the Microsoft Excel Solver tool to perform only a continuous-variable,

low-cost footing design. The objectives of the second example are; first, to examine the effects of applying the ACI 318-11 requirements for structural concrete to the first example by performing a single-objective, low-cost and low-CO_2-emission optimization; and second, to perform a multi-objective optimization to gain insight on the relationship between low-cost and low-CO_2 emission designs.

7.1.1 Concentric loading: example one

Example One was originally developed by Wang and Kulhawy (2008) and only considered the geotechnical limit states of soil bearing capacity and vertical settlement, given by Equations (269) through (281). Wang and Kulhawy (2008) only considered three design variables: length of the footing L, width B, and depth from the ground surface to the bottom of the footing D. Since structural limit states were not considered in this example, the mass of reinforcement M_r is calculated as:

$$M_r = mV_c \tag{338}$$

where m is a proportionality coefficient taken as 29.67 kg/m^3 (Wang and Kulhawy 2008).

Both a continuous and discrete variable formulation are used for Example One. Table 3 gives the ranges of the design variables used for both the continuous and discrete variable formulations.

Table 3. Concentric Loading Design Variables for Example One

Design variables	Unit	Lower bound	Upper bound	Increment (discrete variable)
B	m	0.01	5.0	0.01
L	m	0.01	5.0	0.01
D	m	0.50	2.0	0.01

Numerical results indicate that a population of 300 candidate solutions is adequate to balance computational efficiency and overall algorithm performance for both the continuous and discrete variable formulations, using both the cost and CO_2 emissions fitness functions. Figure 68 shows the average cost as a function of population size. It can be seen that the solutions are not sensitive to the population size. This is due to the simplicity of the problem. With only three design variables, the size of the search space is relatively small. A general stopping criterion of 2,000 analyses without any change in $\vec{x}_g^{best}$ (overall best feasible design) has been shown to be sufficient for both the continuous and discrete variable formulations, using both the cost and CO_2 emissions fitness functions. Figure 69 shows the average cost as a function of the number of analyses. The size of the Phase 2 search space reduction around $\vec{x}_g^{best}$ varies with the size of the problem; however, approximately 10% of the original size has been shown to be sufficient to obtain improved designs while reducing overall computational time (Camp and Bichon 2004 and Camp 2007).
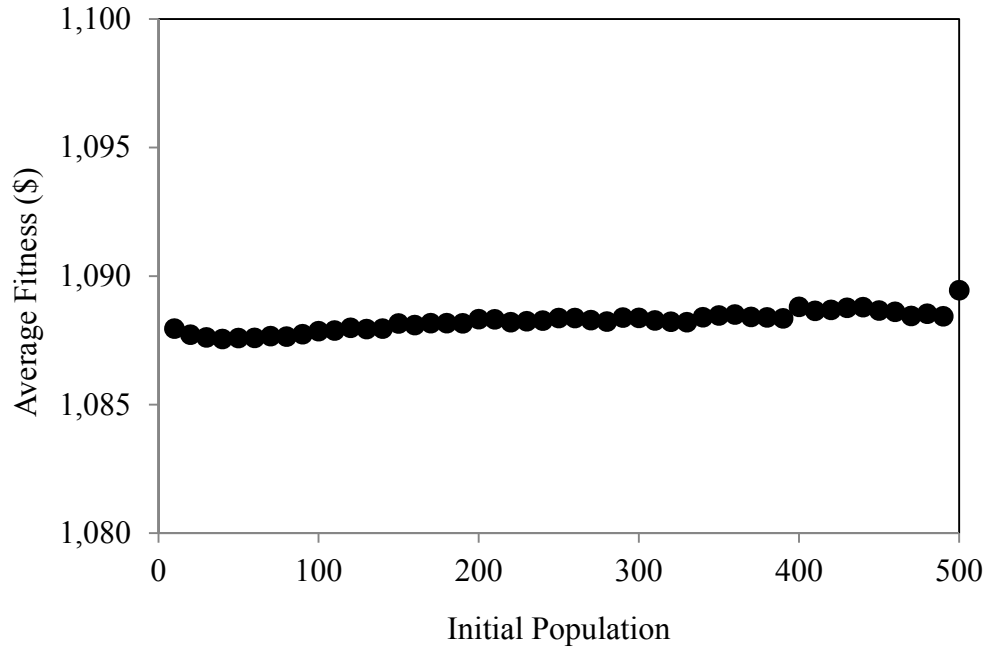
Figure 68. Initial Population Parameter Study for Concentric Loading, Example One.
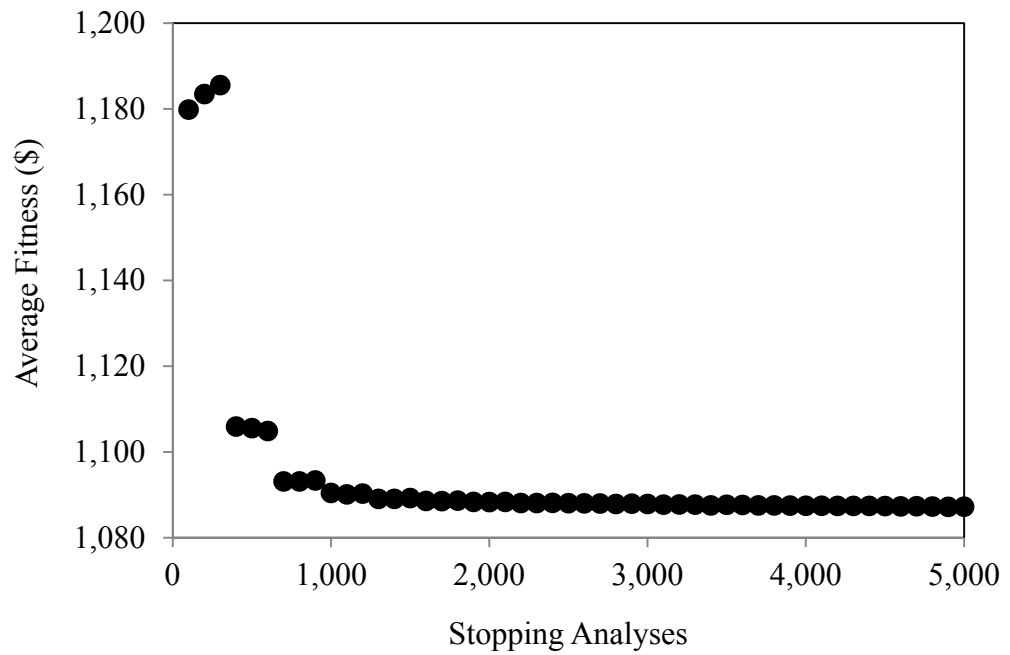
Figure 69. Stopping Analysis Parameter Study for Concentric Loading, Example One.

Appropriate values for ω_1 and ω_2 required in Equation (332) for spread footing design are established based upon a sensitivity study. Computational results from Example One show that $\omega_1 = 0.3$ and $\omega_2 = 0.5$ routinely provide the best footing designs for this example for both the continuous and discrete variable formulations, using both the cost and CO_2 emissions fitness functions. Figure 70 shows how the average fitness varies with ω_1 and ω_2. The relatively small value for ω_1 indicates that better designs are obtained when the center of the new population of normally distributed candidates is shifted more towards the local and global best designs than the population center of mass. The value of $\omega_2 = 0.5$ indicates an equal weight between the local best and global best designs tends to produce overall better results. Camp and Akin (2012) and Camp and Huq (2013) showed that using a value of $\tau = 1$ in Equation (332) enables the initial search to sample the full range of values for each design variable.
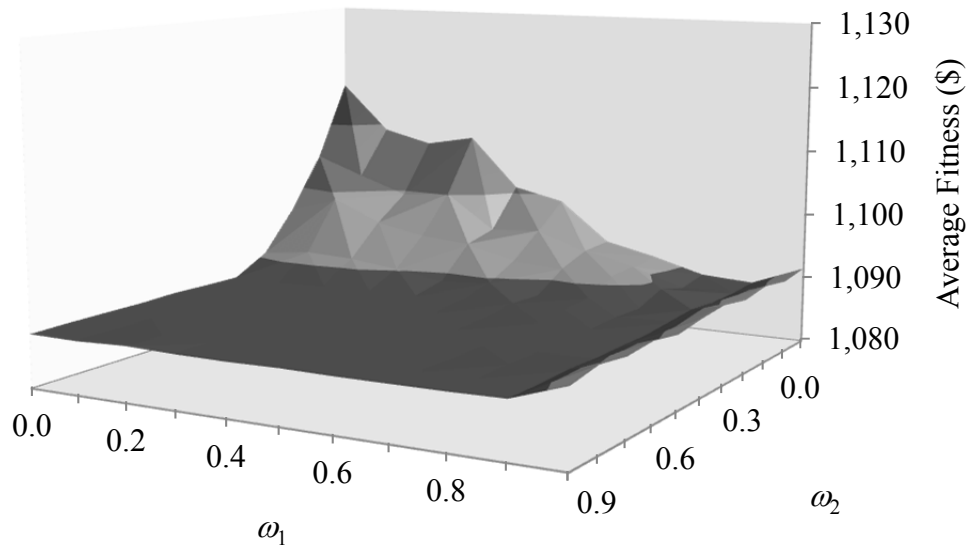
Figure 70. ω_1 and ω_2 Parameter Study for Concentric Loading, Example One.

In order to compare with the results presented by Wang and Kulhawy (2008), the scale factors used in Equations (302) and (303) are taken as $\xi = 1$ and $f'_{cmin} = f'_c$ and are applied to both the continuous and discrete variable formulations. Also, since Wang and Kulhawy (2008) did not consider structural limit states, the compressive strength of concrete is not considered a design variable in this example. Table 4 shows the design parameters for Example One (Wang and Kulhawy, 2008).

Table 4. Concentric Loading Design Parameters for Example One

Input parameter	Unit	Symbol	Value
Internal friction angle of soil	degree	ϕ'	35
Unit weight of soil	kN/m^3	γ_s	18.5
Poisson ratio of soil	—	ν	0.3
Modulus of elasticity of soil	MPa	E	50
Applied vertical force	kN	P	3,000
Over-excavation length	m	L_0	0.3
Over-excavation width	m	B_0	0.3
Thickness of footing	m	H	0.6
Factor of safety for bearing capacity	—	FS	3.0
Maximum allowable settlement	mm	δ	25

In a series of 1,000 runs, the BB-BC procedure, using the cost objective function and continuous variable formulation, had a low cost of $1,086.15 (with an average cost of $1,087.88 and standard deviation of $1.35) and an associated CO_2 emission value of 1,122.15 kg. When rounded to the nearest dollar, this low-cost value is the same as presented by Wang and Kulhawy (2008). For the same number of runs, the BB-BC procedure, using the CO_2 objective function and continuous variable formulation, had a low-CO_2-emission value of 1,119.53 kg (with an average CO_2 emission value of 1,124.23 kg and standard deviation of 3.80 kg) and an associated cost value of $1,087.32 kg. Table 5 shows a summary of the designs developed by the BB-BC procedure using continuous variable formulation. On average, the multiphase BB-BC design procedure used 62% of the computational effort in Phase 1 for both the cost and CO_2 emission functions. On average, the multiphase BB-BC procedure completed 62% of the computational effort in

Phase 1 for the cost function and 63% of the computational effort in Phase 1 for the CO_2 emission function. On average, the percent difference between the Phase 1 and Phase 2 solutions is 0.12% for the cost function and 0.21% for the CO_2 emission function.

Table 5. Designs for Example One (Continuous Variables)

Design variables	Wang and Kulhawy (2008)	BB-BC COST	BB-BC CO_2
B (m)	1.86	1.865	2.089
L (m)	2.30	2.297	2.101
D (m)	1.38	1.374	1.256
Excavation (m^3)	7.75	7.72	7.20
Concrete Formwork (m^2)	5.00	5.00	5.03
Reinforcement (kg)	76.16	76.26	78.12
Concrete (m^3)	2.57	2.57	2.63
Compacted Backfill (m^3)	5.18	5.15	4.57
Design Objective	$1,086	$1,086.15	1,119.53 kg
Secondary Objective	—	1,122.15 kg	$1,087.32
Average Fitness	—	$1,087.88	1,124.23 kg
Std. Dev. Fitness	—	$1.35	3.80 kg
Average No. Analyses	—	10,207	10,958

Table 6 shows a summary of the designs developed by the BB-BC procedure using discrete variable formulation. For the discrete variable formulation, the size of the resulting search space is approximately $3.78(10^7)$ possible designs. For the cost objective function, the best BB-BC design is approximately $1,086.54 (with an average cost of $1,088.28 and standard deviation of $1.33) and an associated CO_2 value of 1,121.06 kg. When rounded to the nearest dollar this low-cost value is the same as presented by Wang

and Kulhawy (2008). For the same number of runs, the BB-BC procedure, using the CO_2 objective function and discrete variable formulation, had a low-CO_2 emission value of 1,120.74 kg (with an average CO_2 emission value of 1,125.50 kg and standard deviation of 12.84 kg) and an associated cost value of $1,088.22. On average, the multiphase BB-BC design procedure used 67% of the computational effort in Phase 1 for both the cost and CO_2 emission functions. On average, the percent difference between the Phase 1 and Phase 2 solutions is 0.10% for the cost function and 0.16% for the CO_2 emission function.

Table 6. Designs for Example One (Discrete Variables)

Design variables	Wang and Kulhawy (2008)	BB-BC COST	BB-BC CO_2
B (m)	1.86	1.96	2.08
L (m)	2.30	2.21	2.11
D (m)	1.38	1.32	1.26
Excavation (m^3)	7.75	7.49	7.23
Concrete Formwork (m^2)	5.00	5.00	5.03
Reinforcement (kg)	76.16	77.11	78.13
Concrete (m^3)	2.57	2.60	2.63
Compacted Backfill (m^3)	5.18	4.89	4.59
Design Objective	$1,086	$1,086.54	1,120.74 kg
Secondary Objective	—	1,121.06 kg	$1,088.22
Average Fitness	—	$1,088.28	1,125.50 kg
Std. Dev. Fitness	—	$1.33	12.84 kg
Average No. Analyses	—	9,325	9,725

7.1.2 Concentric loading: example two

For the second design example, the discrete variable BB-BC footing design procedure
is applied once for the cost objective function and again for the CO_2 objective function.
In addition, the design will satisfy the ACI 318-11 requirements for reinforced concrete.
This example considers the four design variables associated with the geometry of the
footing ($X_1 - X_4$), six design variables representing the steel reinforcement ($R_1 - R_6$), and
one design variable representing the strength of the concrete (S_1), as defined in Section
6.2. The size of the resulting search space is approximately $1.13(10^{17})$ possible designs.
Table 7 lists the ranges of the design variables for Example Two.

Table 7. Concentric Loading Design Variables for Example Two

Design variables	Unit	Lower bound	Upper bound	Increment
X_1	m	0.30	3.00	0.01
X_2	m	0.02	8.00	0.02
X_3	m	0.02	8.00	0.02
X_4	m	0.01	2.00	0.01
R_1	—	3	12	1
R_2	—	2	20	1
R_3	—	3	12	1
R_4	—	2	20	1
R_5	—	3	11	1
R_6	—	4	12	2
S_1	MPa	20	55	5

Table 8 lists the specified column, footing, soil, and design parameters. For a comparison to Wang and Kulhawy (2008), all of the design parameters are the same as in Example One, with the exception of the parameters that are utilized for the structural analysis. Values needed for the structural aspects of the footing design include: concrete unit weight, steel elastic modulus, column dimensions, concrete cover, and minimum footing thickness. The concrete unit weight, steel elastic modulus, and column dimensions are assumed based on typical values used in practice. Concrete cover and minimum footing thickness are specified in ACI 318-11.

Table 8. Concentric Loading Design Parameters for Example Two

Input parameter	Unit	Symbol	Value
Internal friction angle of soil	degree	ϕ'	35
Unit weight of soil	kN/m^3	γ_s	18.5
Poisson Ratio of soil	—	ν	0.3
Modulus of elasticity of soil	MPa	E	50
Applied vertical force	kN	P	3,000
Over excavation length	m	L_o	0.3
Over excavation width	m	B_o	0.3
Factor of safety for bearing capacity	—	FS	3.0
Maximum allowable settlement	mm	δ	25
Unit weight of concrete*	kN/m^3	γ_c	23.56
Modulus of elasticity of steel*	GPa	E_s	199.95
Column length*	mm	l_{col}	457.2
Column width*	mm	b_{col}	457.2
Concrete Cover in Footing*	mm	$cover$	76.2
Minimum Footing Thickness*	mm	T_{min}	228.6

Note: All values given by Wang and Kulhawy (2008) except for * values which are assumed.

As in Example One, numerical results indicate that a population of 300 candidate

solutions is adequate to balance computational efficiency and overall algorithm

performance, and a general stopping criterion of 2,000 analyses without any change in

$\vec{x}_g^{\,best}$ has been shown to be sufficient. Figure 71 shows the average cost as a function of

population size. Figure 72 shows the average cost as a function of the number of

analyses.
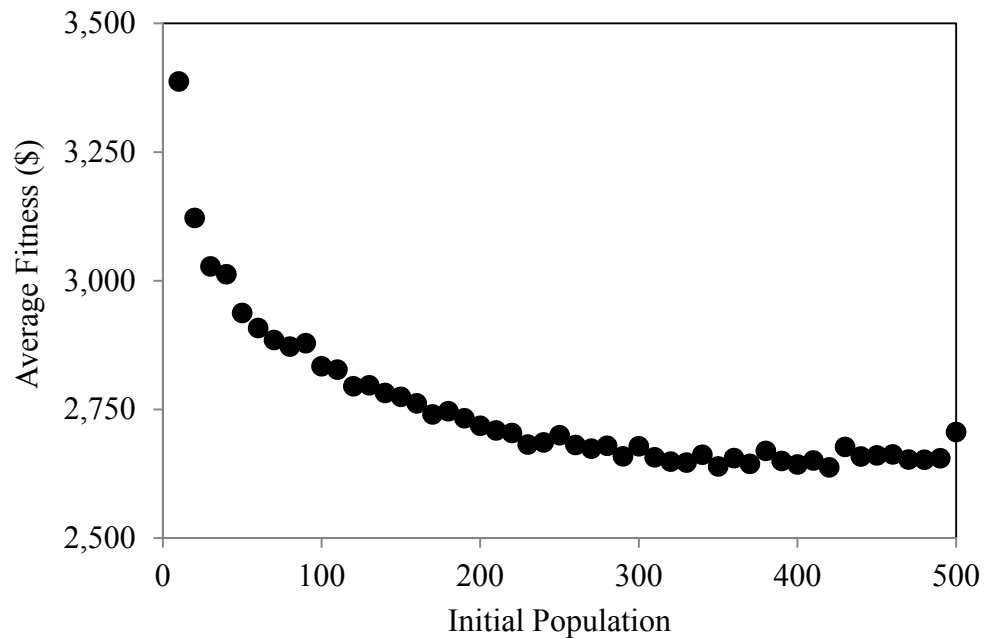
Figure 71. Initial Population Parameter Study for Concentric Loading, Example Two.
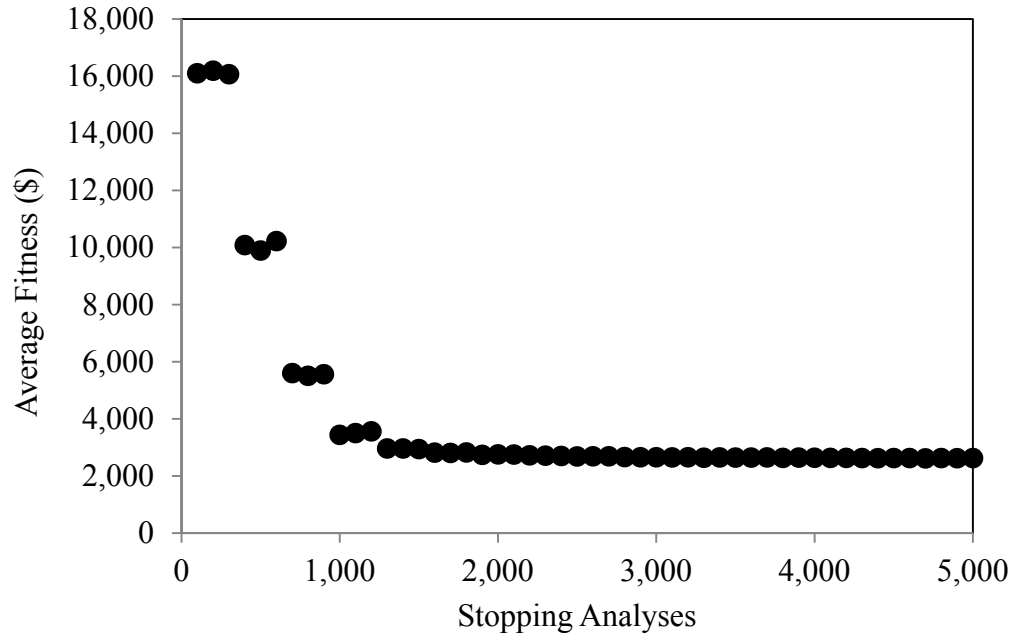
Figure 72. Stopping Criteria Parameter Study for Concentric Loading, Example Two.

Appropriate values for ω_1 and ω_2 required in Equation (332) for spread footing design are established based upon a sensitivity study that show $\omega_1 = 0.3$ and $\omega_2 = 0.6$ routinely provide the best footing designs for this example. Figure 73 shows how the average fitness varies with ω_1 and ω_2. As in Example One, a value of $\tau = 1$ is also used in Equation (332). In order to give the steel reinforcing term in the objective function a magnitude comparable to that of the other terms, the scale factors used in Equations (302) and (303) are taken as $\xi = 10$ and $f'_{cmin} = 20$ MPa.
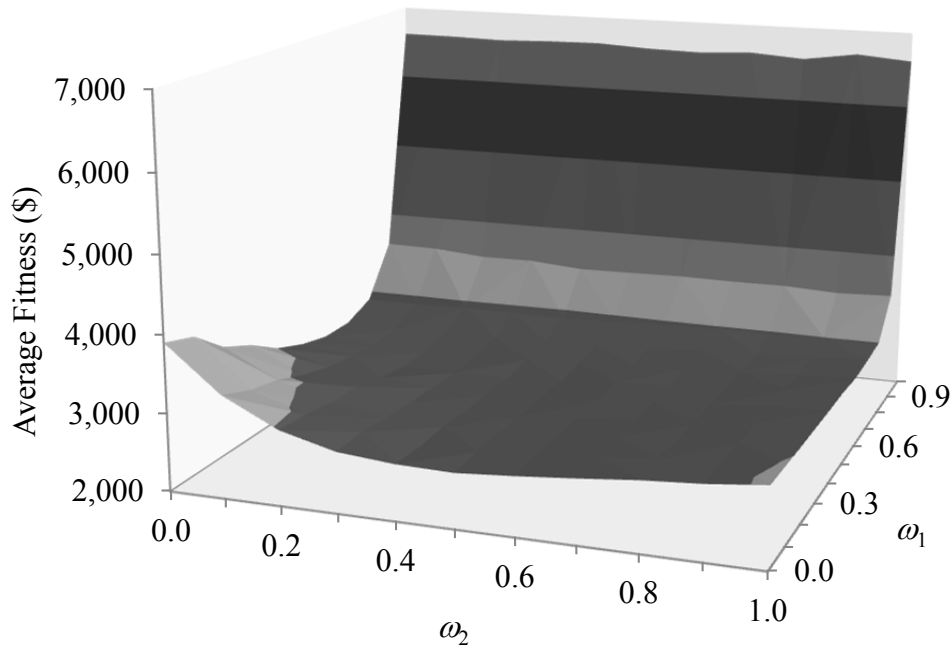
Figure 73. ω_1 and ω_2 Parameter Study for Concentric Loading, Example Two.

Table 9 lists a summary of the results developed by the BB-BC procedure, using the cost fitness function. From 1,000 designs, the best low-cost design is \$1,189.55 (with an average cost of \$1,321.66 and standard deviation of \$78.63) with a corresponding CO_2 emission value of 1,500.82 kg. Several important observations can be made by comparing the cost of the spread footing design in Example Two with the one presented by Wang and Kulhawy (2008). First, the mass of steel reinforcement from the BB-BC design is 29% lower; resulting in an equivalent proportionality coefficient of 17.85 kg/m^3. Second, while there is a modest cost savings associated with the reduction in the required reinforcing, the additional cost of the spread footing design in Example Two is primarily due to a 19% increase in the volume of concrete in the footing. Increased values for length, width, and height of the footing are required to meet strength and reinforcing

details specified in ACI 318-11. On average, the multiphase BB-BC procedure completed

64% of the computational effort in Phase 1. The increase in the average number of

analyses to convergence from Example One is due to the increased complexity of the

problem as well as the significantly larger search space.

Table 9. Concentric Load Designs Based on Scaled Cost Fitness for Example Two

Design Variables			
X_1 (m)	1.78	R_1	5
X_2 (m)	1.66	R_2	19
X_3 (m)	1.19	R_3	5
X_4 (m)	0.42	R_4	18
S_1 (MPa)	40	R_5	4
		R_6	10
Excavation (m^3)			7.298
Concrete Formwork (m^2)			5.649
Reinforcement (kg)			54.707
Concrete (m^3)			3.065
Compacted Backfill (m^3)			4.113
Best Cost			$ 1,189.55
Average Cost			$ 1,321.66
Std. Dev. Cost			$ 78.63
Corresponding CO_2			1,500.82 kg
Average CO_2			1,398.39 kg
Std. Dev. CO_2			130.31 kg
Average No. Analyses			24,281

Table 10 lists a summary of the results developed by the BB-BC procedure using the CO_2 emissions fitness function. From 1,000 designs, the best low-CO_2 emission design is 1,205.70 kg (with an average CO_2 emission value of 1,337.09 kg and standard deviation of 112.29 kg) with a corresponding cost of $1,248.25. Compared to Wang and Kulhawy (2008), the mass of steel reinforcement from the spread footing design in Example Two is 32% lower; resulting in an equivalent proportionality coefficient of 14.90 kg/m^3. Second, while there is a modest emission savings associated with the reduction in the required reinforcing, the additional emissions of the spread footing design in Example Two is primarily due to a 35% increase in the volume of concrete in the footing. Increased values for length, width, and height of the footing are required to meet strength and reinforcing details specified in ACI 318-11. On average, the multiphase BB-BC procedure completed 68% of the computational effort in Phase 1. The increase in the average number of analyses to convergence from Example One is due to the increased complexity of the problem as well as the significantly larger search space.

Table 10. Concentric Load Designs Based on Scaled CO_2 Fitness for Example Two

Design Variables			
X_1 (m)	1.74	R_1	5
X_2 (m)	1.70	R_2	16
X_3 (m)	1.18	R_3	5
X_4 (m)	0.52	R_4	16
S_1 (MPa)	20	R_5	4
		R_6	10
Excavation (m^3)			7.241
Concrete Formwork (m^2)			6.519
Reinforcement (kg)			52.773
Concrete (m^3)			3.541
Compacted Backfill (m^3)			3.602
Best CO_2			1,205.70 kg
Average CO_2			1,337.09 kg
Std. Dev. CO_2			112.29 kg
Corresponding Cost			$ 1,248.25
Average Cost			$ 1,363.73
Std. Dev. Cost			$ 88.48
Average No. Analyses			23,714

A sensitivity analysis was performed to assess the impact of different design parameters on the cost and CO_2 emissions. Figure 74 shows that the cost and CO_2 emissions increase dramatically as the applied column load increases, as one would expect. Figure 75 shows that as the soil becomes stiffer, the cost and CO_2 emission values greatly decrease. The only limit state that the soil stiffness influences is settlement. Footings resting on stiffer soils will tend to settle less, which can lead to the settlement

limit state not significantly controlling the design. Figure 76 shows that as the Poisson ratio of the soil increases, the cost and CO_2 emission values slightly decrease, which suggests that the soil Poisson ratio does not have a significant impact on designs. Figure 77 shows that as the internal angle of friction of the soil increases, the cost and CO_2 emission values decrease. The lack of smoothness in these curves is most likely due to the internal friction angle value being in the trigonometric functions of the bearing capacity, shape, and depth factors of the soil bearing capacity analysis. Figure 78 shows that as the minimum required factor of safety against bearing failure of the soil increases, the cost and CO_2 emission values increase. Figure 79 shows that as the maximum allowable settlement increases, the cost and CO_2 emissions of the spread footing designs significantly decrease until a point where settlement no longer controls the design ($\delta > 35$ mm).

Impact of the concrete compressive strength on footing cost and CO_2 emissions is investigated using a modified form of the design example that does not consider the concrete compressive strength as a design variable. The four geometric design variables and six reinforcement design variables are defined in the same manner as stated in Section 6.2. Figure 80 shows the impact of the concrete strength on average footing cost for various applied loads. For a given applied load, it is seen that the concrete compressive strength has little effect on average cost. Figure 81 shows the average CO_2 emissions as a function of the concrete strength. For a given applied load, it is seen that as the concrete compressive strength is increased, the average CO_2 emissions increase. For higher applied loads, it is seen that the average CO_2 emissions increase more dramatically as concrete compressive strength increases.
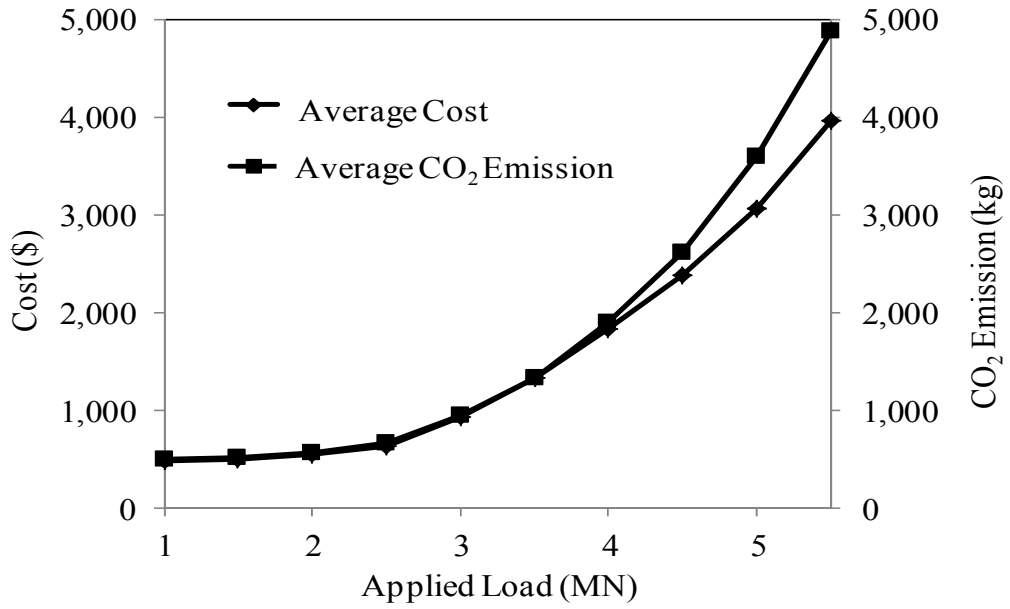
Figure 74. Sensitivity of Cost and CO_2 Emissions to Applied Load.
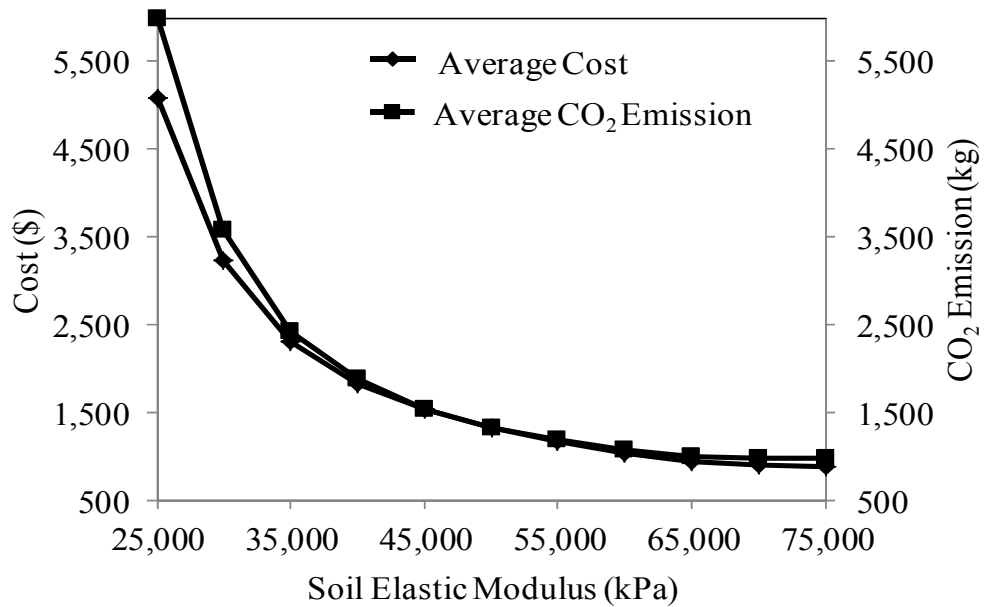
Figure 75. Sensitivity of Cost and CO_2 Emissions to Soil Elastic Modulus.
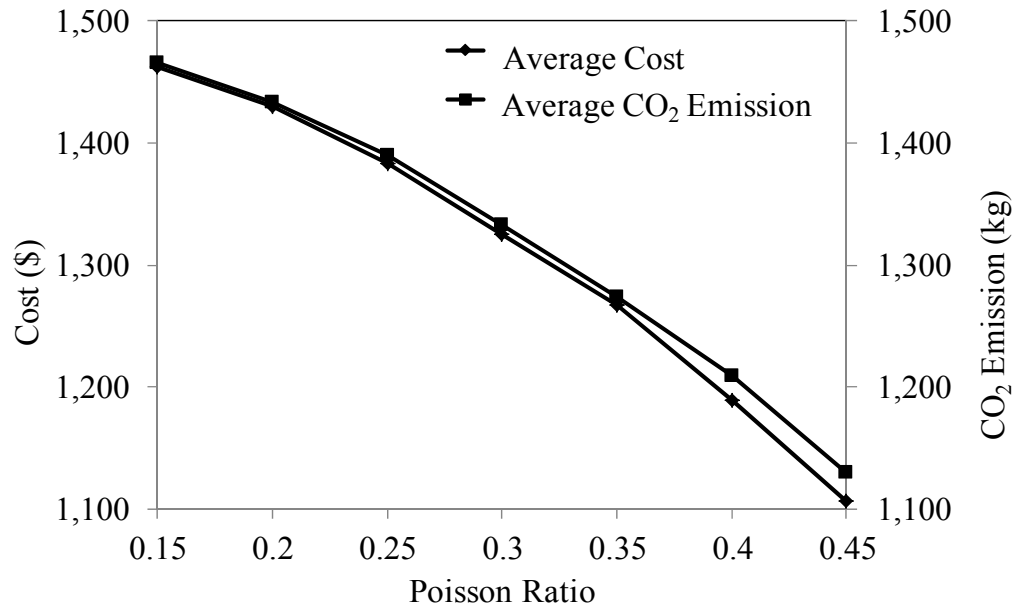
Figure 76. Sensitivity of Cost and CO_2 Emissions to Poisson Ratio.
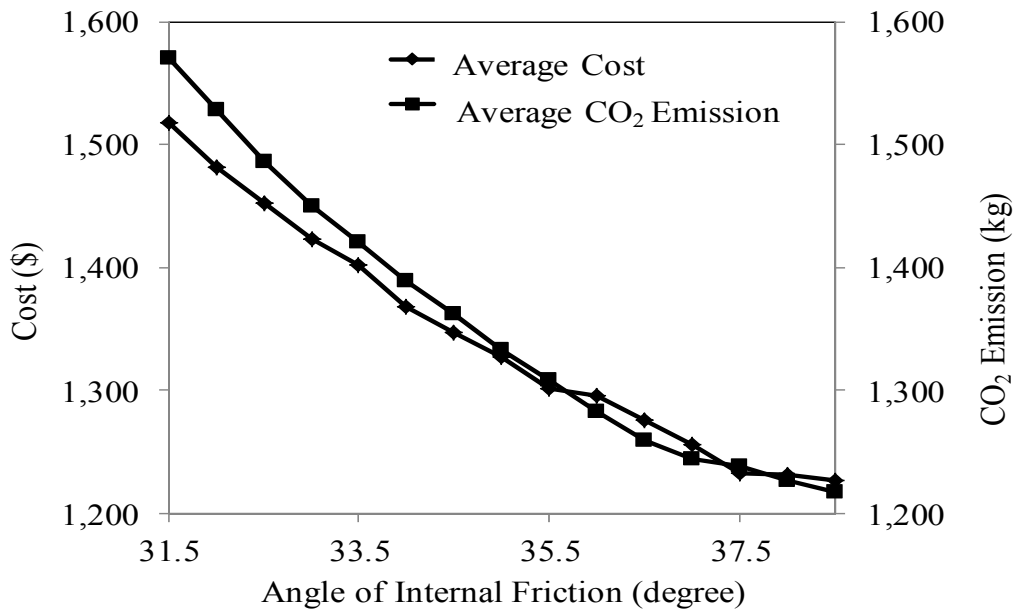
Figure 77. Sensitivity of Cost and CO_2 Emissions to Angle of Internal Friction.
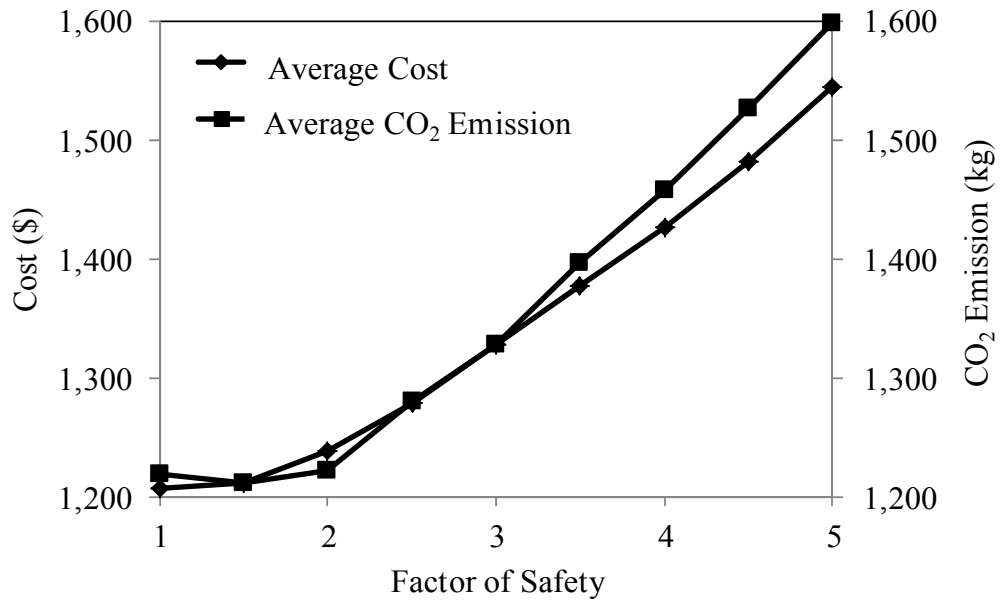
Figure 78. Sensitivity of Cost and CO_2 Emissions to Factor of Safety.
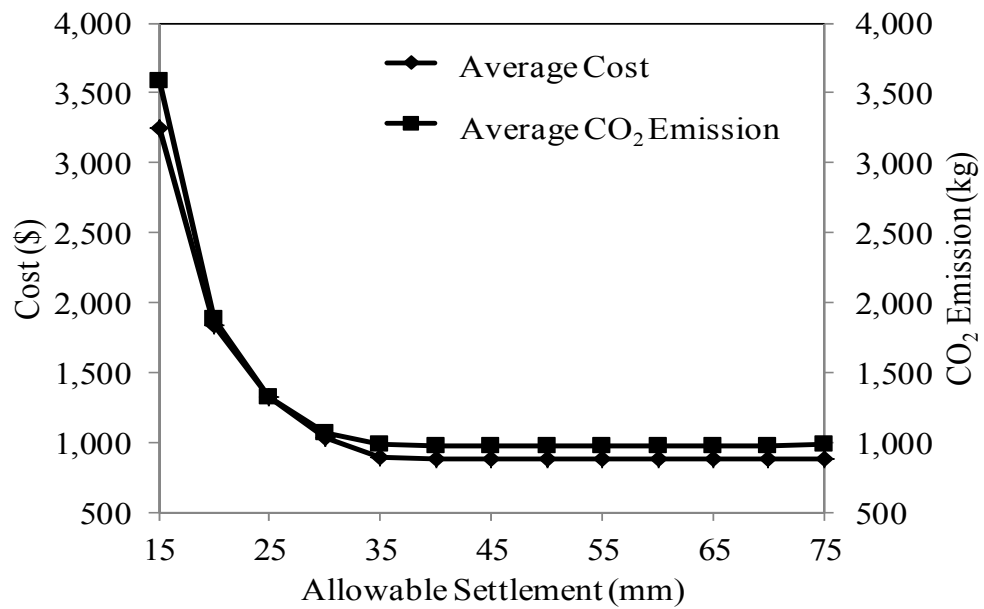
Figure 79. Sensitivity of Cost and CO_2 Emissions to Allowable Settlement.
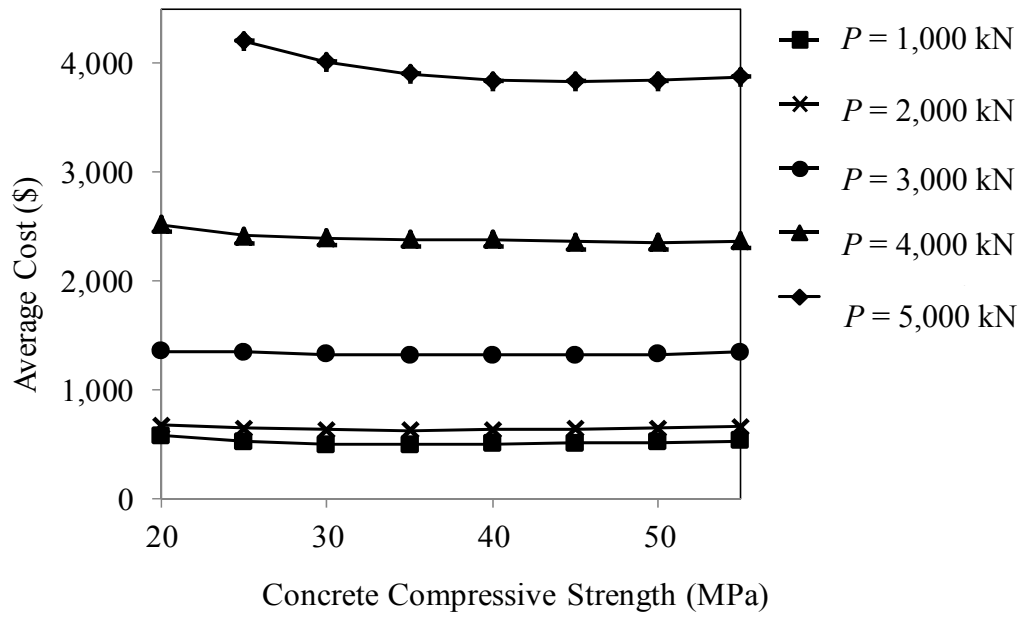
Figure 80. Cost vs. Concrete Compressive Strength.
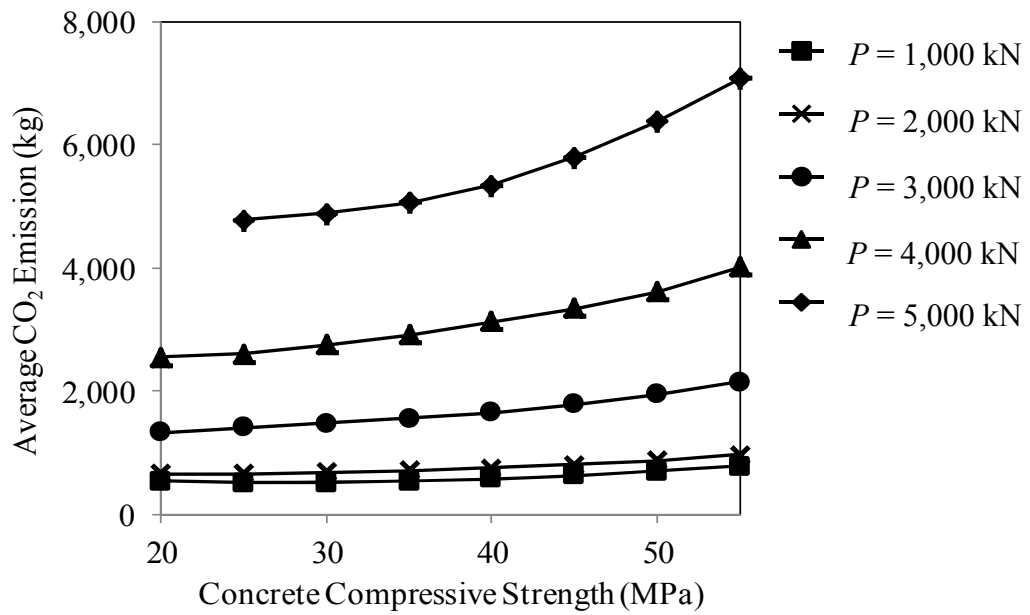
Figure 81. CO_2 Emissions vs. Concrete Compressive Strength.

7.1.3 Multi-objective optimization

In order to observe a relationship between the cost and CO_2 emissions, the BB-BC algorithm is applied to the multi-objective fitness function given by Equation (306). To better reflect the tradeoff between cost and CO_2 emissions, the reinforcement scale factor ξ used in the single objective fitness functions is taken as 1 and $f'_{cmin} = f'_c$. The value of ζ was varied from 0 to 1 by 0.01. Figure 82 shows that, on average, as cost increases, CO_2 emissions decrease. That is, as the value of ζ approaches 1, cost decreases and CO_2 emissions increase. The steeper slope of the data when the multi-objective function is weighted more heavily for cost indicates a drastic decrease in average CO_2 emissions for a relatively small increase in average cost. As the weights on the cost and CO_2 emission components of the multi-objective function become equal and the CO_2 emissions become weighted more heavily, the data shows a smaller decrease in CO_2 emissions with increasing cost. Also, the data shows that when more weight is on the cost function, designs are produced with a higher average concrete compressive strength. As the CO_2 emissions function is weighted more heavily, the average concrete compressive strength drops. Figure 83 shows the relationship between best low-CO_2 emissions with best low-cost for different values of the concrete compressive strength. For groups of designs where the strength of concrete is constant, a slight increase in cost has a correspondingly small increase in CO_2 emission. When the entire set of designs is considered, a more significant trend is observed where the strength of concrete has a more significant effect on both cost and CO_2 emissions. As the strength of concrete decreases, CO_2 emissions decrease by up to 12% while cost increases only 0.8%. This difference is due to the increased CO_2 emission associated with the larger quantities of cement in the higher

strength mix designs. The few designs produced with $f'_c = 30$ MPa occur when the multi-objective fitness function is weighted more heavily on the CO_2 fitness function. The fewer designs with the $f'_c = 30$ MPa suggest that using lower strength concrete causes a higher required volume of concrete, as well as a higher required mass of rebar, which may tend to inflate CO_2 emissions.
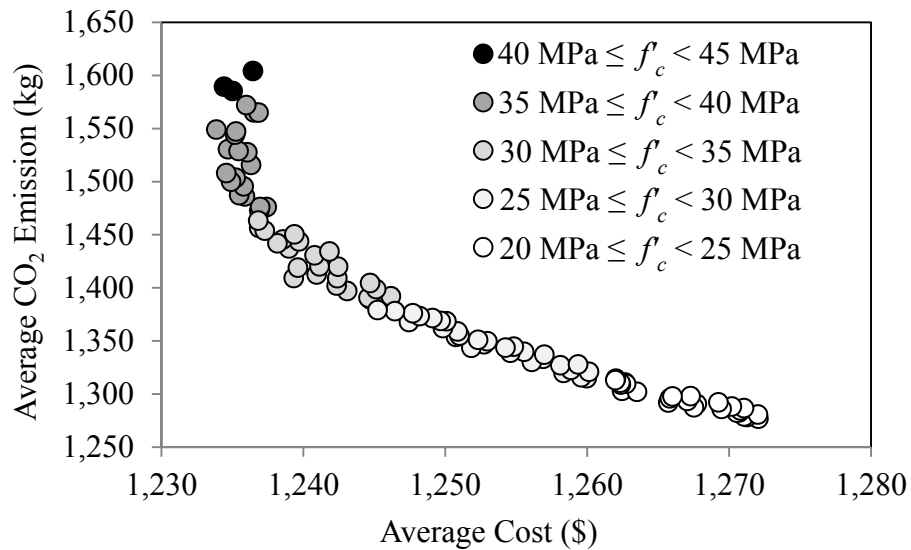
Figure 82. Pareto Front for Cost and CO_2 Emissions for
Concentric Loading, Example One.
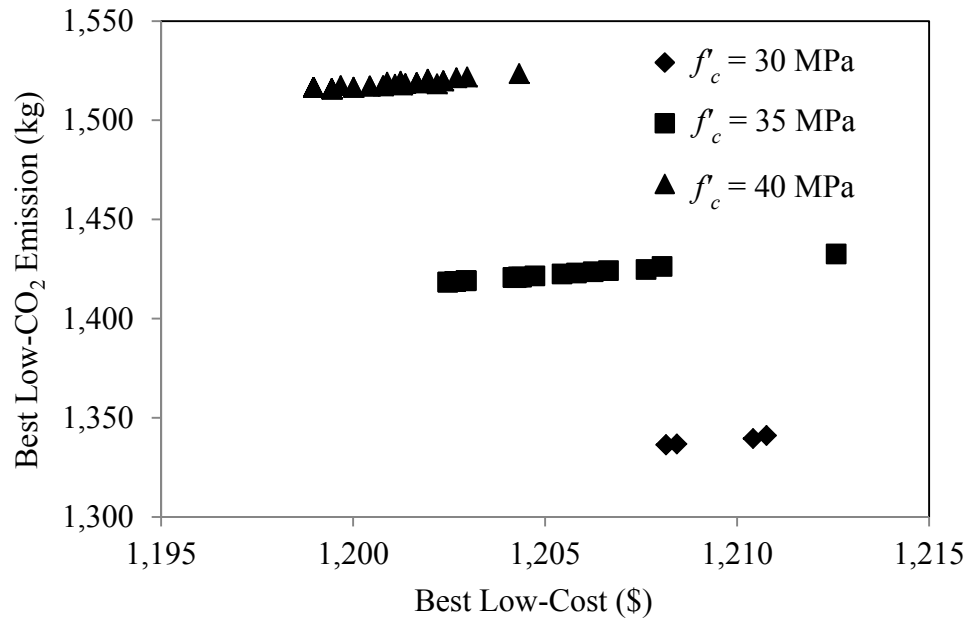
Figure 83. Effects of Concrete Strength on Cost and CO_2 Emissions
for Concentric Loading, Example One.

7.2 Uniaxial Loading

The objective of these design examples is to investigate the cost and CO_2 emission

impact between using the theoretical analysis procedures and simplified analysis

procedures, commonly used by practitioners, when designing a spread footing subjected

to a uniaxial bending moment. The discrete variable BB-BC footing design procedure is

applied for the cost objective function and again for the CO_2 objective function. All

designs will satisfy geotechnical limit states, as well as the ACI 318-11 requirements for

reinforced concrete. Both examples consider the four design variables associated with the

geometry of the footing ($X_1 - X_4$), six design variables representing the steel

reinforcement ($R_1 - R_6$), and one design variable representing the strength of the concrete

(S_1), as defined in Section 6.2. The size of the resulting search space is approximately

$4.75(10^{17})$ possible designs. Table 11 lists the ranges of the design variables.

Table 11. Uniaxial Loading Design Variables

Design variables	Unit	Lower bound	Upper bound	Increment
X_1	m	0.30	3.00	0.01
X_2	m	0.02	8.00	0.02
X_3	m	0.02	8.00	0.02
X_4	m	0.01	2.00	0.01
R_1	—	3	12	1
R_2	—	2	40	1
R_3	—	3	12	1
R_4	—	2	40	1
R_5	—	3	11	1
R_6	—	4	12	2
S_1	MPa	20	55	5

Table 12 lists the specified column, footing, and soil design parameters. In order to build upon the concentric loading design examples, all of the design parameters remain the same with the only additional information being an applied bending moment about the y-axis, M_y. Recall that the applied moment can be written in terms of the applied point load acting at an equivalent eccentricity e_x away from the center of the footing, along the positive x-axis. The equivalent eccentricity e_x is defined as:

$$e_x = \frac{M_y}{P} \tag{339}$$

The applied moment value was chosen based on a force equal to the one used by Wang and Kulhawy (2008) with values of e_x varying from 0 m to 1 m. As the optimization procedure sizes the footing, the weight of the footing W_f is included in the equivalent

eccentricity as part of the point load P. Concrete cover and minimum footing thickness are specified in ACI 318-11.

Table 12. Uniaxial Example Input Parameters

Input parameter	Unit	Symbol	Value
Internal friction angle of soil	degree	ϕ'	35
Unit weight of soil	kN/m^3	γ_s	18.5
Poisson Ratio of soil	—	ν	0.3
Modulus of elasticity of soil	MPa	E	50
Applied vertical force	kN	P	3,000
Over excavation length	m	L_o	0.3
Over excavation width	m	B_o	0.3
Factor of safety for bearing capacity	—	FS	3.0
Maximum allowable settlement	mm	δ	25
Applied Moment*	kN-m	M	3,000
Unit weight of concrete*	kN/m^3	γ_c	23.56
Modulus of elasticity of steel*	GPa	E_s	199.95
Column length*	mm	l_{col}	457.2
Column width*	mm	b_{col}	457.2
Concrete Cover in Footing*	mm	$cover$	76.2
Minimum Footing Thickness*	mm	T_{min}	228.6

Note: All values given by Wang and Kulhawy (2008) except for * values which are assumed.

As with the concentric loading examples, numerical results indicate that a population of 300 candidate solutions is adequate to balance computational efficiency and overall algorithm performance, and a general stopping criterion of 2,000 analyses without any

change in $\vec{x}_g^{\,best}$ has been shown to be sufficient. Figure 84 shows the average fitness as a

function of population size. Figure 85 shows the average fitness as a function of the

number of analyses.
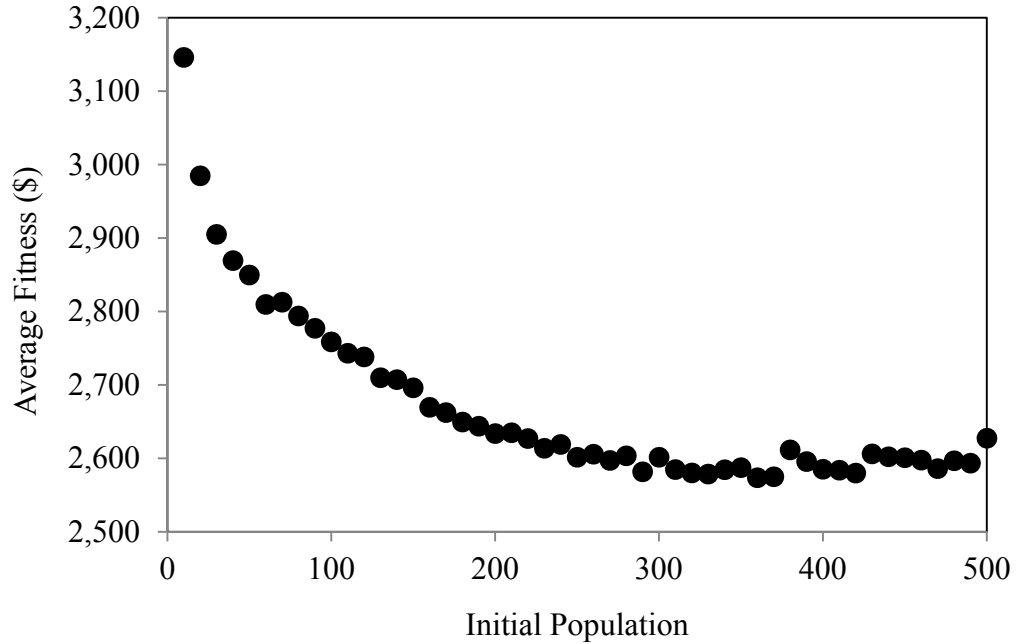
Figure 84. Initial Population Parameter Study for Uniaxial Loading Examples.
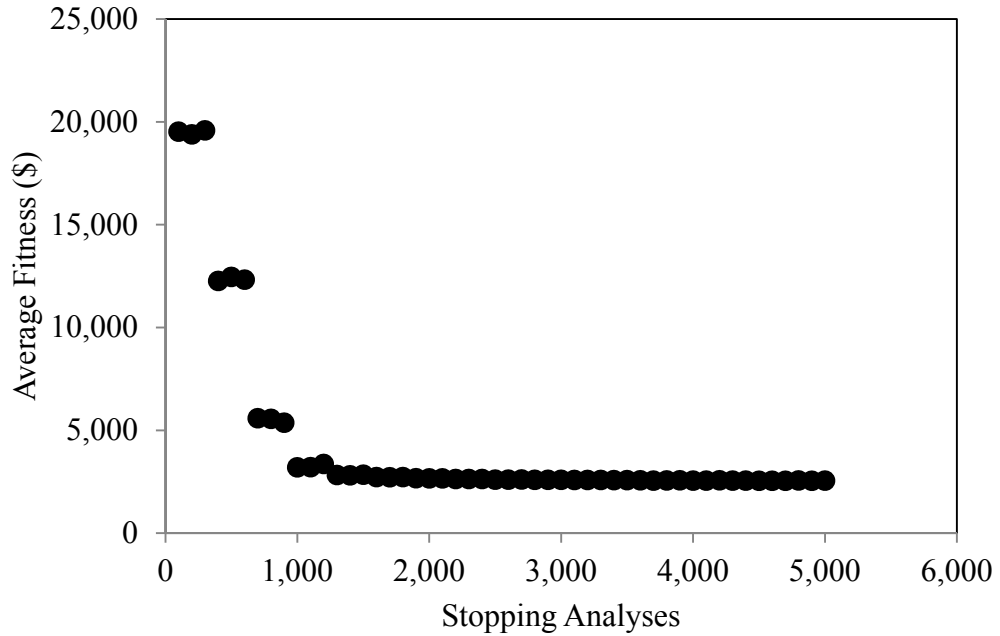
Figure 85. Stopping Criteria Parameter Study for Uniaxial Loading Examples.

Based upon a sensitivity study, $\omega_1 = 0.3$ and $\omega_2 = 0.6$ required in Equation (332) routinely provide the best footing designs for this example. Figure 86 shows the average fitness as a function of ω_1 and ω_2. As in the concentric loading examples, a value of $\tau = 1$ is used in Equation (332). In order to give the reinforcing term a magnitude comparable to that of the other terms, the scale factors used in Equations (302) and (303) are taken as $\xi = 10$ and $f'_{cmin} = 20$ MPa for both uniaxial loading examples.
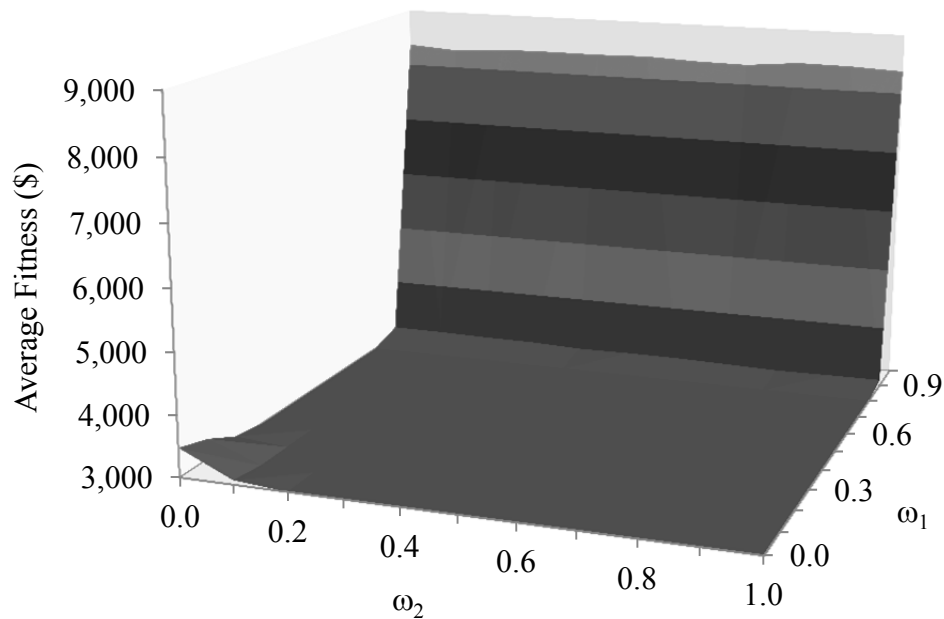
Figure 86. ω_1 and ω_2 Parameter Study for Uniaxial Loading Examples.

7.2.1 Uniaxial loading: example one

The first set of footing designs considers the scaled cost fitness function defined in

Equation (302) with the input design parameters given in Table 12. From 1,000 designs,

the best low-cost design using the simplified analysis procedures commonly used in

practice is $6,030.79, with an average cost of $6,911.92 and standard deviation of

$444.85. On average, the multiphase BB-BC procedure performed 21,793 analyses

before convergence and completed 63% of the computational effort in Phase 1 when

using the simplified analysis procedures. The best low-cost design using the theoretical

analysis procedures is $4,316.57, with an average cost of $5,203.72 and standard

deviation of $418.45. On average, the multiphase BB-BC procedure performed 22,631

analyses before convergence and completed 59% of the computational effort in Phase 1 when using the theoretical analysis procedures.

Table 13 summarizes the low-cost designs developed by the BB-BC procedure. Several important observations can be made by comparing the cost of the spread footing design based on the simplified analysis procedures with the one based on the theoretical analysis procedures. First, on average, there is a 24.7% savings in cost when using the theoretical procedures. Although the excavation volume is slightly higher for the design based on the theoretical analysis procedures, the other quantities are significantly less. In particular, there is approximately 70% less rebar mass in the design based on the theoretical analysis procedures. Since the moment at the face of the column is based on the maximum bearing pressure beneath the footing, and the rebar length extends from between the clear covers in both directions of the footing; the mass of reinforcement is significantly higher for the design based on the simplified analysis procedures. Second, when using the theoretical analysis procedures, some soil detachment is allowed; whereas for the simplified analysis procedures, it is not. The detached distance for the design presented in this example is 0.311 m, with a percentage of detachment of approximately 6.5%. For 1000 runs, the average percent detachment is approximately 1.1%.

A sensitivity study is done by varying the applied vertical force and equivalent eccentricity. Table 14 shows the range of applied vertical force and equivalent eccentricity considered. Figure 87 shows a surface plot of the lowest cost footing designs using the theoretical analysis procedures. The general trend shows that as the applied load and equivalent eccentricity increase, cost values increase drastically. Figure 88 shows a surface plot of the difference between the average low-cost designs using both simplified

186

analysis procedures and the theoretical analysis procedures. The general trend shows that as the applied load and equivalent eccentricity increase, the difference in average cost increases dramatically. For example, the average cost is approximately a 31% higher when the simplified analysis procedures are used for a footing subjected to a load of 3,000 kN and moment of 3,000 kN-m. Figure 89 shows a contour plot of average cost when using the theoretical analysis procedures, where each contour represents a $1,000 increment in average cost. The bold boundary indicates where detachment first occurs. Designs to the right of the boundary have loading outside of the kern. A general trend shows an inflection point in the contours, located approximately where designs first have soil detachment.

Table 13. Uniaxial Loading Designs Based on Scaled Cost Fitness

Design Variables	Simplified Analysis	Theoretical Analysis
X_1 (m)	2.32	1.76
X_2 (m)	2.18	2.68
X_3 (m)	0.31	0.31
X_4 (m)	0.96	0.75
R_1	7	8
R_2	34	25
R_3	9	6
R_4	18	30
R_5	7	4
R_6	4	10
S_1 (MPa)	45	45
L	5.32	4.76
B	2.64	3.14
H	1.19	0.98
Detached Distance (m)	—	0.311
Excavation (m^3)	5.117	5.392
Concrete Formwork (m^2)	18.916	15.456
Reinforcement (kg)	769.843	237.477
Concrete (m^3)	16.578	14.583
Compacted Backfill (m^3)	0.768	0.762
Best Cost	$ 6,030.79	$ 4,316.57
Average Cost	$ 6,911.92	$ 5,203.72
Std. Dev. Cost	$ 444.85	$ 418.45
Average No. Analyses	21,793	22,631

Table 14. Uniaxial Loading Force and Eccentricity Parameters

Parameter	Unit	Lower bound	Upper bound	Increment
F	kN	500.0	5,000.0	500.0
e_x	m	0.0	1.0	0.1
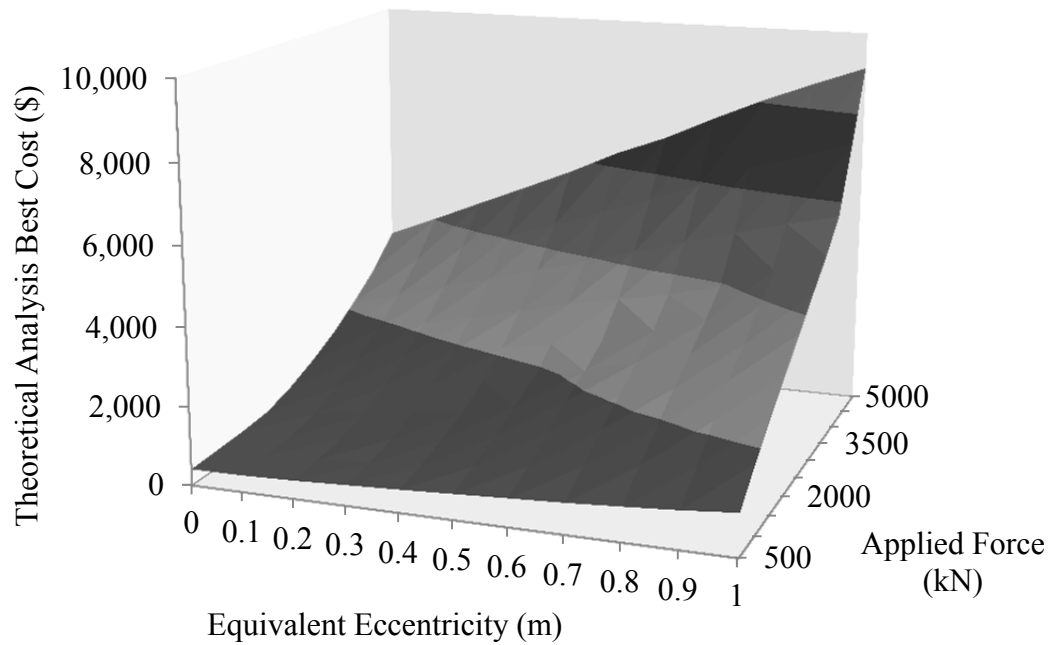
Figure 87. Lowest Cost Designs using Theoretical Analysis
Procedures for Uniaxial Loading.
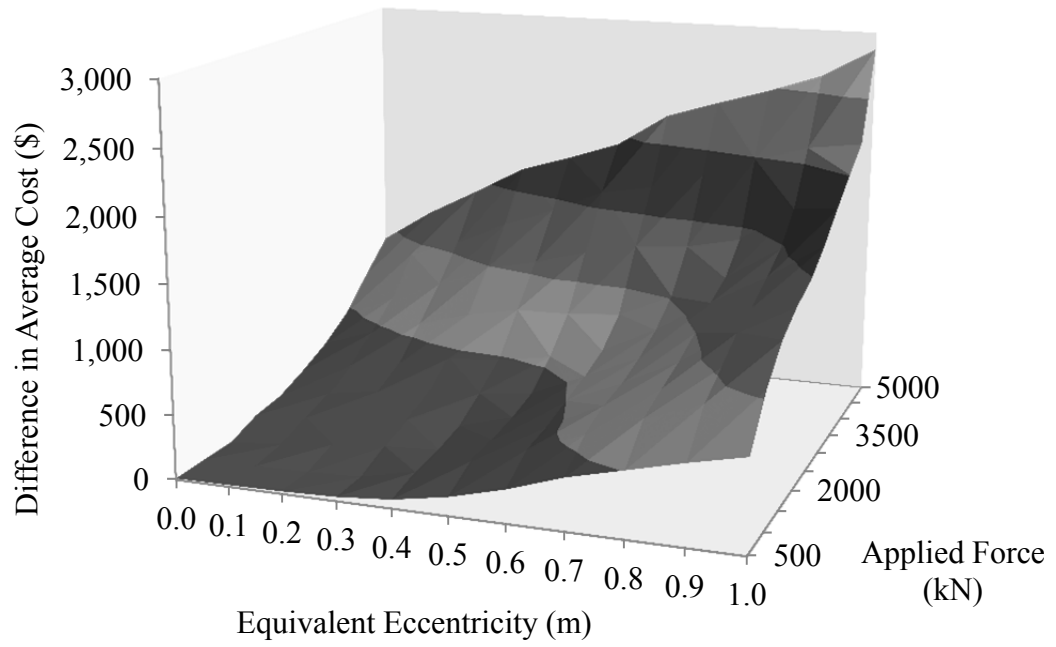
Figure 88. Difference in Cost between Designs using Simplified Analysis Procedures and Theoretical Analysis Procedures for Uniaxial Loading.
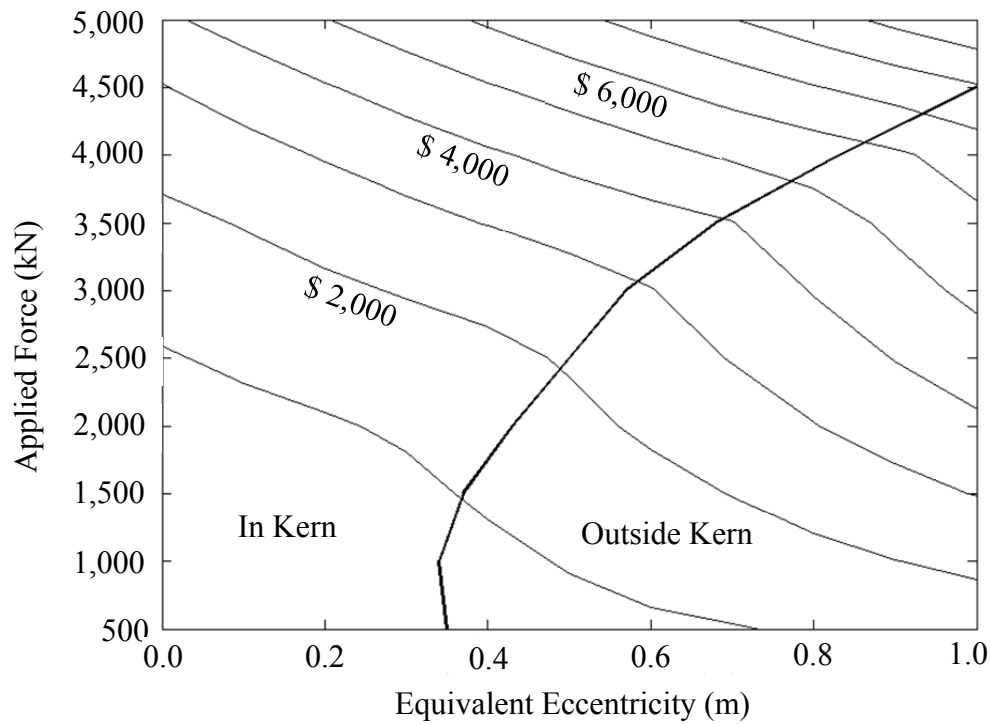
Figure 89. Cost Contour Plot for Theoretical Analysis Procedures for Uniaxial Loading.

7.2.2 Uniaxial loading: example two

The second set of footing designs considers the scaled CO_2 fitness function defined in

Equation (303) with the design parameters given in Table 12. From 1,000 designs, the

lowest CO_2 emission design using the simplified analysis procedures is 7,920.67 kg, with

an average CO_2 emission value of 8,520.88 kg and standard deviation of 423.57 kg. On

average, the multiphase BB-BC procedure performed 21,490 analyses before

convergence completed 63% of the computational effort in Phase 1 when using the

simplified analysis procedures. The lowest CO_2 emission design using the theoretical

analysis procedures is 5,675.44 kg, with an average CO_2 emission value of 6,268.98 kg

and standard deviation of 370.04 kg. On average, the multiphase BB-BC procedure

performed 22,949 analyses before convergence and completed 59% of the computational effort in Phase 1 when using the theoretical analysis procedures.

Table 15 summarizes of the lowest CO_2 emission designs developed by the BB-BC procedure. Several observations can be made by comparing the CO_2 emissions of the spread footing design based on the simplified analysis procedures with the one based on the theoretical analysis procedures. On average, there is a 26.4% savings in CO_2 emissions when the theoretical analysis procedures are used. As with cost, the excavation volume is slightly higher based on the theoretical analysis procedures; however, more significantly, all of the other quantities are less. There is approximately 70% less rebar mass in the design based on the theoretical analysis procedures. Also, when using the theoretical analysis procedures, some soil detachment is allowed. The detached distance for the design presented in this example is 0.0397 m, with a percentage of detachment of approximately 0.8%. For 1,000 runs, the average percent detachment is nearly zero. Although the average percent of detachment is nearly zero, the allowance of possible detachment that the theoretical analysis procedures provide, coupled with the more realistic triangular-shaped bearing pressure distribution, results in a significant savings in CO_2 emissions.

Figure 90 shows a surface plot of the best CO_2 emission values based upon the theoretical analysis procedures. The general trend shows that as the applied load and equivalent eccentricity increase, the best CO_2 emission values increase drastically. Figure 91 shows a surface plot of the difference between the average of the low CO_2 emission designs using both simplified analysis procedures and the theoretical analysis procedures. The general trend shows that as the applied load and equivalent eccentricity increase, the

additional CO_2 emission associated with the simplified analysis procedures increases

dramatically. Figure 92 shows a contour plot of average low-CO_2 emission designs using

the theoretical analysis procedures, where each contour represents a 1,000 kg increment

in average CO_2 emission. The bold boundary indicates where detachment first occurs. As

with low cost designs, the area to the right of the boundary indicate designs where the

loading is outside of the kern. A general trend shows an inflection point in the contours

located approximately where designs first have soil detachment.

Table 15. Uniaxial Loading Designs Based on Scaled CO_2 Fitness

Design Variables	Simplified Analysis	Theoretical Analysis
X_1 (m)	2.40	2.14
X_2 (m)	2.56	2.74
X_3 (m)	0.31	0.31
X_4 (m)	1.07	0.93
R_1	7	6
R_2	32	40
R_3	8	6
R_4	25	38
R_5	6	4
R_6	8	12
S_1 (MPa)	25	25
L	5.40	5.14
B	3.02	3.20
H	1.30	1.16
Detached Distance (m)	—	0.0397
Excavation (m^3)	5.861	5.898
Concrete Formwork (m^2)	21.861	19.319
Reinforcement (kg)	809.033	240.521
Concrete (m^3)	21.055	19.009
Compacted Backfill (m^3)	0.811	0.803
Best CO_2	7,920.67 kg	5,675.44 kg
Average CO_2	8,520.88 kg	6,268.98 kg
Std. Dev. CO_2	423.57 kg	370.04 kg
Average No. Analyses	21,490	22,949
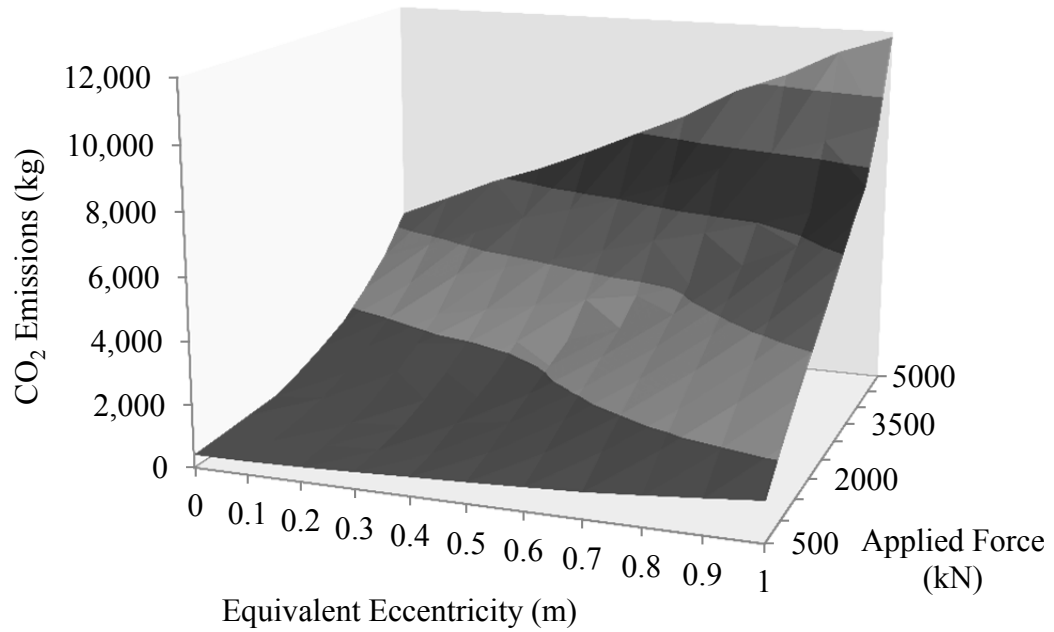
Figure 90. Best CO_2 Emissions Designs using Theoretical Analysis
Procedures for Uniaxial Loading.
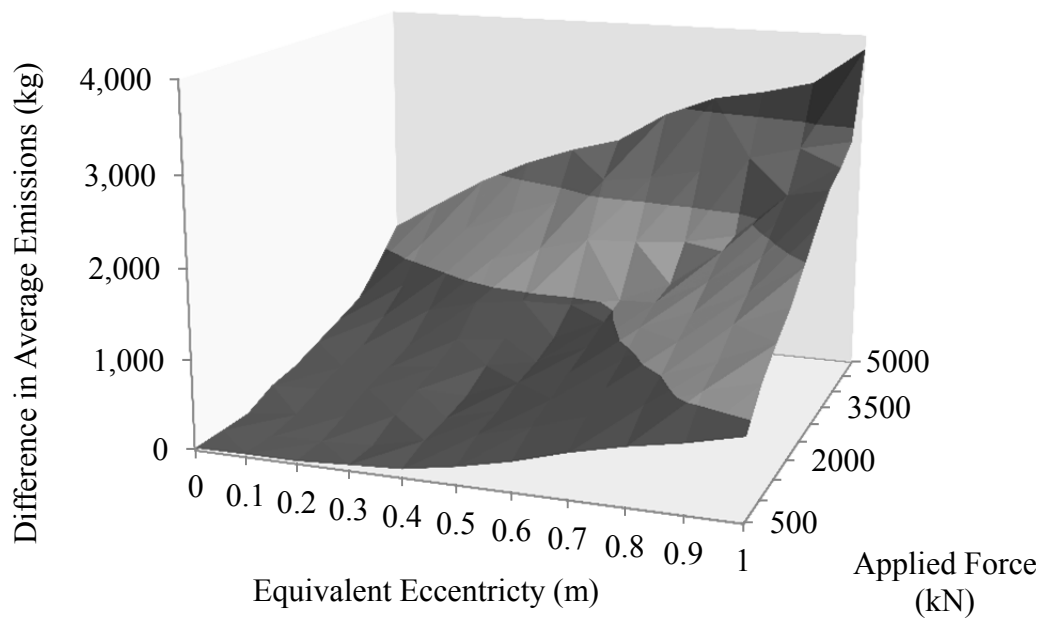
Figure 91. Difference in low-CO_2 Emissions Designs using Simplified Analysis
Procedures and Theoretical Analysis Procedures for Uniaxial Loading.
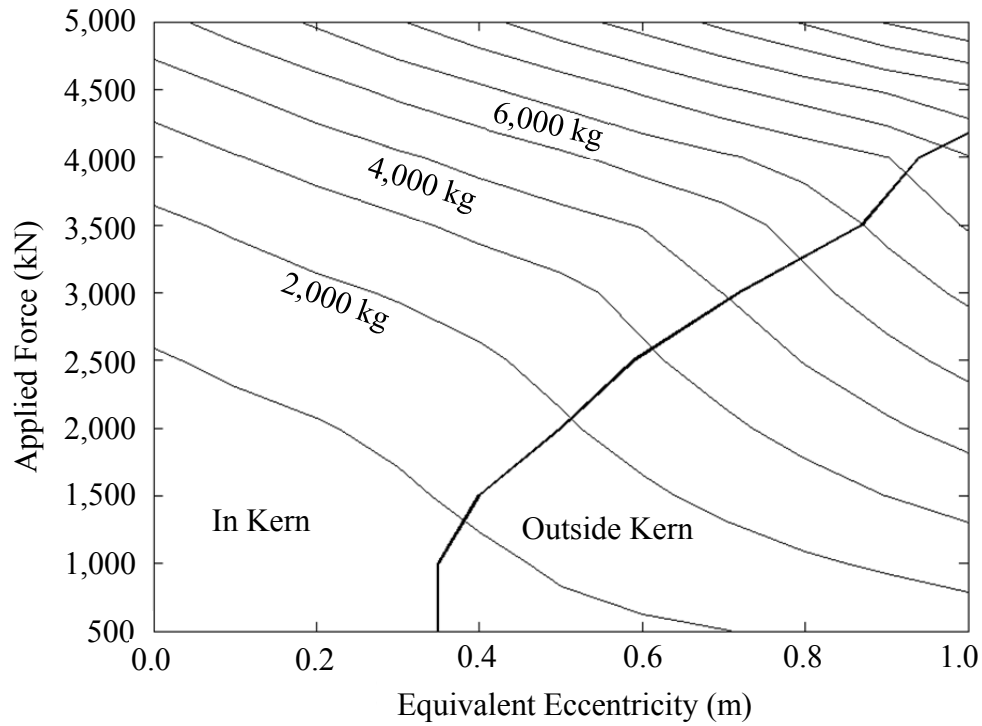
Figure 92. CO_2 Emission Contour Plot for Theoretical Analysis
Procedures for Uniaxial Loading.

7.2.3 Multi-objective optimization

In order to observe a relationship between the cost and CO_2 emissions for the

theoretical and simplified analysis procedures, the BB-BC algorithm was applied to the

multi-objective fitness function, using the weighted aggregation approach given by

Equation (306) with the design input parameters given in Table 12. To better reflect the

tradeoff between cost and CO_2 emissions, the reinforcement scale factor ξ used in the

single objective fitness functions was taken as 1 and $f'_{cmin} = f'_c$. The value of ζ was varied

from 0 to 1 by 0.01.

Figure 93 shows that, on average, as cost increases CO_2 emissions decrease when the

theoretical analysis procedures are applied to the design example. That is, as the value of

ζ approaches 1, cost decreases and CO_2 emissions increase. Also, the data shows that when more weight is on the cost function, designs are produced with a higher average concrete compressive strength. As the CO_2 emissions function is weighted more heavily, the average concrete compressive strength drops. Figure 94 shows the relationship between best low-CO_2 emissions with best low-cost for different values of the concrete compressive strength when the theoretical analysis procedures are applied to the design example. For groups of designs where the strength of concrete is constant, a slight increase in cost has a correspondingly small increase in CO_2 emission. When the entire set of designs is considered, a more significant trend is observed where the strength of concrete has a more significant effect on both cost and CO_2 emissions. In this case, as the strength of concrete decreases, CO_2 emissions decrease by up to 20% while cost increases only 6%. This difference is due to the increased CO_2 emission associated with the larger quantities of cement in the higher strength mix designs.

Figure 93. Pareto Front for Average Cost and CO_2 Emissions using Theoretical Analysis Procedures for Uniaxial Loading.
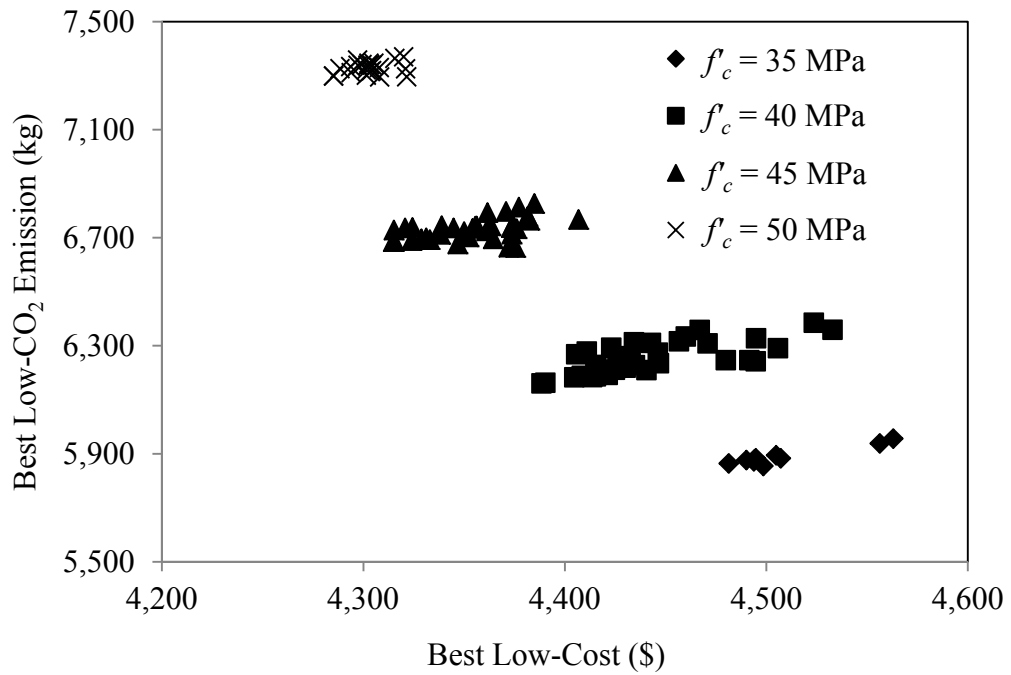
Figure 94. Effects of Concrete Strength on Cost and CO_2 Emissions using Theoretical Analysis Procedures for Uniaxial Loading.

Figure 95 shows that, on average, as cost increases CO_2 emissions decrease when the simplified analysis procedures are applied to the design example. The steeper slope of the data when the multi-objective function is weighted more heavily for cost indicates a drastic decrease in average CO_2 emissions for a relatively small increase in average cost. As the weights on the cost and CO_2 emission components of the multi-objective function become equal and the CO_2 emissions become weighted more heavily, the data shows a smaller decrease in CO_2 emissions with increasing cost. Like with the theoretical analysis procedures, the data shows that when more weight is on the cost function, designs are produced with a higher average concrete compressive strength. As the CO_2 emissions function is weighted more heavily, the average concrete compressive strength drops. Figure 96 shows the relationship between best low-CO_2 emissions with best low-cost for different values of the concrete compressive strength when the simplified analysis procedures are applied to the design example. For groups of designs where the strength of concrete is constant, a slight increase in cost has a correspondingly small increase in CO_2 emission. When the entire set of designs is considered, a more significant trend is observed where the strength of concrete has a more significant effect on both cost and CO_2 emissions. In this case, as the strength of concrete decreases, CO_2 emissions decrease by up to 12% while cost increases only 2.5%. Compared to the theoretical analysis procedure multi-objective optimization, there is less decrease in CO_2 emissions for a relatively small increase in cost.
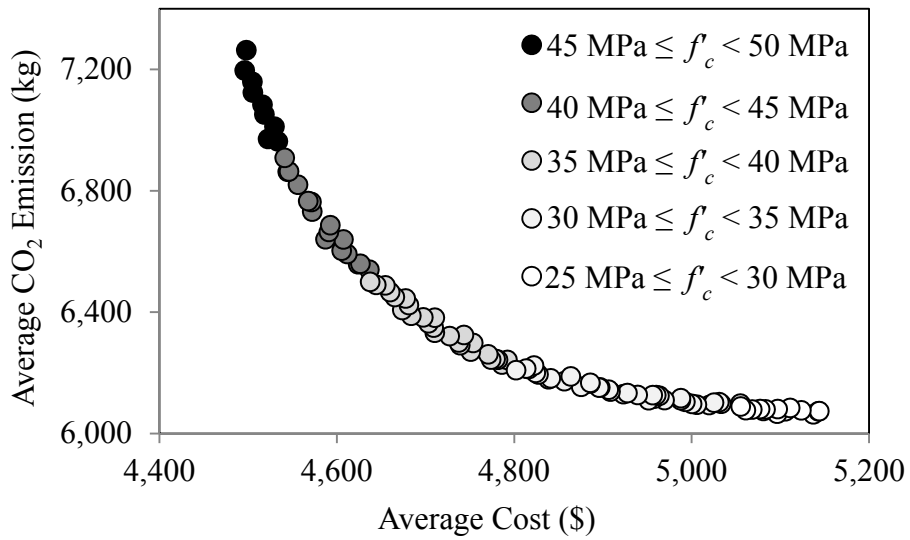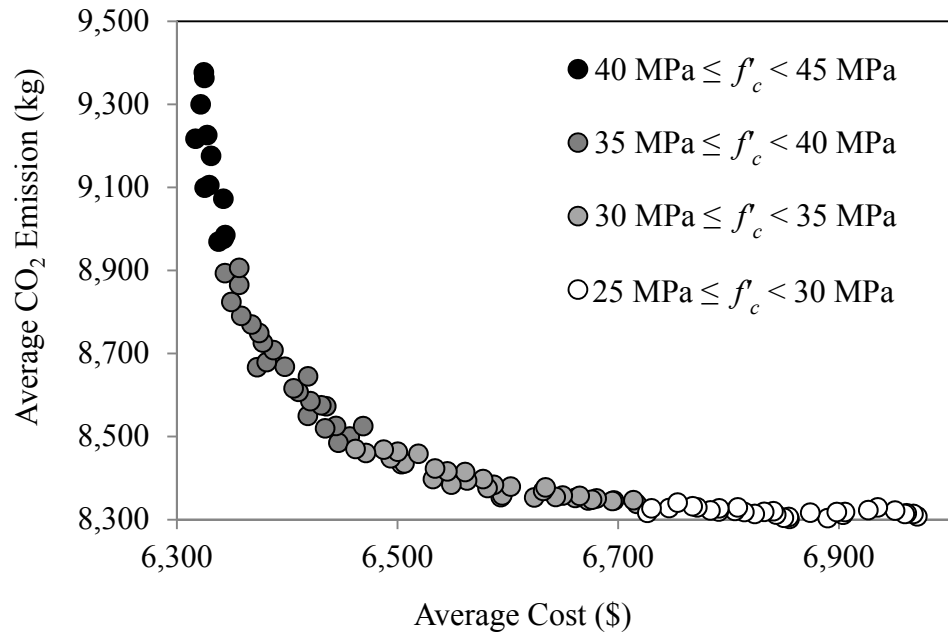
Figure 95. Pareto Front for Average Cost and CO_2 Emissions using Simplified Analysis Procedures for Uniaxial Loading.
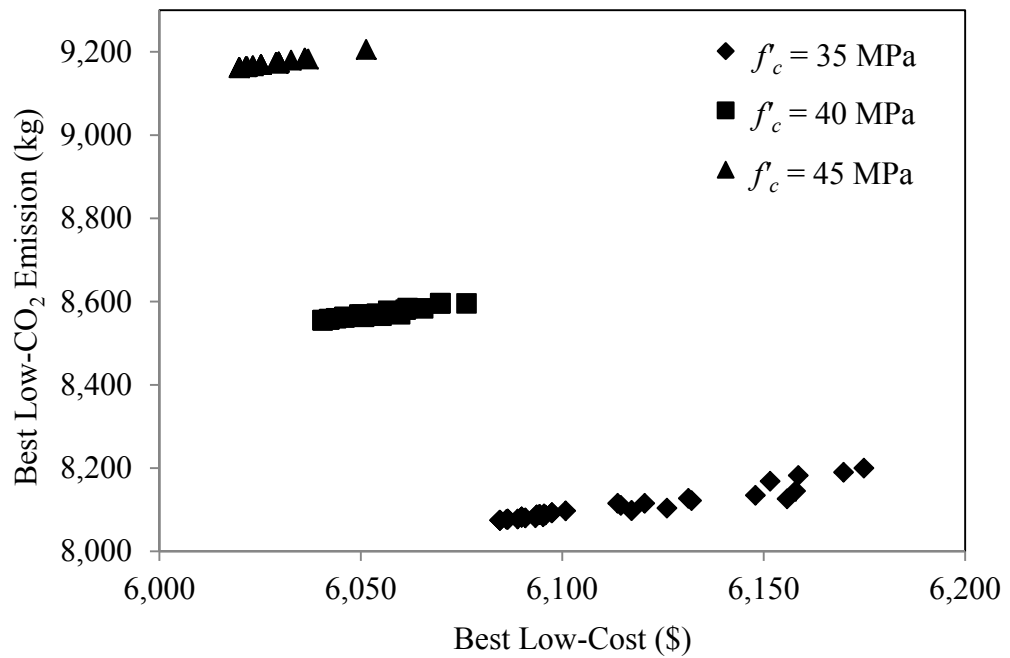
Figure 96. Effects of Concrete Compressive Strength on Cost and CO_2 Emissions using Simplified Analysis Procedures for Uniaxial Loading.

Figure 97 shows the data from Figure 93 and Figure 95 plotted on the same set of axes, without coloring based on concrete compressive strength. It is clear that there is a significant savings in both cost and CO_2 emissions when the theoretical analysis procedures are used over the simplified analysis procedures. In addition, the curvature of the data shows a smoother transition from the low-cost to low-CO_2 emissions when the theoretical analysis procedures are used. Due to the nature of the simplified analysis procedures, the multi-objective optimization is utilizing less of a variety of concrete compressive strengths, with more of the designs having lower concrete compressive strengths. This causes a steep decrease in CO_2 emissions as more weight is applied to the CO_2 emission component of the multi-objective function.
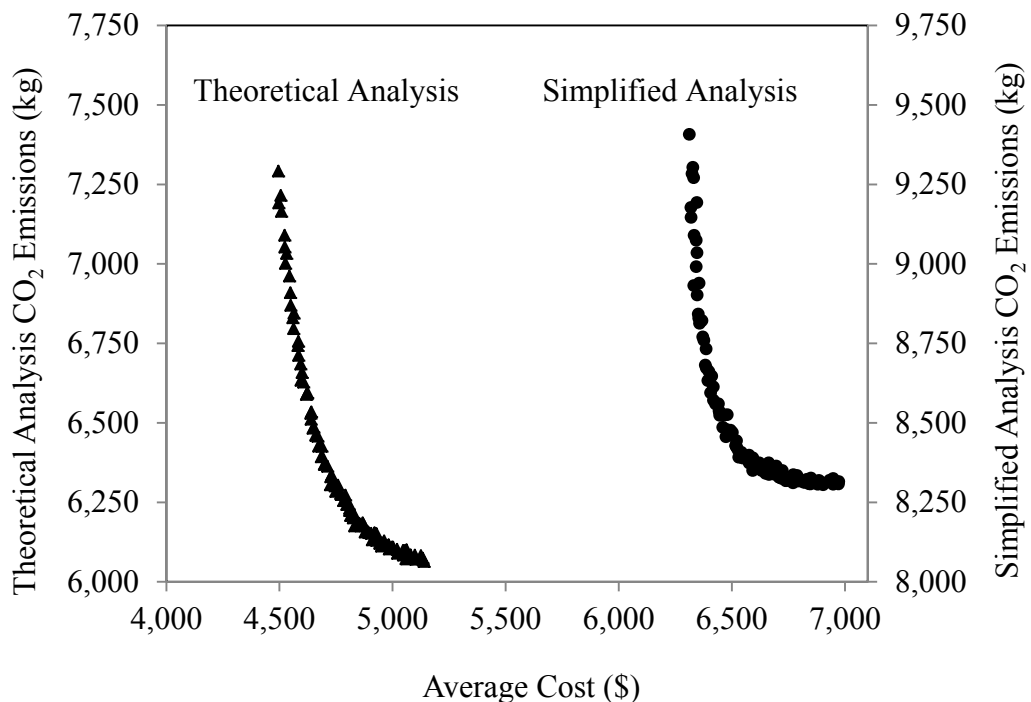
Figure 97. Pareto Fronts for Theoretical and Simplified Analysis for Uniaxial Loading.

7.3 Biaxial Loading

The objective of these design examples is to investigate the cost and CO_2 emission impact between using the theoretical analysis procedures and simplified analysis procedures when designing a spread footing subjected to a biaxial bending moment. Recall that the applied bending moments may also be expressed as an applied point load acting at equivalent eccentricities along the positive x and y axes. The discrete variable BB-BC footing design procedure is applied for the cost objective function and again for the CO_2 objective function. All designs will satisfy geotechnical limit states, as well as the ACI 318-11 requirements for reinforced concrete. As with uniaxial loading, both examples considers the four design variables associated with the geometry of the footing $(X_1 - X_4)$, six design variables representing the steel reinforcement $(R_1 - R_6)$, and one design variable representing the strength of the concrete (S_1), as defined in Section 6.2. Table 11 lists the upper and lower limits of the design variables, which are identical to the uniaxial loading examples. The size of the resulting search space is approximately $4.75(10^{17})$ possible designs.

As with the concentric and uniaxial loading examples, parametric studies suggest that a population of 300 candidate solutions and a general stopping criterion of 2,000 analyses without any change in $\vec{x}_g^{best}$ are sufficient. Based upon a sensitivity study, $\omega_1 = 0.3$ and $\omega_2 = 0.6$ required in Equation (332) routinely provide the best footing designs for this example. Since the uniaxial optimization problem is a simplification of the biaxial optimization problem and the design variables along with their ranges have not changed between the uniaxial and biaxial analysis, the parameter studies for initial population, stopping criteria and ω_1 and ω_2 are the uniaxial and biaxial analyses are identical.

Therefore, Figures 84, 85, and 86 are applicable to the biaxial loading case. A value of $\tau = 1$ is also used in Equation (332). In order to give the steel reinforcing term a magnitude comparable to that of the other terms, the scale factors used in Equations (302) and (303) are taken as $\xi = 10$ and $f''_{cmin} = 20$ MPa for both biaxial loading examples. In order to show how different applied loads and moments affect the average cost and average CO_2 emission designs, applied loads of 1,000 kN, 3,000 kN, and 5,000 kN are applied for equivalent eccentricities ranging from 0 m to 1 m along the positive x and y axes. Figure 98 shows surface plots of average cost for equivalent eccentricities along the x and y axes for (a) 5,000 kN, (b) 3,000 kN, and (c) 1,000 kN. Figure 99 shows surface plots for average CO_2 emissions versus equivalent eccentricities along the x and y axes for (a) 5,000 kN, (b) 3000 kN, and (c) 1,000 kN. Both figures show the significant upward shift in cost and CO_2 emissions as load increases. For the two biaxial design examples, the applied load will be taken as 3,000 kN and the applied moments will be taken as 3,000 kN-m each, which represents one specific point in the middle plots of Figures 98 and 99.

Table 16 lists the specified column, footing, and soil design parameters. In order to build upon the uniaxial loading design examples, all of the design parameters remain the same with the only additional information being the second applied moment.
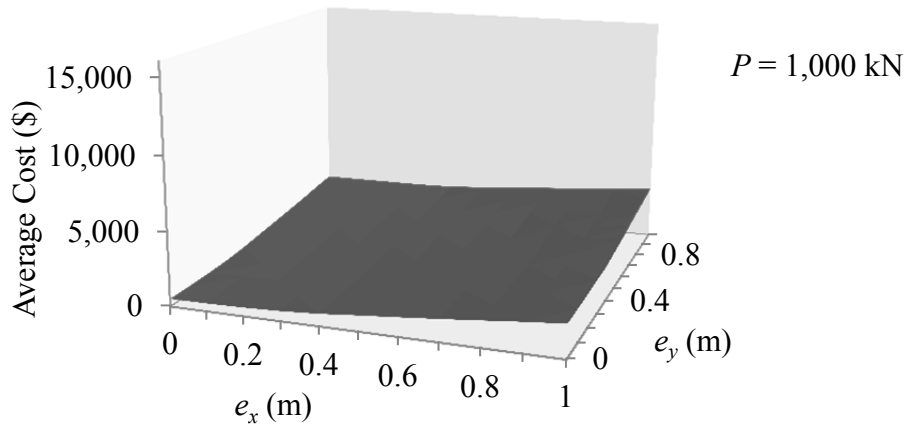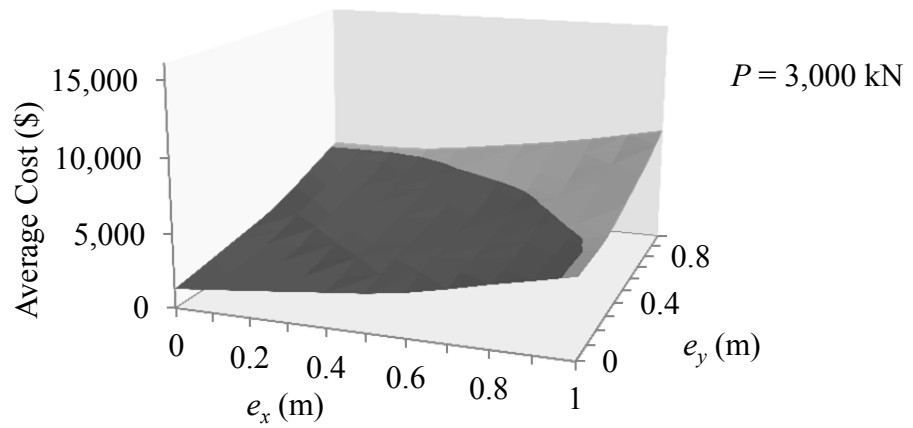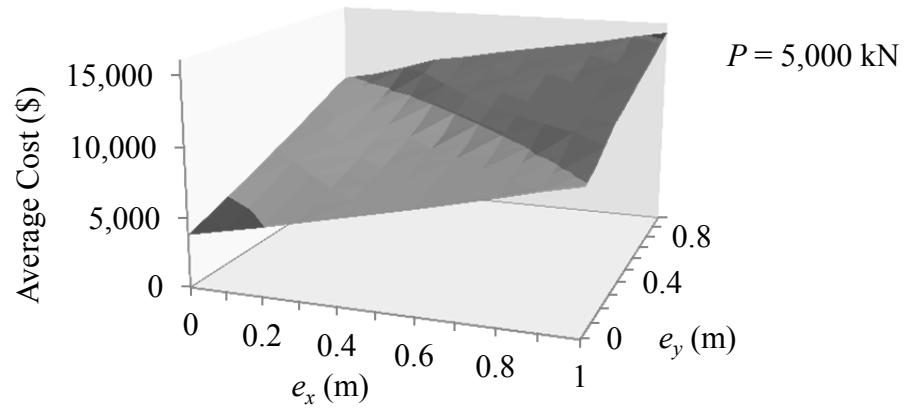
Figure 98. Average Cost for Various Applied Loads and Equivalent Eccentricities for Biaxial Loading.
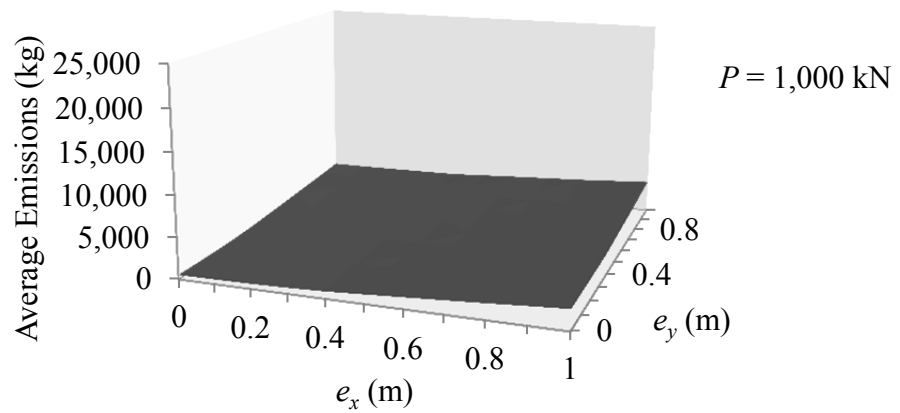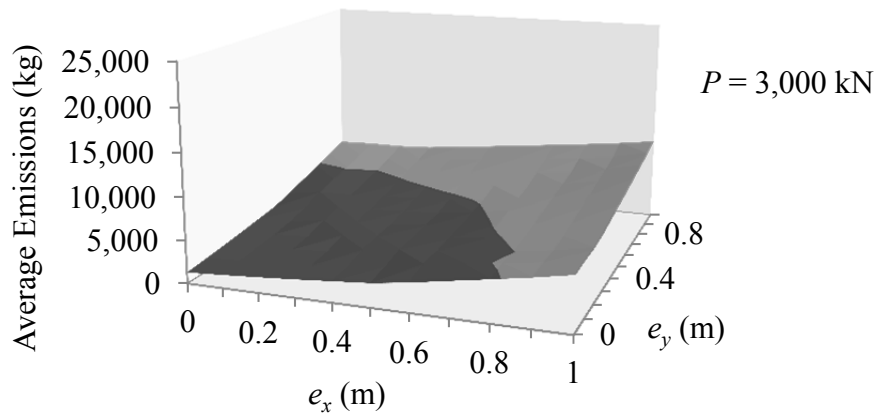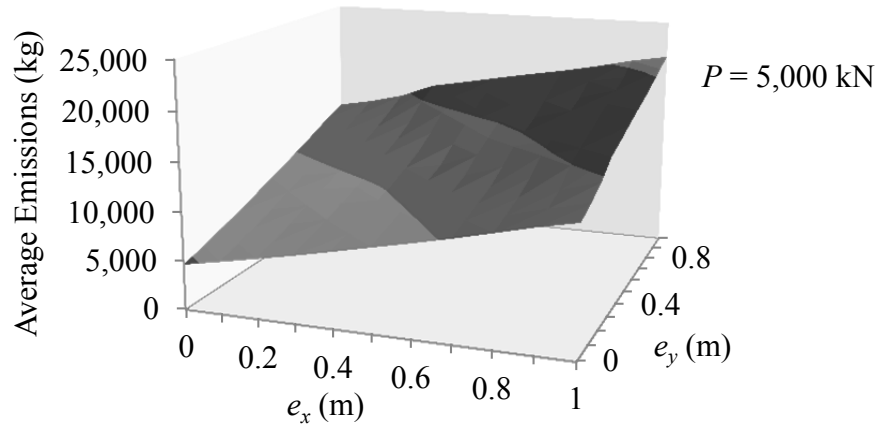
Figure 99. Average CO_2 Emissions for Various Applied Loads and Equivalent Eccentricities for Biaxial Loading.

Table 16. Biaxial Loading Example Input Parameters

Input parameter	Unit	Symbol	Value
Internal friction angle of soil	degree	ϕ'	35
Unit weight of soil	kN/m^3	γ_s	18.5
Poisson Ratio of soil	—	ν	0.3
Modulus of elasticity of soil	MPa	E	50
Applied vertical force	kN	P	3,000
Over excavation length	m	L_o	0.3
Over excavation width	m	B_o	0.3
Factor of safety for bearing capacity	—	FS	3.0
Maximum allowable settlement	mm	δ	25
Applied Moment about x-axis*	kN-m	M_x	3,000
Applied Moment about y-axis*	kN-m	M_y	3,000
Unit weight of concrete*	kN/m^3	γ_c	23.56
Modulus of elasticity of steel*	GPa	E_s	199.95
Column length*	mm	l_{col}	457.2
Column width*	mm	b_{col}	457.2
Concrete Cover in Footing*	mm	*cover*	76.2
Minimum Footing Thickness*	mm	T_{min}	228.6

Note: All values given by Wang and Kulhawy (2008) except for * values which are assumed.

7.3.1 Biaxial loading: example one

The first set of footing designs considers the scaled cost fitness function defined by Equation (302). The applied column load is $P = 3,000$ kN and applied column moments are $M_x = 3,000$ kN-m and $M_y = 3,000$ kN-m. From 1,000 optimization runs, the best low-cost design using the simplified analysis procedures is $21,595.39, with an average cost of $22,414.92 and standard deviation of $528.88. On average, the multiphase BB-BC procedure performed 25,032 analyses before convergence and completed 71% of the computational effort in Phase 1 when using the simplified analysis procedures. The best low-cost design using the theoretical analysis procedures is $6,888.80, with an average cost of $8,177.29 and standard deviation of $517.33. On average, the multiphase BB-BC procedure performed 24,185 analyses before convergence and completed 63% of the computational effort in Phase 1 when using the theoretical analysis procedures.

Table 17 summarizes the low-cost designs developed by the BB-BC procedure. Several important observations can be made by comparing the cost of the spread footing design based on the simplified analysis procedures with the one based on the theoretical analysis procedures. First, on average, there is a 63.5% savings in cost when using the theoretical procedures. While all material quantities are significantly less when the theoretical analysis procedures are used, most notably there is approximately 88% less rebar mass in the design based on the theoretical analysis procedures. Since the moment at the face of the column is based on the maximum bearing pressure beneath the footing, and the rebar length spans between the clear covers in both directions of the footing, the mass of reinforcement is significantly higher for the design based on the simplified analysis procedures. Secondly, when using the theoretical analysis procedures, some soil

detachment is allowed whereas for the simplified analysis procedures it is not. The equivalent eccentricities fall within Region A in Figure 6, causing approximately 14.6% of the plan area of the footing to detach from the soil.

A sensitivity study is done by varying the applied column bending moments. Table 18 shows the variation of eccentricities. Figure 100 shows a surface plot of the best low-cost designs using the theoretical analysis procedures. The general trend shows that as the eccentricities increase, the cost increases drastically. Figure 101 shows a surface plot of the difference between average low-cost designs based on the simplified analysis procedures and the theoretical analysis procedures. The general trend shows that as the eccentricities increase, the difference in cost increases dramatically.

Table 17. Biaxial Loading Designs Based on Scaled Cost Fitness

Design Variables	Simplified Analysis	Theoretical Analysis
X_1 (m)	3.26	1.96
X_2 (m)	3.62	1.96
X_3 (m)	2.96	0.39
X_4 (m)	1.35	0.84
R_1	9	7
R_2	31	33
R_3	10	7
R_4	27	34
R_5	9	4
R_6	12	10
S_1 (MPa)	25	40
B	6.26	4.96
L	6.62	4.96
H	1.58	1.07
Region	Kern	A
Detached Area (m^2)	—	3.98
Detached Percent	—	14.6 %
excavation (m^3)	134.370	10.790
Concrete Formwork (m^2)	40.665	21.201
Reinforcement (kg)	2,105.785	259.568
Concrete (m^3)	65.151	26.256
Compacted Backfill (m^3)	68.662	1.196
Best Cost	$ 21,595.39	$ 6,888.80
Average Cost	$ 22,414.92	$ 8,177.29
Std. Dev. Cost	$ 528.88	$ 517.33
Average No. Analyses	25,032	24,185

Table 18. Biaxial Loading Eccentricity Parameters

Parameter	Unit	Lower bound	Upper bound	Increment
e_x	m	0.0	1.0	0.1
e_y	m	0.0	1.0	0.1
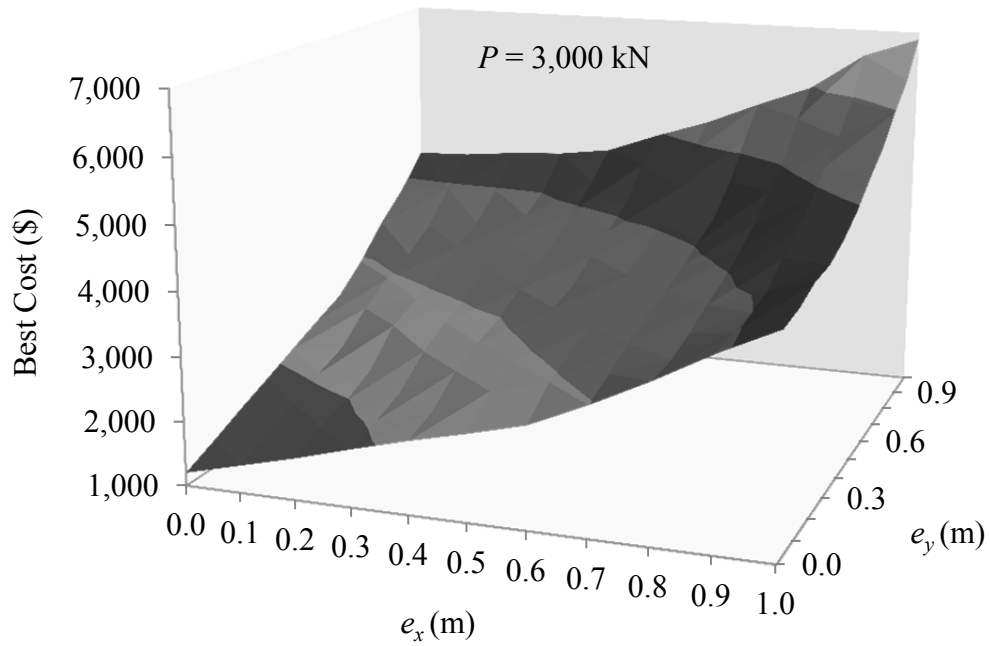
Figure 100. Cost of Biaxial Loading Designs using Theoretical Analysis Procedures.
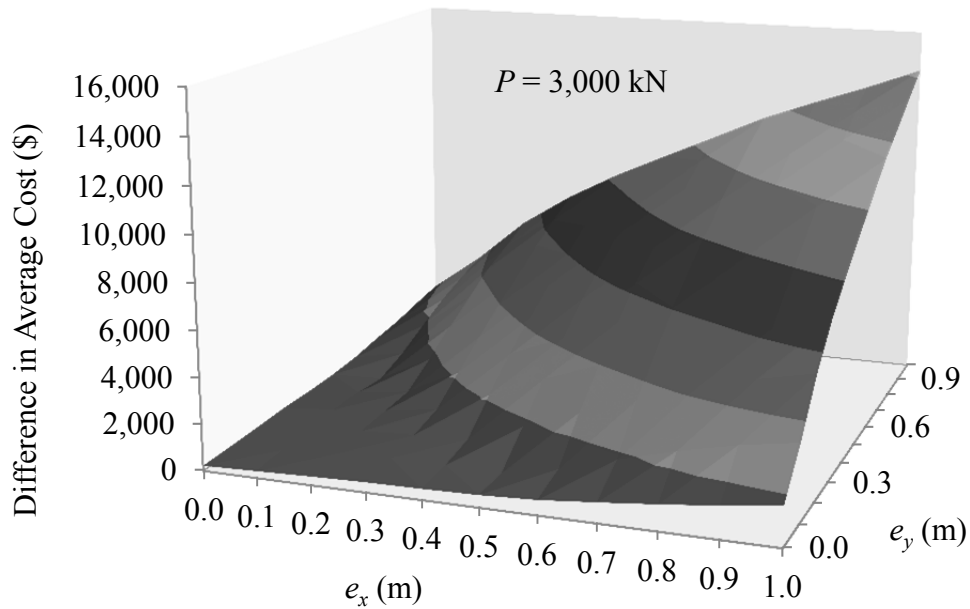
Figure 101. Difference in Average Low-Cost Designs using Simplified Analysis
Procedures and Theoretical Analysis Procedures for Biaxial Loading.

Since detachment is allowed in the theoretical analysis procedures, the area of

detachment is estimated. Figure 102 shows a plot of the average area of the footing that

has become detached from the soil. As equivalent eccentricities increase, the average

detached area increases drastically. Figure 103 shows a plot of the average percent of

area of the footing that has become detached from the soil. The surface shows that the

maximum percentage of area that has become detached from the soil is approximately

14.6%. Figure 104 shows a plot of the kern area, Region A, Region B, and Region C of

detachment overlain by a scatter plot of the eccentricity ratios e_x/L and e_y/B of the best

low-cost designs. Recall that the equivalent eccentricities for these designs include the

weight of the footing itself. It is seen that as eccentricity ratios grow, the optimization

yields footing designs in which one corner has become detached from the soil. For the

uniaxial cases, some low-cost designs just fall within Regions B and C, yielding two

detached corners. Figure 104 shows that footings with some detachment are still feasibly

designed. The trend seen in Figure 101 coupled with that shown in Figure 104 provide

evidence that by allowing some detachment of the footing from the soil, there is a

significant savings in cost.
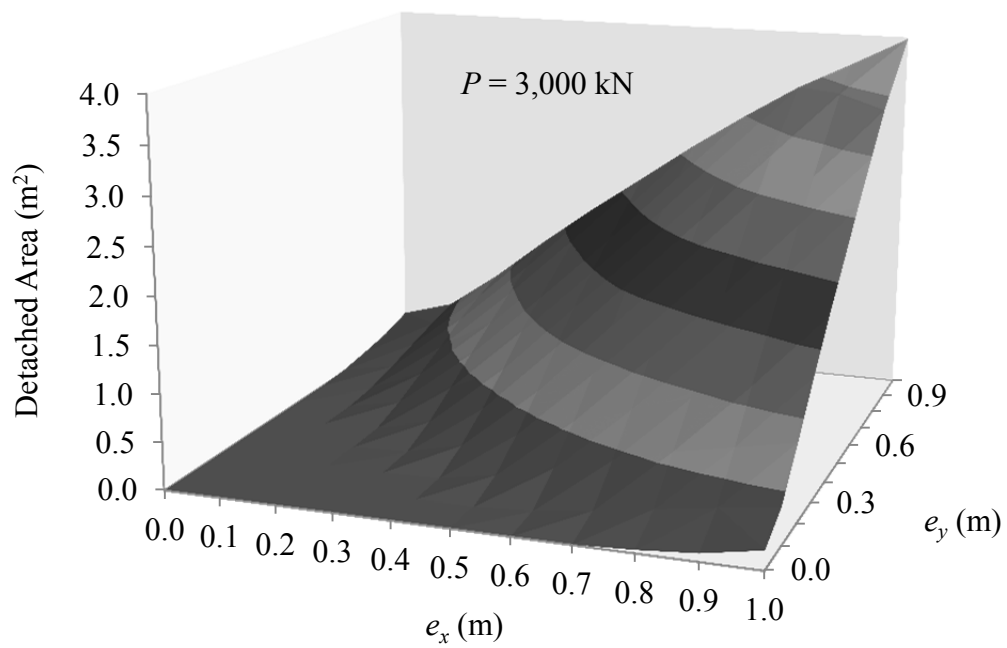
Figure 102. Average Detached Area of Biaxial Loaded Footing.
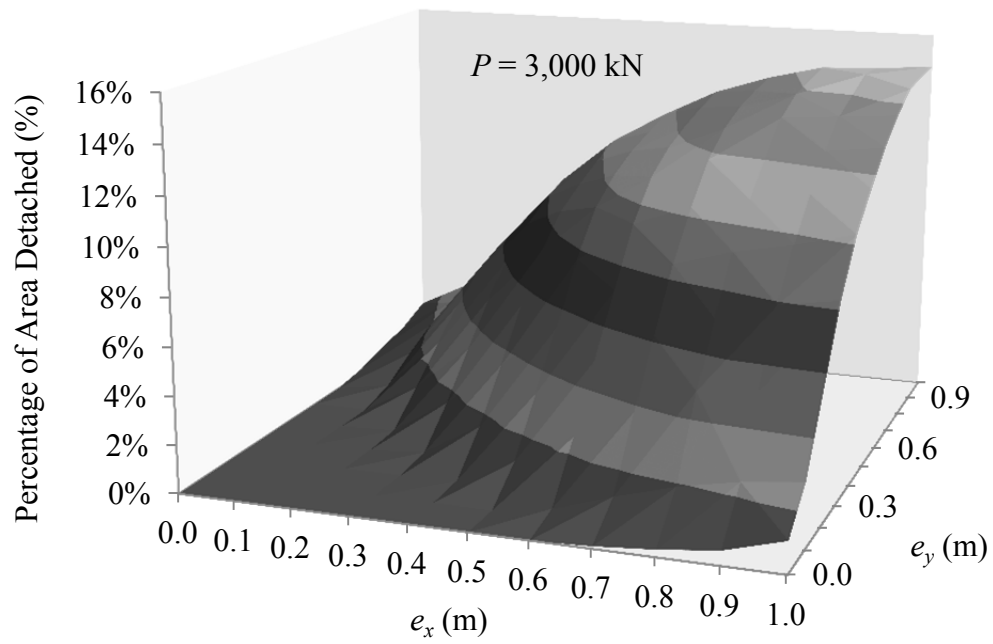
Figure 103. Average Percentage of Detached Area of Biaxial Loaded Footing.
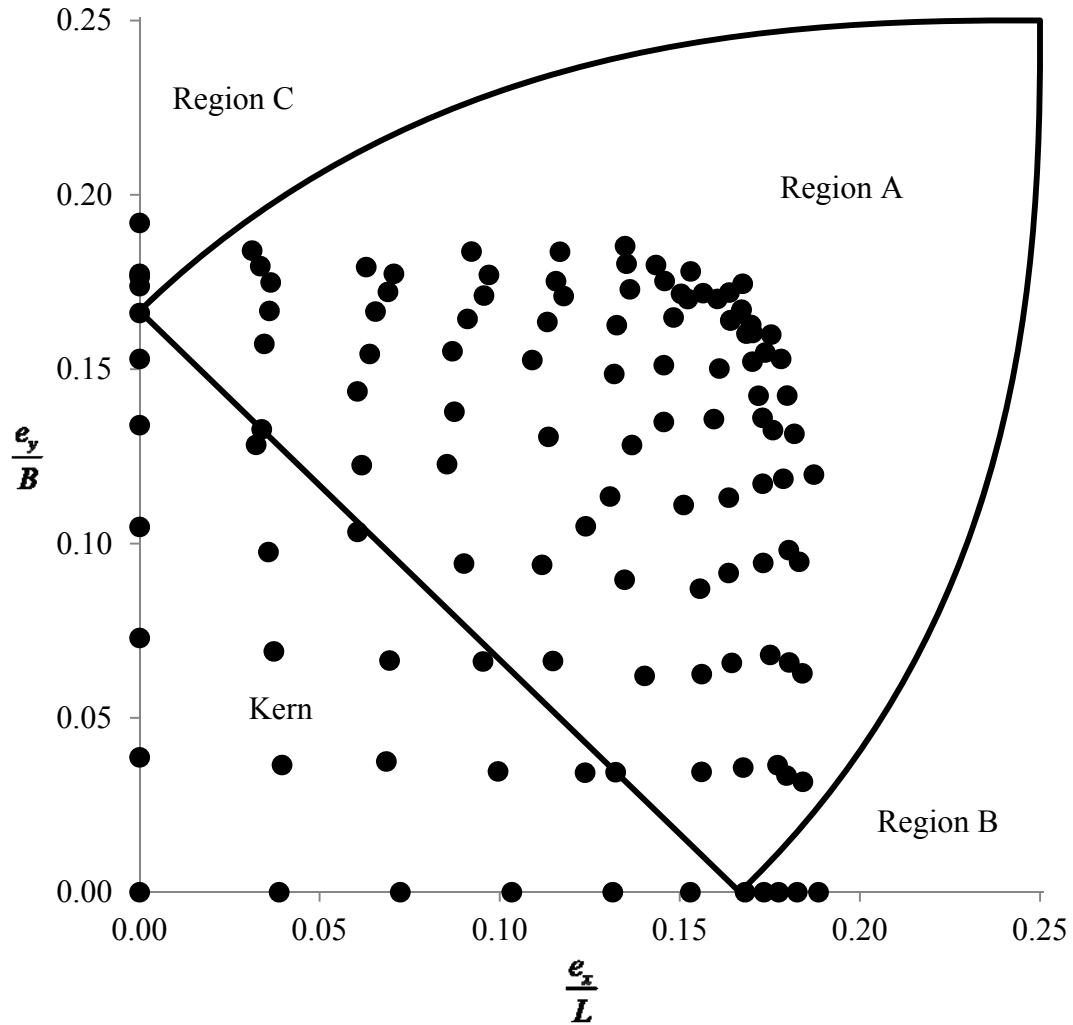
Figure 104. Biaxial Loading Low-Cost Designs by Detachment Region for $P = 3,000$ kN.

In practice, engineers may want to apply all of the simplified analysis procedures, except for allowing uplift. To determine the impact of allowing uplift, Example One was run based on theoretical analysis procedures without allowing uplift. That is, the theoretical analysis procedures were used, with the exception that the kern penalty was applied. Table 19 summarizes the low-cost designs developed by the BB-BC procedure. Several important observations can be made by comparing the cost of the spread footing

design based on theoretical analysis procedures that do not allow uplift with the one based on the theoretical analysis procedures that allow uplift. First, on average, there is a 50.3% savings in cost when uplift is allowed. All material quantities are significantly less when uplift is allowed. There is approximately 92% less excavation volume, 35% less rebar mass, 48% less concrete volume, and 99% less backfill volume in the design based on allowing uplift. This data shows that not allowing uplift but applying the other theoretical analysis procedures (i.e., not applying the simplified analysis procedures) results in significant cost savings. It shows that allowing uplift can result in a significant savings in cost, while still satisfying geotechnical and structural limit states.

Table 19. Biaxial Loading Designs Based on Scaled Cost Fitness with and without Uplift

Design Variables	Theoretical Analysis without Uplift	Theoretical Analysis
X_1 (m)	3.56	1.96
X_2 (m)	3.40	1.96
X_3 (m)	2.97	0.39
X_4 (m)	0.98	0.84
R_1	8	7
R_2	36	33
R_3	8	7
R_4	36	34
R_5	4	4
R_6	12	10
S_1 (MPa)	35	40
B	6.56	4.96
L	6.40	4.96
H	1.21	1.07
Region	Kern	A
Detached Area (m^2)	—	3.98
Detached Percent	—	14.6 %
excavation (m^3)	136.507	10.790
Concrete Formwork (m^2)	31.327	21.201
Reinforcement (kg)	398.873	259.568
Concrete (m^3)	50.691	26.256
Compacted Backfill (m^3)	85.397	1.196
Best Cost	$ 15,509.73	$ 6,888.80
Average Cost	$ 16,462.61	$ 8,177.29
Std. Dev. Cost	$ 470.44	$ 517.33
Average No. Analyses	22,797	24,185

7.3.2 Biaxial loading: example two

The second set of footing designs considers the scaled CO_2 fitness function. As with

cost, to build upon the concentric and uniaxial loading cases, the applied load is 3,000 kN

and applied column moments are $M_x = 3,000$ kN-m and $M_y = 3,000$ kN-m. From 1,000

optimization runs, the best low-CO_2 emission design using the simplified analysis

procedures is 25,041.20 kg, with an average CO_2 emission value of 27,415.41 kg and

standard deviation of 1,426.30 kg. On average, the multiphase BB-BC procedure

performed 25,304 analyses before convergence and completed 71% of the computational

effort in Phase 1 when using the simplified analysis procedures. The best low-CO_2

emission design using the theoretical analysis procedures is 9,279.84 kg, with an average

CO_2 emission value of 9,939.03 kg and standard deviation of $ 413.03. On average, the

multiphase BB-BC procedure performed 23,424 analyses before convergence and

completed 64% of the computational effort in Phase 1 when using the theoretical analysis

procedures. Table 20 summarizes the low-CO_2 emission designs developed by the BB-

BC procedure. Several observations can be made by comparing the CO_2 emissions of the

biaxial loaded spread footing design based on the simplified analysis procedures with the

one based on the theoretical analysis procedures. On average, there is a 63.7% savings in

CO_2 emissions when the theoretical analysis procedures are used. All material quantities

are significantly less when the theoretical analysis procedures are used; most notably,

there is approximately 88% less rebar and 98% less backfill in the design based on the

theoretical analysis procedures.

A sensitivity study is done by varying the applied column bending moments. Table 18

shows the variation of equivalent applied eccentricities. Figure 105 shows a surface plot

of the best CO_2 emission values based upon the theoretical analysis procedures. The general trend shows that as the eccentricities increase, the CO_2 emission values increase drastically. Figure 106 shows a surface plot of the difference between average CO_2 emission values of designs based on the simplified analysis procedures and the theoretical analysis procedures. The general trend shows that as the eccentricities increase, the difference in CO_2 emissions increases dramatically.

Table 20. Biaxial Loading Designs Based on Scaled CO_2 Fitness

Design Variables	Simplified Analysis	Theoretical Analysis
X_1 (m)	3.50	2.24
X_2 (m)	3.58	2.24
X_3 (m)	2.73	0.34
X_4 (m)	1.39	0.98
R_1	9	7
R_2	31	31
R_3	8	7
R_4	39	31
R_5	11	4
R_6	12	12
S_1 (MPa)	20	25
B	6.50	5.24
L	6.58	5.24
H	1.62	1.21
Region	kern	A
Detached Area (m^2)	—	3.66
Detached Percent	—	12.9 %
Excavation (m^3)	127.720	10.435
Concrete Formwork (m^2)	42.343	25.332
Reinforcement (kg)	2,118.037	257.114
Concrete (m^3)	68.958	33.153
Compacted Backfill (m^3)	58.260	1.100
Best CO_2 Emission	25,041.20 kg	9,279.84 kg
Average CO_2 Emission	27,415.41 kg	9,939.03 kg
Std. Dev. CO_2 Emission	1,426.30 kg	413.03 kg
Average No. Analyses	25,304	23,424
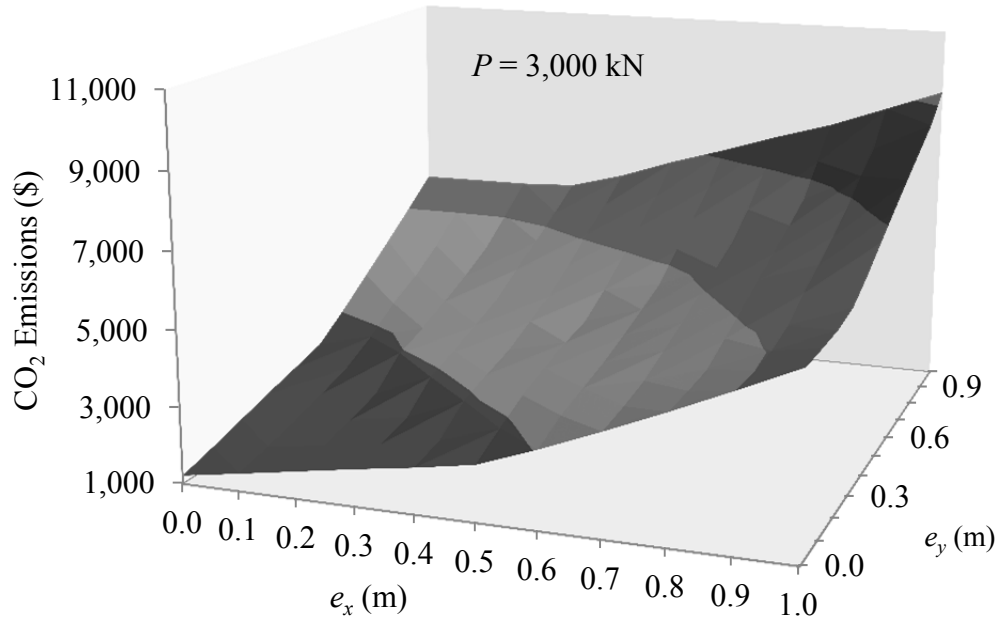
Figure 105. CO$_2$ Emissions of Biaxial Loading Designs using Theoretical Analysis Procedures.
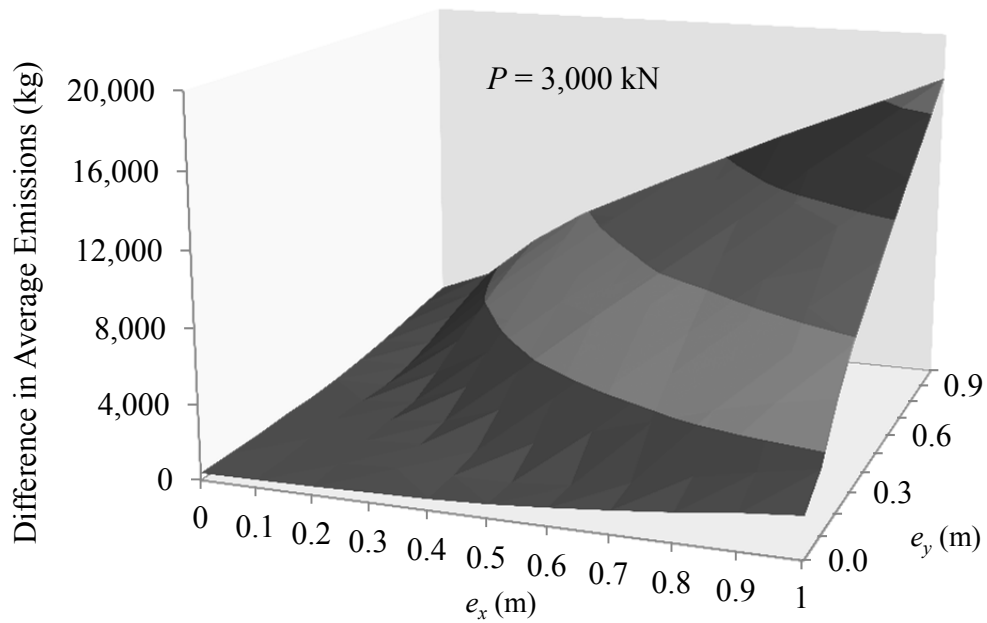
Figure 106. Difference in Average Low-CO$_2$ Emission Biaxial Loading Designs between Simplified Analysis Procedures and Theoretical Analysis Procedures.

As with the cost fitness function designs, detachment is allowed in the theoretical procedures. Figure 107 shows a plot of the average area of the footing that has become detached from the soil. As eccentricities increase, the detached area increases drastically. Figure 108 shows a plot of the average percent of area of the footing that has become detached from the soil. The surface shows that the maximum percentage of area that has become detached from the soil is approximately 13%. Figure 109 shows a plot of the kern area, Region A, Region B, and Region C of detachment overlain by a scatter plot of the eccentricity ratios e_x/L and e_y/B of the best low-CO_2 emission designs. It is seen that as eccentricity ratios grow, the optimization yields footing designs in which one corner has become detached from the soil. For the uniaxial cases, some low-cost designs just fall within Regions B and C, yielding two detached corners. This plot shows that footings with some detachment are still feasibly designed. As with cost, the trend seen in Figure 106 coupled with that shown in Figure 109 suggests a significant savings in CO_2 emissions can be achieved by allowing some detachment of the footing from the soil.
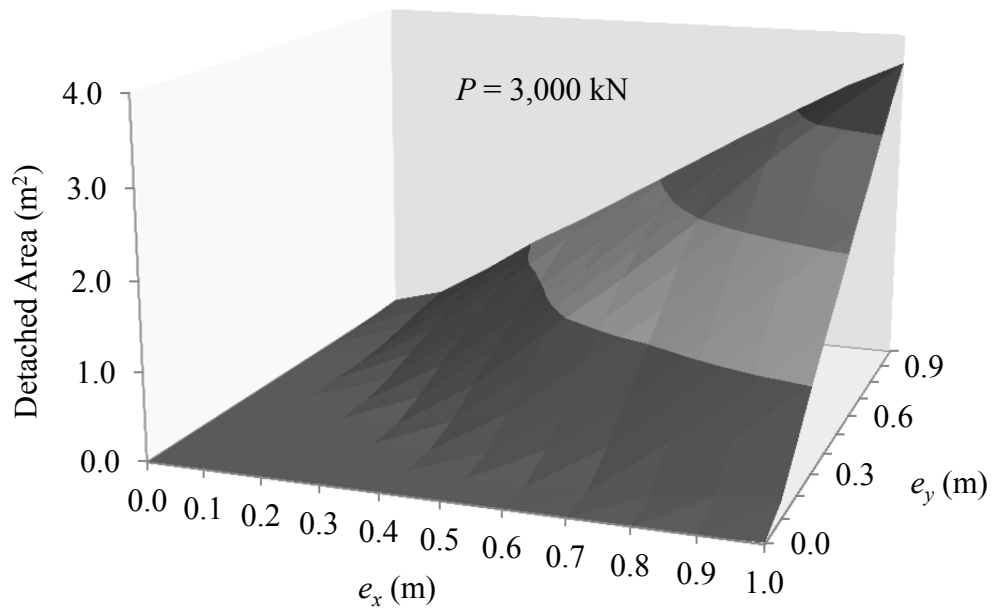
Figure 107. Average Detached Area of Biaxial Loaded Footing.
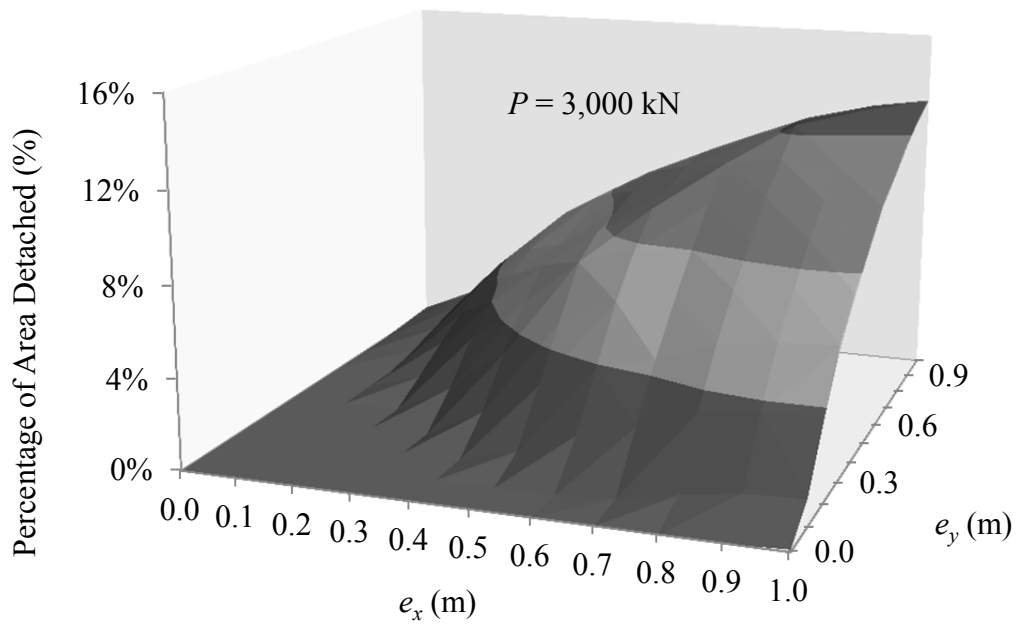
Figure 108. Average Percentage of Detached Area of Biaxial Loaded Footing.
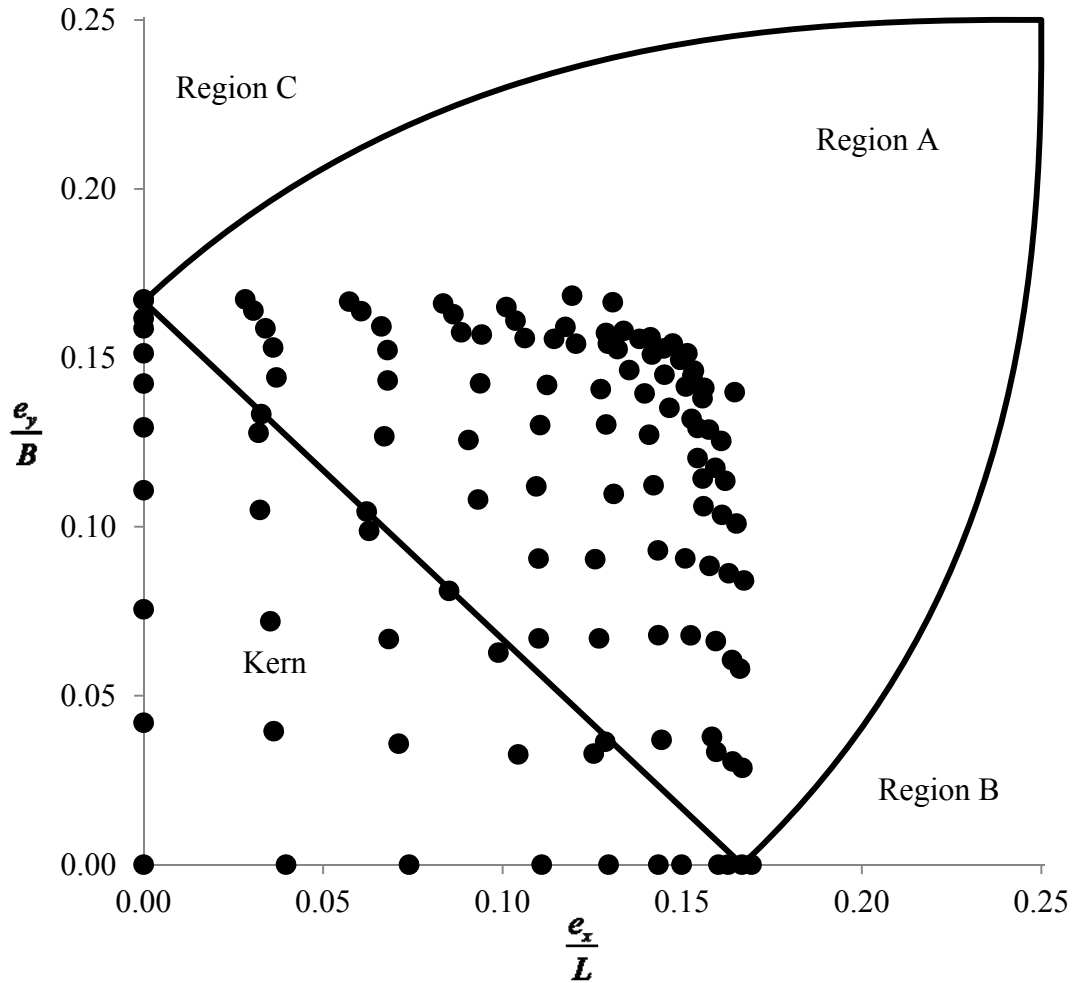
Figure 109. Biaxial Loading Low-CO$_2$ Emission Designs by
Detachment Region for $P = 3,000$ kN.

To determine the impact of allowing uplift on CO$_2$ emissions, Example Two was run

based on theoretical analysis procedures without allowing uplift. That is, the theoretical

analysis procedures were used, with the exception that the kern penalty was applied.

Table 21 summarizes the low-CO$_2$ emission designs developed by the BB-BC procedure.

Several important observations can be made by comparing the cost of the spread footing

design based on theoretical analysis procedures that do not allow uplift with the one

based on the theoretical analysis procedures that allow uplift. First, on average, there is a

50.0% savings in cost when uplift is allowed. All material quantities are significantly less

when uplift is allowed. There is approximately 92% less excavation volume, 54% less

rebar mass, 44% less concrete volume, and 98% less backfill volume in the design based

on allowing uplift. This data shows that not allowing uplift but applying the other

theoretical analysis procedures (i.e., not applying the simplified analysis procedures)

results in significant savings in CO_2 emissions. It shows that allowing uplift can result in

a significant savings in cost, while still satisfying geotechnical and structural limit states.

Table 21. Biaxial Loading Designs Based on Scaled CO_2 Emission Fitness with and without Uplift

Design Variables	Theoretical Analysis without Uplift	Theoretical Analysis
X_1 (m)	3.70	2.24
X_2 (m)	3.50	2.24
X_3 (m)	2.68	0.34
X_4 (m)	1.14	0.98
R_1	8	7
R_2	32	31
R_3	8	7
R_4	33	31
R_5	11	4
R_6	12	12
S_1 (MPa)	20	25
B	6.70	5.24
L	6.50	5.24
H	1.37	1.21
Region	Kern	A
Detached Area (m^2)	—	3.66
Detached Percent	—	12.9 %
excavation (m^3)	127.568	10.435
Concrete Formwork (m^2)	36.131	25.332
Reinforcement (kg)	562.070	257.114
Concrete (m^3)	59.531	33.153
Compacted Backfill (m^3)	67.691	1.100
Best CO_2 Emission	18,488.13 kg	9,279.84 kg
Average CO_2 Emission	19,912.92 kg	9,939.03 kg
Std. Dev. CO_2 Emission	707.67 kg	413.03 kg
Average No. Analyses	23,115	23,424

7.3.3 Multi-objective optimization

As with the concentric and uniaxial loading cases, to observe a relationship between the cost and CO_2 emissions for the theoretical and simplified analysis procedures, the BB-BC algorithm was applied to the multi-objective fitness function, using the weighted aggregation approach given by Equation (306) with the design input parameters given in Table 16. As with the concentric and uniaxial loading examples, the reinforcement scale factor ξ used in the single objective fitness functions is taken as 1 and $f'_{cmin} = f'_c$ to better reflect the tradeoff between cost and CO_2 emissions. The value of ζ was varied from 0 to 1 by 0.01.

Figure 110 shows that, on average, as cost increases CO_2 emissions decrease when the theoretical analysis procedures are applied to the design example. That is, as the value of ζ approaches 1, cost decreases and CO_2 emissions increase. Also, the data shows that when more weight is on the cost function, designs are produced with a higher average concrete compressive strength. As the CO_2 emissions function is weighted more heavily, the average concrete compressive strength drops. Figure 111 shows the relationship between best low-CO_2-emissions with best low-cost for different values of the concrete compressive strength when the theoretical analysis procedures are applied to the design example. For groups of designs where the strength of concrete is constant, a slight increase in cost has a correspondingly small increase in CO_2 emission. When the entire set of designs is considered, a more significant trend is observed where the strength of concrete has a more significant effect on both cost and CO_2 emissions. In this case, as the strength of concrete decreases, CO_2 emissions decrease by up to 20% while cost increases

only 7%. This difference is due to the increased CO_2 emission associated with the larger

quantities of cement in the higher strength mix designs.

Figure 110. Pareto Front for Average Cost and CO_2 Emissions using Theoretical Analysis Procedures for Biaxial Loading.
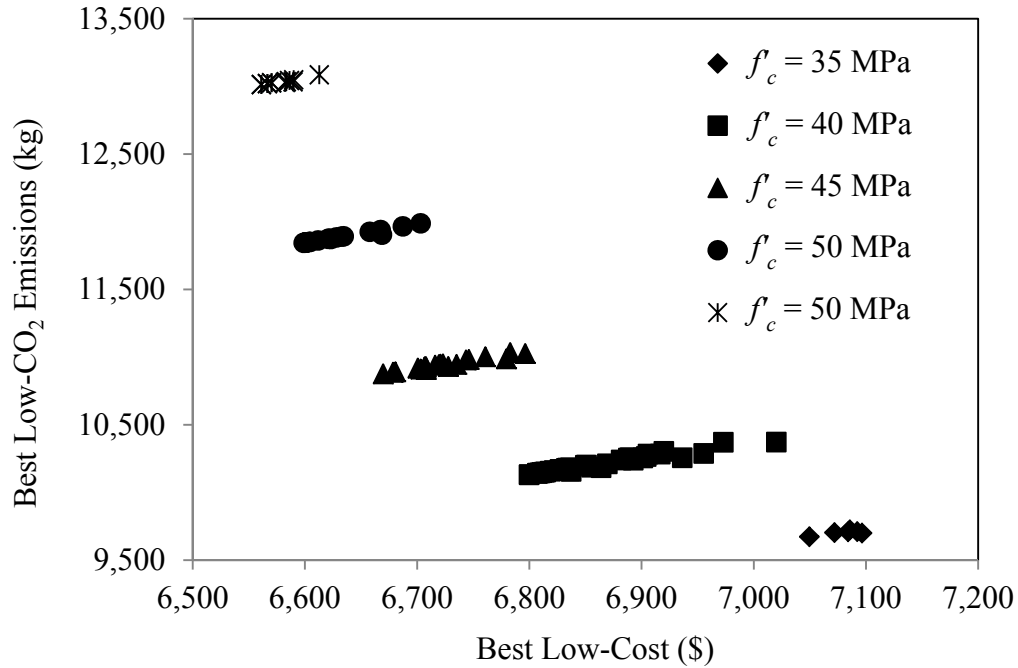
Figure 111. Effects of Concrete Strength on Cost and CO_2 Emissions using Theoretical Analysis Procedures for Biaxial Loading.

Figure 112 shows that, on average, as cost increases CO_2 emissions decrease when the simplified analysis procedures are applied to the design example. The designs shown in Figure 112 do not form a noticeable pareto front due to the nature of the simplified analysis procedures applied to the biaxial loading case. Recall that the maximum corner bearing pressure is assumed to be constant beneath the entire footing. Because of this, all of the structural limit states are based upon a substantially higher bearing pressure than what is actually occurring due to the loading. Many of the structural analysis procedures are highly sensitive to the bearing pressure distribution. For the simplified analysis procedures, the bearing pressure distribution is constant and no detachment is allowed. However, as with the theoretical analysis procedures, the data shows that when more weight is on the cost function, designs are produced with a higher average concrete

compressive strength. As the CO_2 emissions function is weighted more heavily, the average concrete compressive strength drops. Figure 113 shows the relationship between best low-CO_2-emissions based on concrete compressive strength when the simplified analysis procedures are applied to the design example. From this multi-objective optimization, concrete compressive strength for all designs is 30 MPa. As with Figure 112, this is most likely due to the nature of the simplified analysis procedures applied to the biaxial loading case. Figure 113 shows a slight increase in cost has a correspondingly small increase in CO_2 emission.

For biaxial loading, there is a significant savings in both cost and CO_2 emissions when the theoretical analysis procedures are used over the simplified analysis procedures, as was the case with uniaxial loading. In addition, optimization results show a much clearer relationship between the low-cost and low-CO_2-emissions when the theoretical analysis procedures are used.
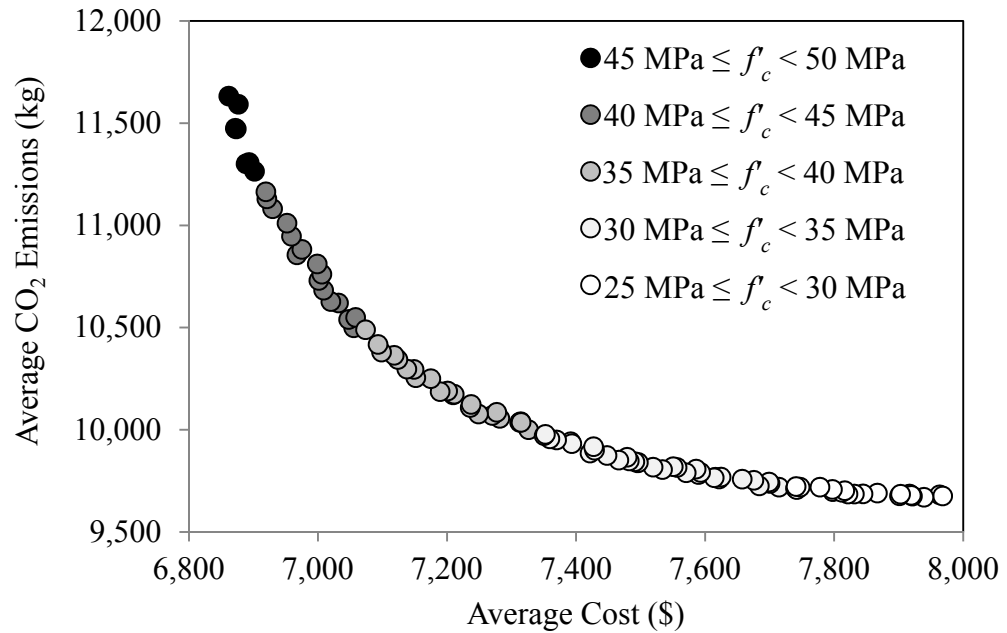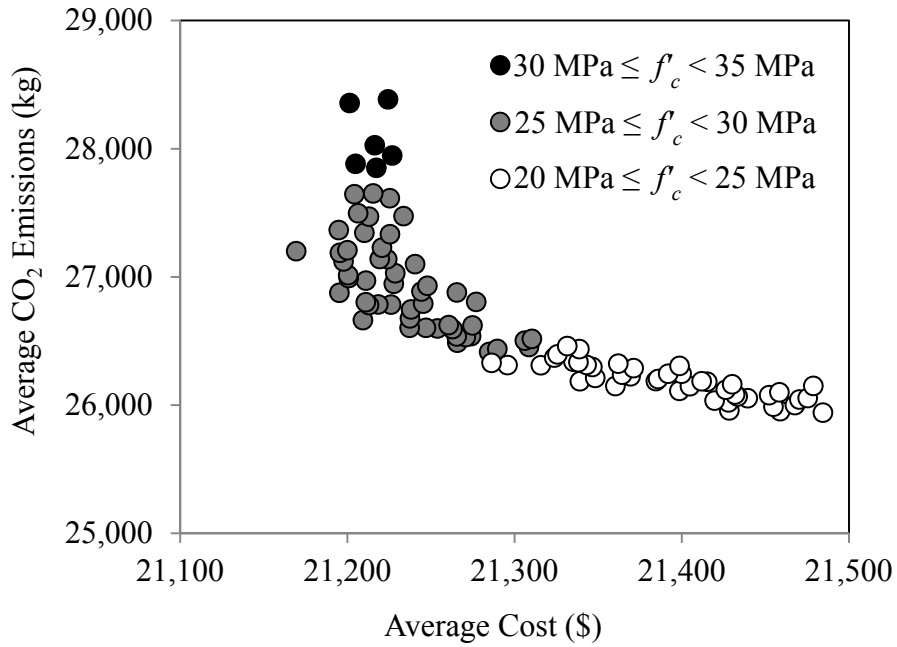
Figure 112. Front for Average Cost and CO_2 Emissions using Simplified Analysis Procedures for Biaxial Loading.
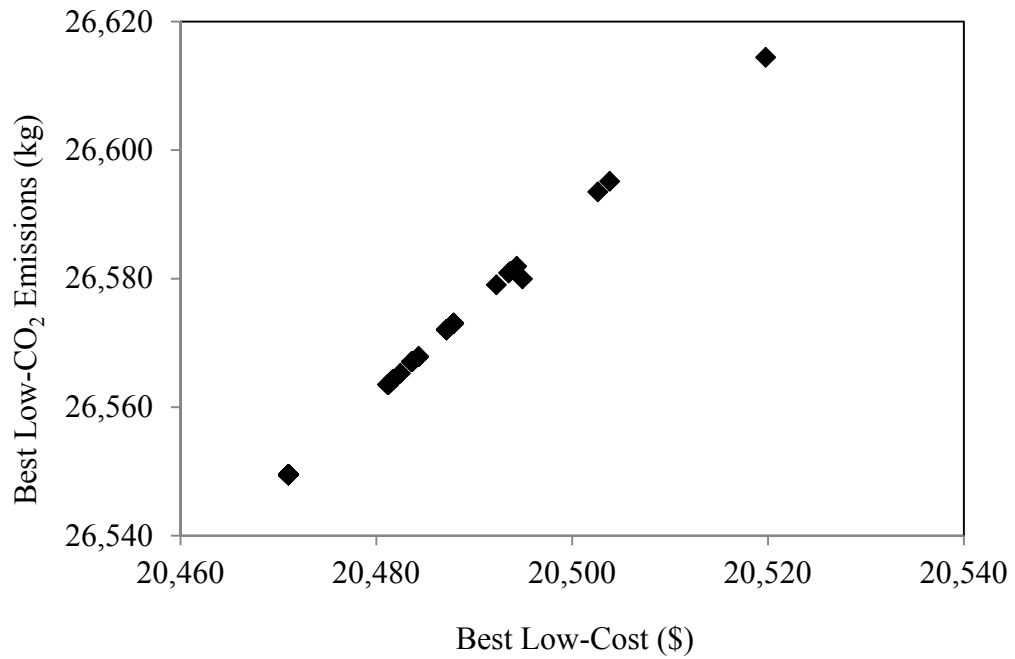
Figure 113. Effects of Concrete Strength on Cost and CO_2 Emissions using Simplified Analysis Procedures for Biaxial Loading.

CHAPTER 8

SUMMARY AND DISCUSSION

A BB-BC optimization algorithm was applied to the analysis and design of rigid reinforced concrete spread footings subjected to concentric, uniaxial, and biaxial loading. For spread footings subjected to eccentric loading conditions, it is convenient to assume that the entire base of the footing remains in contact with the soil, resulting in a compressive bearing pressure distribution. These conditions occur when the eccentricities of the load are within the kern area of the footing and the flexure formula, given by Equation (1), is valid. By designing a spread footing such that the kern area is large enough to contain the eccentricities, the footing will become larger than what is required to satisfy service and ultimate limit states. Then, by assuming the bearing pressure distribution is constant beneath the entire footing with a value of q_{max}, the analysis of a spread footing subjected to eccentric loads greatly simplifies and becomes similar to a concentrically loaded footing. However, these assumptions do not accurately describe the nature of the bearing pressure distribution. In addition, knowledge of the soil pressure distribution for spread footings subjected to uplift may be necessary to evaluate an existing footing in which the original loading pattern has been modified. Therefore, the first objective of this research was to develop analysis procedures for rigid spread footings underlain by a uniform, homogeneous, isotropic, cohesionless, linear-elastically behaving soil, subjected to eccentric loading conditions that allow uniaxial and biaxial uplift. Different boundary conditions, based upon one, two, and three corners detached, were applied to the general bearing pressure surface equation, given by Equation (10). From these formulations, an analysis chart of the bearing pressure surface equations for

one, two, and three footing corners detached was developed to determine percentages of detachment along the edges of a spread footing that is subjected to biaxial uplift.

The second objective was to compare the theoretical structural analysis procedures that account for uplift with simplified analysis procedures, discussed in Section 5.3, using a BB-BC optimization algorithm. For reinforced spread footings subjected to uniaxial and biaxial loading, it was shown that there is significant savings in cost and CO_2 emissions when the theoretical analysis procedures are used over the simplified analysis procedures. Figure 88 showed a dramatic increase in average cost difference between the theoretical and simplified analysis procedures as applied load and eccentricity increased for uniaxial loading. For a load of 5,000 kN at a 1-m eccentricity, there was close to a 30% difference in average cost between the theoretical and simplified analysis procedures. Figure 91 also showed a drastic increase in the difference in average CO_2 emissions between the theoretical and simplified analysis procedures as applied load and eccentricity increased for uniaxial loading. For a load of 5,000 kN at a 1 m eccentricity, there was close to a 30% difference in average CO_2 emissions between the theoretical and simplified analysis procedures. For biaxial loading, significant differences in average cost and CO_2 emissions between theoretical and simplified analysis procedures were also observed. Figure 101 showed that for footings subjected to biaxial loading with an applied load of 3,000 kN and $e_x = e_y = 1$ m, there was approximately a 175% difference in average cost between the theoretical and simplified analysis procedures. Figure 106 also showed nearly 175% difference in average CO_2 emissions for the same loading condition between the theoretical and simplified analysis procedures. In addition, it was shown that when large applied moments cause detachment of the footing from the soil, feasible designs are

232

still produced for both uniaxial and biaxial loading cases. Figures 104 and 109 showed several low-cost and low-CO_2 emission designs that yield one and two corners detached. This is a significant observation since in practice it is convenient and typical to increase the footing size if there is concern for soil detachment. Applying the BB-BC algorithm to a uniaxial and biaxial loaded footing shows that even though there may be some detachment of the footing from the soil, this does not cause ultimate or service limit state failure.

The third objective was to study the relationship between cost and CO_2 emissions associated with the design of reinforced spread footings subjected to concentric, uniaxial, and biaxial loading. By utilizing a multi-objective optimization, it was shown that for a moderate increase in cost, there was a substantial savings in CO_2 emissions for concentric, uniaxial, and biaxial loading conditions. For engineers striving to be environmentally friendly, spending a little extra money on a spread footing project can result in a decrease in CO_2 emissions.

REFERENCES

American Concrete Institute (2011) Building code requirements for structural concrete and commentary. ACI 318-11

American Society of Civil Engineers (2010) Minimum design loads for buildings and other structures. ASCE/SEI 7-10

Camp C, Pezeshk S, Hansson H (2003) Flexural design of reinforced concrete frames using a genetic algorithm. J Struct Eng 129(1):1-11

Camp CV, Bichon BJ (2004) Design of space trusses using ant colony optimization. J Struct Eng 130(5):741-751

Camp C (2007) Design of space trusses using big bang-big crunch optimization. J Struct Eng 133(7):999-1007

Camp CV, Akin A (2012) Design of retaining walls using big bang-big crunch optimization. J Struct Eng 138(3):438-448

Camp CV, Assadollahi A (2013) CO_2 and cost optimization of reinforced concrete footings using a hybrid big bang-big crunch algorithm. Struct Multidisc Optim http://link.springer.com/content/pdf/10.1007%2Fs00158-013-0897-6

Camp CV, Huq F (2013) CO_2 and cost optimization of reinforced concrete frames using a big bang-big crunch algorithm. Eng Struct 48:363–372

Coello CA, Christiansen AD, Santos F (1997) A simple genetic algorithm for the design of reinforced concrete beams. Eng. Comput 13:185-96

Coello CA (1999) A comprehensive survey of evolutionary-based multi-objective optimization techniques. Know Inf Syst 1:269-308

Das BM (2008) Fundamentals of geotechnical engineering, 3 Ed. Cengage Learning, Stamford, CT

Erol OK, Eksin I (2006) A new optimization method: big bang-big crunch. Adv Eng Softw 37:106-111

Galton F (1907) Vox Populi. Nature 75:450-451

Govindaraj V, Ramasamy JV (2005) Optimum detailed design of reinforced concrete continuous beams using genetic algorithms. Comput Struct 84:34-48

Highter WH, Anders JC (1985) Dimensioning footings subjected to eccentric loads. J Geotech Eng, American Society of Civil Engineers 111, GT5:659-665

Irles R, Irles F (1994) Explicit stresses under rectangular footings. J Geotech Eng, American Society of Civil Engineers 120:444-450

Kaveh A, Talatahari S (2009) Size optimization of space trusses using big bang-big crunch algorithm. Comput Struct 87:1129-1140

Kaveh A, Talatahari, S (2010) A discrete big bang-big crunch algorithm for optimal design of skeletal structures. Asian J of Civil Eng 11(1):103-122

Khajehzadeh M, Taha MR, El-Shafie A, Eslami M (2011) Modified particle swarm optimization for optimum design of spread footing and retaining wall. J Zheijiang Univ-Sci A (Applied Physics & Engineering) 12(6):415-426

Kwak HG, Kim J (2008) Optimum design of reinforced concrete plane frames based on predetermined section database. Comput Aided Des 40:396-408

Kwak HG, Kim J (2009) An integrated genetic algorithm complemented with direct search for optimum design of RC frames. Comput Aided Des 41:490-500

Lee CL, Ahn, J (2003) Flexural design of reinforced concrete frames by genetic algorithm. J Struct Eng 129(6):762-774

Lepš M, Šejnoha M (2003) New approach to optimization of reinforced concrete beams. Comput Struct 81:1957-1966

Marler RT, Arora JS (2004) Survey of multi-objective optimization methods for engineering. Structural and Multidisc Optim 26:369-395

Mehta PK (2002) Greening of the concrete industry for sustainable development. In: Concrete International, July 23-28

Mehta PK, Merman H (2009) Tools for reducing carbon emissions due to cement consumption. In: Structure, January 11-15

Meyerhof GG (1953) The bearing capacity of foundations under eccentric and inclined loads. Proceedings, 3rd Int Conf Soil Mech and Foundation Eng 1:440-445, Zurich

Mineral Products Association (2010) Summary data. www.mineralproducts.org/sustainability/data.html. 2 August 2012

Parsopoulos KE, Vrahatis MN (2002) Particle swarm optimization method in multi-objective problems. ACM Symposium on Applied Computing SAC, Madrid, Spain, pp 603-607, March 10 - 14

Paya I, Yepes V, González-Vidosa F, Hospitaler A (2008) Multiobjective optimization of concrete building frames by simulated annealing. Comput-Aided Civil Infrastruct Eng 23(8):596-610

Paya-Zaforteza I, Yepes V, Hospitaler A, González-Vidosa F (2009) CO_2-optimization of reinforced concrete frames by simulated annealing. Eng Struct 31:1501-1508

Perea C, Alcala J, Yepes V, González-Vidosa F, Hospitaler A (2008) Design of reinforced concrete bridge frames by heuristic optimization. Adv Eng Softw 39:676-688

Poulos HG, Davis EH (1974) Elastic solutions for soil and rock mechanics. Wiley, New York

Rafiqa MY, Southcombea C (1998) Genetic algorithms in optimal design and detailing of reinforced concrete biaxial columns supported by a declarative approach for capacity checking. Comput Struct 69:443-457

Rajeev S, Krishnamoorthy CS (1998) Genetic algorithms-based methodology for design optimization of reinforced concrete frames. Computer-Aided Civil Infrastruct Eng 13:63-74

Rodriguez JA, Aristizabal-Ochoa JD (2012) Rigid spread footings resting on soil subjected to axial load and biaxial bending: I) simplified analytical method. Int J Geomech, American Society of Civil Engineers 13:109-119

Sahaba MG, Ashourb AF, Toropovc VV (2004) Cost Optimisation of Reinforced Concrete Flat Slab Buildings. Eng Struct 27:313-322

Sarma KC, Adeli H (1998) Cost optimization of concrete structures. J Struct Eng 124(5):570-578

Teng WC (1962) Foundation design. Prentice-Hall, Inc., Englewood Cliffs, N.J

United Nations Intergovernmental Panel on Climate Change (2007) Climate change 2007: synthesis report. Contribution of Working Groups I, II and III to the Fourth Assessment Report of the Intergovernmental Panel on Climate Change. IPCC, Geneva, Switzerland

Vesic AS (1975) Bearing capacity of shallow foundations. In: H Winterkorn and HY Fang, (eds) Foundation Engineering Handbook, Chap 3. Van Nostrand Reinhold, New York

Villalba P, Alcalá J, Yepes V, González-Vidosa F (2010) CO_2 optimization of reinforced concrete cantilever retaining walls. In: 2nd International Conference on Engineering Optimization, September 6 – 9. Lisbon, Portugal

Wang Y, Kulhawy FH (2008) Economic design optimization of foundations. J Geotech Geoenviron 134(8):1097-1105

Wang Y (2009) Reliability-based economic design optimization of spread foundations. J Geotech Geoenviron 135(7):954-959

Whitman RV, Richart FE (1967) Dynamic procedures for dynamically loaded foundations. J Soil Mech Found Div 93(SM6):169-193

Wilson KE (1997) Bearing pressures for rectangular footings with biaxial uplift. J Bridge Eng, American Society of Civil Engineers 2:27-33

Yepes V, González-Vidosa F, Alcalá J, Villalba P (2012) CO_2 optimization design of reinforced concrete cantilever retaining walls based on a VNS-threshold acceptance strategy. J Comput Civ Eng 26(3):378-386

APPENDIX

$$V_{one-way} = \frac{-L(b_{col} - B + 2d_a)}{16B}\left(Bq_1 + Bq_2 + 3Bq_3 + 3Bq_4 - b_{col}q_1 - b_{col}q_2 + \right.$$
$$\left. + b_{col}q_3 + b_{col}q_4 - 2d_aq_1 - 2d_aq_2 + 2d_aq_3 + 2d_aq_4\right) \tag{A1}$$

$$V_{one-way} = \frac{-B(b_{col} - L + 2d_a)}{16L}\left(Lq_1 + 3Lq_2 + 3Lq_3 + Lq_4 - b_{col}q_1 + b_{col}q_2 + \right.$$
$$\left. + b_{col}q_3 - b_{col}q_4 - 2d_aq_1 + 2d_aq_2 + 2d_aq_3 - 2d_aq_4\right) \tag{A2}$$

$$V_{punch} = P_u - \left(-\frac{q_1(b_{col} + d_a)^2(\alpha + \beta - 2\alpha\beta)}{2\alpha\beta} \right.$$
$$\left. -\frac{q_1(\beta b_{col}B - \alpha BL - \beta BL + \beta d_aB + \alpha b_{col}L + \alpha d_aL + 2\alpha\beta BL)^3}{48(\alpha\beta BL)^2} \right) \tag{A3}$$

$$V_{punch} = P_u - \left(-\frac{q_1\beta B(b_{col} + d_a)^3}{24(\alpha L)^2} \right.$$
$$\left. -\frac{q_1(b_{col} + d_a)(\alpha BL + \beta BL + \alpha d_aL + \alpha b_{col}L - 2\alpha\beta BL)^2}{8(\alpha L)^2\beta B} \right) \tag{A4}$$

$$V_{punch} = P_u - \left(-\frac{q_1\alpha L(b_{col} + d_a)^3}{24(\beta B)^2} \right.$$
$$\left. -\frac{q_1(b_{col} + d_a)(\alpha BL + \beta BL + \beta d_aL + \beta b_{col}L - 2\alpha\beta BL)^2}{8\alpha L(\beta B)^2} \right) \tag{A5}$$

$$V_{one-way} = \frac{q_1 B}{48(\alpha L)^2 \beta}\left(12(\alpha\beta)^2 L^3 - 8(\alpha L)^3 \beta^2 - 6\alpha\beta^2 L^3 + \beta^2 L^3 + 24\alpha^2\beta L^3 \right.$$

$$-18\alpha\beta L^3 - 12\alpha^2 L^3 + 12(\alpha\beta)^2 b_{col} L^2 + 24(\alpha\beta)^2 d_a L^2$$

$$-12\alpha\beta^2 b_{col} L^2 - 24\alpha\beta^2 d_a L^2 + 3\beta^2 b_{col} L^2 + 6\beta^2 d_a L^2$$

$$-24\alpha^2\beta b_{col} L^2 - 48\alpha^2\beta d_a L^2 + 12\alpha\beta b_{col} L^2 + 24\alpha\beta d_a L^2$$

$$+12\alpha^2 b_{col} L^2 + 24\alpha^2 d_a L^2 - 6\alpha\beta^2 b_{col}^2 L - 24\alpha\beta^2 b_{col} d_a L$$

$$-24\alpha\beta^2 d_a^2 L + 3\beta^2 b_{col}^2 L + 12\beta^2 b_{col} d_a L + 12\beta^2 d_a^2 L$$

$$+6\alpha\beta b_{col}^2 L + 24\alpha\beta b_{col} d_a L + 24\alpha\beta d_a^2 L + \beta^2 b_{col}^3$$

$$\left. +6\beta^2 d_a b_{col}^2 + 12\beta^2 b_{col} d_a^2 + 8\beta^2 d_a^3 \right) \tag{A6}$$

$$V_{one-way} = \frac{q_1 L}{48\alpha(\beta B)^2}\left(12(\alpha\beta)^2 B^3 - 8(\beta B)^3 \alpha^2 - 6\alpha^2\beta B^3 + \alpha^2 B^3 + 24\alpha\beta^2 B^3 \right.$$

$$-18\alpha\beta B^3 - 12\beta^2 B^3 + 12(\alpha\beta)^2 b_{col} B^2 + 24(\alpha\beta)^2 d_a B^2$$

$$-12\alpha^2\beta b_{col} B^2 - 24\alpha^2\beta d_a B^2 + 3\alpha^2 b_{col} B^2 + 6\alpha^2 d_a B^2$$

$$-24\alpha\beta^2 b_{col} B^2 - 48\alpha\beta^2 d_a B^2 + 12\alpha\beta b_{col} B^2 + 24\alpha\beta d_a B^2$$

$$+12\beta^2 b_{col} B^2 + 24\beta^2 d_a B^2 - 6\alpha^2\beta b_{col}^2 B - 24\alpha^2\beta b_{col} d_a B$$

$$-24\alpha^2\beta d_a^2 B + 3\alpha^2 b_{col}^2 B + 12\alpha^2 b_{col} d_a B + 12\alpha^2 d_a^2 B$$

$$+6\alpha\beta b_{col}^2 B + 24\alpha\beta b_{col} d_a B + 24\alpha\beta d_a^2 B + \alpha^2 b_{col}^3$$

$$\left. +6\alpha^2 d_a b_{col}^2 + 12\alpha^2 b_{col} d_a^2 + 8\alpha^2 d_a^3 \right) \tag{A7}$$

$$V_{punch} = P_u - \left(\frac{q_4 \left(b_{col}+d_a\right)^2 \left(\alpha+\gamma-1\right)}{2\gamma} - \frac{q_4}{48\gamma\left(\alpha-\gamma\right)\left(BL\right)^2}\left(b_{col}B - BL + d_a B\right. \right.$$
$$\left.\left. +\gamma BL + \alpha BL - \gamma b_{col}L - \gamma d_a L + \alpha b_{col}L + \alpha d_a L\right)^3 \right) \tag{A8}$$

$$V_{punch} = P_u - \left(\frac{-q_4 B\left(b_{col}+d_a\right)^3}{24\gamma\left(\alpha-\gamma\right)L^2} - \frac{q_4\left(b_{col}+d_a\right)}{8\gamma\left(\alpha-\gamma\right)BL^2}\left(\gamma BL - BL + \alpha BL + \gamma b_{col}L\right.\right.$$
$$\left.\left. +\gamma d_a L - \alpha b_{col}L - \alpha d_a L\right)^2 \right) \tag{A9}$$

$$V_{one-way} = \frac{q_4 B\left(b_{col}-L+2d_a\right)\left(3L+b_{col}+2d_a-2\gamma L-2\alpha L\right)}{8\gamma L}$$
$$+\frac{q_4 B\left(L+b_{col}+2d_a-2\alpha L\right)^3}{48\gamma\left(\alpha-\gamma\right)L^2} \tag{A10}$$

$$V_{one-way} = \frac{q_4 L\left(b_{col}-B+2d_a\right)}{48\gamma B^2}\left(12B^2 - 6\alpha B^2 + 7\left(\gamma B\right)^2 + \left(\alpha B\right)^2 + \left(\gamma b_{col}\right)^2\right.$$

$$+4\left(\gamma d_a\right)^2 + \left(\alpha b_{col}\right)^2 + 4\left(\alpha d_a\right)^2 - 18\gamma B^2$$

$$+4\alpha\gamma B^2 + 4\gamma^2 b_{col}B + 8\gamma^2 d_a B - 2\alpha^2 b_{col}B$$

$$-4\alpha^2 d_a B - 2\alpha\gamma b_{col}^2 - 8\alpha\gamma d_a^2 + 4\gamma^2 b_{col}d_a$$

$$+4\alpha^2 b_{col}d_a - 6\gamma b_{col}B - 12\gamma d_a B + 6\alpha b_{col}B$$

$$\left. +12\alpha d_a B - 2\alpha\gamma b_{col}B - 4\alpha\gamma d_a B - 8\alpha\gamma d_a b_{col}\right) \tag{A11}$$

$$M_B = \frac{-q_4 BL}{24\gamma}\Big(2L - 6b_{col} - 2\gamma^2 b_{col} - 2\alpha^2 L + \alpha^3 L - 2\alpha^2 b_{col} + 6\gamma b_{col} + 6\alpha b_{col}$$
$$-2\gamma^2 L + \gamma^3 L + \alpha^2 \gamma L + \alpha\gamma^2 L - 2\alpha\gamma L - 2\alpha\gamma b_{col}\Big) \tag{A12}$$

$$M_L = \frac{-q_4 L\left(B - b_{col}\right)^2}{384\gamma B^2}\Big(24B^2 - 8\alpha B^2 + 17\left(\gamma B\right)^2 + \left(\alpha B\right)^2 + \left(\gamma b_{col}\right)^2 + \left(\alpha b_{col}\right)^2$$
$$-40\gamma B^2 + 6\alpha\gamma B^2 + 6\gamma^2 b_{col} B - 2\alpha^2 b_{col} B - 2\alpha\gamma b_{col}^2$$
$$-8\gamma b_{col} B + 8\alpha b_{col} B - 4\alpha\gamma b_{col} B\Big) \tag{A13}$$

$$V_{punch} = P_u - \left(\frac{q_2 \left(b_{col} + d_a\right)^2 \left(\beta + \eta - 1\right)}{2\eta} - \frac{q_2}{48\gamma\left(\alpha - \gamma\right)\left(BL\right)^2}\left(b_{col}L - BL + d_a L\right.\right.$$
$$\left.\left.+\eta BL + \beta BL - \eta b_{col} B - \eta d_a B + \beta b_{col} B + \beta d_a B\right)^3\right) \tag{A14}$$

$$V_{punch} = P_u - \left(\frac{-q_2 L\left(b_{col} + d_a\right)^3}{24\eta\left(\beta - \eta\right)B^2} - \frac{q_2 \left(b_{col} + d_a\right)}{8\eta\left(\beta - \eta\right)B^2 L}\left(\eta BL - BL + \beta BL + \eta b_{col} B\right.\right.$$
$$\left.\left.+\eta d_a B - \beta b_{col} B - \beta d_a B\right)^2\right) \tag{A15}$$

$$V_{one-way} = \frac{q_2 B (b_{col} - L + 2d_a)}{48\eta L^2} \left(12L^2 - 6\beta L^2 + 7(\eta L)^2 + (\beta L)^2 + (\eta b_{col})^2 + 4(\eta d_a)^2 \right.$$

$$+ (\beta b_{col})^2 + 4(\beta d_a)^2 - 18\eta L^2 + 4\beta \eta L^2 + 4\eta^2 b_{col} L$$

$$+ 8\eta^2 d_a L - 2\beta^2 b_{col} L - 4\beta^2 d_a L - 2\beta \eta b_{col}^2 - 8\beta \eta d_a^2$$

$$+ 4\eta^2 b_{col} d_a + 4\beta^2 b_{col} d_a - 6\eta b_{col} L - 12\eta d_a L \qquad \text{(A16)}$$

$$+ 6\beta b_{col} L + 12\beta d_a L - 2\beta \eta b_{col} L - 4\beta \eta d_a L$$

$$\left. - 8\beta \eta d_a b_{col} \right)$$

$$V_{one-way} = \frac{q_2 (b_{col} - B + 2d_a)(3B + b_{col} + 2d_a - 2\eta B - 2\beta B)}{8\eta B}$$

$$+ \frac{q_2 L (B + b_{col} + 2d_a - 2\beta B)^3}{48\eta (\beta - \eta) B} \qquad \text{(A17)}$$

$$M_B = \frac{-q_2 B (L - b_{col})^2}{384\eta L^2} \left(24L^2 - 8\beta L^2 + 17(\eta L)^2 + (\beta L)^2 + (\eta b_{col})^2 + (\beta b_{col})^2 \right.$$

$$- 40\eta L^2 + 6\beta \eta L^2 + 6\eta^2 b_{col} L - 2\beta^2 b_{col} L - 2\beta \eta b_{col}^2 \qquad \text{(A18)}$$

$$\left. - 8\eta b_{col} L + 8\beta b_{col} L - 4\beta \eta b_{col} L \right)$$

$$M_L = \frac{-q_2 B L}{24\eta} \left(2B - 6b_{col} - 2\eta^2 b_{col} - 2\beta^2 B + \beta^3 B - 2\beta^2 b_{col} + 6\eta b_{col} + 6\beta b_{col} \right. \qquad \text{(A19)}$$

$$\left. - 2\eta^2 B + \eta^3 B + \beta^2 \eta B + \beta \eta^2 B - 2\beta \eta B - 2\beta \eta b_{col} \right)$$

242

$$V_{punch} = P_u - \left(\frac{q_3 \left(b_{col} + d_a\right)^2 \left(\eta + \gamma - 2\eta\gamma\right)}{2\left(\eta - 1\right)\left(\gamma - 1\right)} + \frac{q_3}{48\left(\gamma - 1\right)^2 \left(\eta - 1\right)^2 \left(BL\right)^2} \left(b_{col}B + d_a B \right. \right.$$
$$\left. \left. + b_{col}L + d_a L + \eta BL + \gamma BL - \eta b_{col}B - \eta d_a B - \gamma b_{col}L - \gamma d_a L - 2\eta\gamma BL\right)^3 \right) \quad \text{(A20)}$$

$$V_{punch} = P_u - \left(\frac{-q_3 B\left(\eta - 1\right)\left(b_{col} + d_a\right)^3}{24\left(\gamma - 1\right)^2 L^2} - \frac{q_3 \left(b_{col} + d_a\right)}{8\left(\gamma - 1\right)^2 \left(\eta - 1\right) BL^2} \left(\eta BL - d_a L - b_{col}L \right. \right.$$
$$\left. \left. + \gamma BL + \gamma b_{col}L + \gamma d_a L - 2\eta\gamma BL\right)^2 \right) \quad \text{(A21)}$$

$$V_{punch} = P_u - \left(\frac{-q_3 B\left(\gamma - 1\right)\left(b_{col} + d_a\right)^3}{24\left(\eta - 1\right)^2 B^2} - \frac{q_3 \left(b_{col} + d_a\right)}{8\left(\gamma - 1\right)\left(\eta - 1\right)^2 B^2 L} \left(\eta BL - d_a B - b_{col}B \right. \right.$$
$$\left. \left. + \gamma BL + \eta b_{col}B + \eta d_a B - 2\eta\gamma BL\right)^2 \right) \quad \text{(A22)}$$

$$V_{punch} = P_u - \left(\frac{-q_3}{48\left(\gamma - 1\right)^2 \left(\eta - 1\right)^2 \left(BL\right)^2} \left(\eta BL - d_a B - b_{col}B - b_{col}L - d_a L + \gamma BL \right. \right.$$
$$\left. \left. + \eta b_{col}B + \eta d_a B + \gamma b_{col}L + \gamma d_a L - 2\eta\gamma BL\right)^3 \right) \quad \text{(A23)}$$

$$V_{one-way} = \frac{q_3 B\left(\eta - 1\right)\left(b_{col} - L + 2d_a\right)}{48\left(\gamma - 1\right)^2 L^2} \left(12\left(\gamma L\right)^2 - 18\gamma L^2 + 7L^2 - 6\gamma b_{col}L - 12\gamma d_a L \right.$$
$$\left. + 4b_{col}L + 8d_a L + b_{col}^2 + 4b_{col}d_a + 4d_a^2\right) \quad \text{(A24)}$$

$$V_{one-way} = \frac{q_3 L\left(\gamma - 1\right)\left(b_{col} - B + 2d_a\right)}{48\left(\eta - 1\right)^2 B^2} \left(12\left(\eta B\right)^2 - 18\eta B^2 + 7B^2 - 6\eta b_{col}B - 12\eta d_a B \right.$$
$$\left. + 4b_{col}B + 8d_a B + b_{col}^2 + 4b_{col}d_a + 4d_a^2\right) \quad \text{(A25)}$$